

A CHEMICAL BIOLOGY APPROACH TO PHOSPHOINOSITIDE METABOLIC
ANALYSIS

Jarod Waybright

A dissertation submitted to the faculty of the University of North Carolina at Chapel Hill in
partial fulfillment of the requirements for the degree of Doctor of Philosophy in the
Division of Chemical Biology and Medicinal Chemistry in the UNC Eshelman School of
Pharmacy.

Chapel Hill
2017

Approved By:

Michael Jarstfer

Nancy Allbritton

David Lawrence

John Sondek

Qisheng Zhang

© 2017
Jarod Waybright
ALL RIGHTS RESERVED

ABSTRACT

Jarod Waybright: A Chemical Biology Approach to Phosphoinositide Metabolic Analysis
(Under the direction of Qisheng Zhang)

Lipids serve a diverse array of functions including maintaining cellular structure and compartmentalization, regulating post-translational modifications of proteins, and as members of complex signaling networks. Despite their importance there is minimal understanding of how bioactive lipids and lipid pathways systematically regulate biological processes. Phosphoinositides (PIPs) are a diverse class of lipid signaling molecule implicated in nearly all facets of cell signaling including migration, proliferation, and apoptosis. Mutations in numerous PIP modifying enzymes occur frequently in human disease, especially cancers, though the effects of these mutations on the global metabolic system have been poorly defined. Likewise, heterogeneous protein expression and undefined feedback loops further complicate obtaining a global view of metabolism and understanding the PIP metabolic pathway's role in disease. Current approaches have been unsuccessful in obtaining a systems-wide analysis due to various technical challenges including low sensitivity, use of indirect measurements of activity, and a lack of validated reporters and delivery methods.

We have developed a new approach to systematic PIP analysis including synthesis and validation of fluorescent reporters, novel PIP delivery methods, and applying these methods to analyze PIP metabolism in breast cancer cell lines. We have shown that hydrophobicity is a key determinant in the ability of fluorescent reporters to serve as substrates for phosphoinositides modifying enzymes, which proceed via interfacial catalysis, through chemical synthesis of fluorescent phosphoinositides with varied hydrophobicity in the diacylglycerol (DAG) side chain and examined their propensity to serve as substrates towards various enzymes. We used these

findings to develop a suite of fluorescent reporters that could subsequently be used as standards and reporters in future experimentation.

To achieve our goal of systematically analyzing cellular metabolism, we examined a variety of delivery methods for fluorescent PIPs as previously reported techniques have failed to achieve a level of delivery sufficient for metabolic analysis. We further developed a fluorescent model phospholipid that allowed us to explore novel delivery techniques including intramolecular charge masking and photocaging methods while simultaneously exploring previously published methods including liposomes and charge altering releasable transporters (CARTs) for the delivery of PIPs.

A PIP₂:CART complex was demonstrated to efficiently deliver fluorescent PIP₂ to cells, which were then analyzed for their metabolite distribution. This method was effective in achieving conversion of the fluorescent reporter to a variety of PIP substrates as judged by comparison with synthetic standards. We further applied this system to preliminary studies on breast cancer cell lines possessing unique mutations in PIP modifying enzymes. We have thus far been successful in demonstrating a platform using fluorescent PIP reporters, novel delivery techniques that lead to a variety of metabolites than can be analyzed by capillary electrophoresis (CE) or thin layer chromatography (TLC). This system could be a powerful tool in future studies of PIP metabolism in human disease with potential diagnostic applications.

For my parents, who encouraged me to always ask 'why' and remind me that 'if you're going to be stupid, you better be strong.. and you aren't very big.'

ACKNOWLEDGEMENTS

*The best journeys answer questions
that in the beginning,
you didn't even think to ask
-Jeff Johnson (180° South)*

In the words of Hunter/Weir: *what a long strange trip it's been*. I would first like to thank Dr. Qisheng Zhang for allowing me to join his lab and help me grow as a scientist and an individual. Members of the research team: Manish K. Singh, Huanyao Guao, and Weigang Wang were also a pleasure to work with and were also eager to help and offer their scientific expertise. It was a more than pleasurable experience scientifically and I enjoyed expanding my cultural horizons throughout our time together.

Thank you to my committee members Dr. Mike Jarstfer (Dr. J), Dr. David Lawrence, Dr. Nancy Allbritton and Dr. John Sondek for their scientific guidance. I would also like to extend a special than you to Dr. J who was a continued positive presence throughout my graduate work in both scientific and personal endeavors. I would also like to thank the entire faculty and staff of CBMC. The people in this program lead me to choosing UNC to pursue my graduate studies and is a large part keeping me here for my future scientific studies. I would also like to acknowledge Dr. Angie Proctor for her assistance throughout my project and always lending a helping hand and a good joke.

I would like to extend the biggest thanks to all of my friends that made this experience both memorable and enjoyable. I cannot describe in words the importance of the camaraderie of friends and fellow students throughout the process. I would like to

give a personal acknowledgment to Carla Coste Sánchez who was a motivating force throughout a crucial time in my graduate studies. Thank you for sticking by me things were hard and the enthusiasm you shared when they were great. I am excited to see where you will go on your journey and enjoyed immensely our time journeying together.

I would also like to extend an acknowledgement to Dr. Kimberly Barnash. I could write an immeasurable amount of great things about Kim the person and scientist, but she would want me to keep it short: you are delightful and a social butterfly. I cannot wait to see where your drive and witty nature take you.

Finally I would like to extend my thanks to the Fantasy Football Focus Podcast (The 06010) crew of Matthew Berry, Stephania Bell, and Field Yates for providing me with mediocre fantasy advice throughout my leagues in graduate school. The pod was a constant source of enjoyment that always made getting through the day a little easier. Put it on the board!

PREFACE

Parts of Chapter 2 of this dissertation are adapted from Waybright, J., Huang, W., Proctor, A. et al. *Required Hydrophobicity of Fluorescent Reporters for Phosphatidylinositol Family of Enzymes* Anal Bioanal Chem (2017).
<https://doi.org/10.1007/s00216-017-0633-y>

Parts of Chapter 3 of this dissertation are adapted from Singh, M.K., J. Waybright, and Q. Zhang. *A facile method to enable a model phospholipid cell-permeable and photoactivatable*. Tetrahedron, 2017. 73(26): p. 3677-3683

TABLE OF CONTENTS

ABSTRACT.....	iii
DEDICATION.....	v
ACKNOWLEDGEMENTS.....	vi
PREFACE.....	ix
TABLE OF CONTENTS.....	x
LIST OF TABLES.....	xiv
LIST OF SCHEMES.....	xv
LIST OF FIGURES.....	xvi
LIST OF ABBREVIATIONS.....	xviii
CHAPTER 1. INTRODUCTION AND IMPORTANCE OF SYSTEMATIC ANALYSIS OF BIOACTIVE LIPIDS.....	1
1.1 Importance of Bioactive Lipids.....	1
1.2 Importance of Systematic Analysis of Lipid metabolites.....	2
1.3 Importance of Phosphoinositides.....	3
1.3.1 Background on Phosphoinositides.....	3
1.3.2 Cellular Distribution of PIPs.....	5
1.3.3 Cellular Functions of Phosphoinositides.....	6
1.4 The PI3K Metabolic Pathway.....	7
1.4.1 Background.....	7
1.4.2 The Importance of PI3K in Human Disease.....	11
1.4.3 Pharmaceutical Targeting of PI3K Pathway.....	11

1.5 Measurement of Lipid Metabolites.....	13
1.5.1 Background.....	13
1.5.2 Radiolabeled Substrate	13
1.5.3 Mass Spectrometry.....	14
1.5.4 Fluorescent Protein Domains	15
1.6 Synthetic Tools for Studying PIP Metabolism.....	15
1.6.1 Fluorescent Substrates.....	15
1.6.2 Chemical Cytometry coupled with Fluorescent Substrates	16
CHAPTER 2. THE IMPORTANCE OF HYDROPHOBICITY IN LIPID SIGNALING REPORTERS: SYNTHESIS AND EVALUATION OF FLUORESCENT LIPID REPORTERS.....	18
2.1 Introduction to Interfacial Catalysis by PIP Modifying Enzymes.....	18
2.2 Results and Discussion.....	19
2.2.1 Design and synthesis of fluorescent PIP2 derivatives.....	19
2.2.2 Biophysical and Biochemical Evaluation of Fluorescent PIP2 Reporters.....	21
2.2.3 In vitro Membrane Association of Fluorescent PIP2 Reporters.....	23
2.2.4 Vesicle Based PI3K Analysis.....	25
2.2.5 Required Hydrophobicity for PI4K Substrate PtdIns.....	26
2.2.6 Synthesis of BODIPY-DAG-C15 and BODIPY-PA-C15	27
2.3 Conclusions and Future Directions	29
2.4 Experimental.....	31
2.4.1 Soluble PI3K Assay Conditions.....	32
2.4.2 Soluble PI4K Assay Conditions.....	32
2.4.3 Vesicle Based PI3K Assay Conditions.....	32
2.4.4 TLC Analysis of Fluorescent Lipid Metabolites	33
2.4.5 CE Analysis of Fluorescent Lipid Metabolite.....	33

2.4.6 Fluorescent lipids/liposome interaction	34
2.4.7 Chemical Synthesis	35
CHAPTER 3. CELLULAR DELIVERY OF SYNTHETIC PIP REPORTERS.....	55
3.1 Introduction.....	55
3.2 Results and Discussion.....	59
3.2.1 Delivery of BODIPY-DAG-C15, BODIPY-PIP2-C15, and model phospholipid 36 to Cells.....	59
3.2.2 Photocaging for the Delivery of Model Phospholipid 36.....	61
3.2.3 Histone Delivery of PIPs.....	64
3.2.4 Cationic Liposomes for the Delivery of PIPs.....	65
3.2.5 Fusogenic Liposomes for the Delivery of PIPs.....	66
3.2.6 Intramolecular Charge Masking Strategy with Guanidine for the Delivery of Phospholipids.....	70
3.2.7 Charge Altering Releasable Transporters (CARTs) for the Delivery of PIPs.....	74
3.3 Conclusions and Future Directions.....	78
3.4 Experimental.....	80
3.4.1 Confocal Microscopy	82
3.4.2 Preparation of Cationic Liposomes.....	82
3.4.3 Preparation of Fusogenic Liposomes.....	82
3.4.4 Extraction of Lipid Metabolites.....	82
3.4.5 TLC analysis of Lipid Metabolites.....	83
3.4.6 CE Analysis of Lipid Analytes.....	83
3.4.7 Chemical Synthesis.....	84
CHAPTER 4. INVESTIGATION OF CELLULAR PHOSPHOLIPID METABOLISM WITH FLUORESCENT REPORTERS.....	94
4.1 Introduction.....	94

4.2 Results and Discussion.....	96
4.2.1 Concentration Dependent Production of PA using BODIPY-DAG-C15.....	96
4.2.2 Delivery of BODIPY-PIP2-C15:CART Complex to Breast Cancer Cells.....	97
4.2.3 Cellular Analysis of BODIPY-PIP2-C15 Metabolites in MDA-MB-436 Cells	98
4.2.4 Cellular Analysis of BODIPY-PIP2-C15 Metabolites in MDA-MB-453 Cells.....	102
4.3 Conclusions and Future Directions.....	103
4.4 Experimental.....	108
4.4.1 Cell Culture.....	108
4.4.2 Delivery of BODIPY-PIP2-C15 to Breast Cancer Cells.....	108
4.4.3 Extraction of Lipids from Cell Pellet.....	109
4.4.4 TLC Analysis of Lipid Metabolites.....	109
Appendix.....	111
References.....	127

LIST OF TABLES

Table 1.1 Table 1.1 Summary of Interactions Within Lipid Signaling Networks.....	3
Table 1.2 Cellular Distribution of PIPs.....	6
Table 1.3 Summary of Frequency of PIK3CA Alterations in Human Cancer.....	10
Table 3.1 Cationic Liposome Formulations for BODIPY-PIP₂-C15 Cellular Delivery.....	66
Table 3.2 Fusogenic Liposome Formulations for BODIPY-PIP₂-C15 Cellular Delivery.....	68

LIST OF SCHEMES

Scheme 2.1 Synthesis of Fluorescent PIP₂ Derivatives with Varied Hydrophobicity.....	20
Scheme 2.2 Synthesis of Fluorescent PtdIns Reporter.....	21
Scheme 2.3 Synthesis of PIP Metabolites.....	29
Scheme 3.1 Synthesis of Fluorescent Model Phospholipid 36.....	60
Scheme 3.2 Synthesis of Intramolecular Charge Masking Model Compound 54.....	73

LIST OF FIGURES

Figure 1.1. Structure and Metabolic Pathway of Phosphoinositides.....	5
Figure 1.2. PIP Binding Effector Protein Domains.....	7
Figure 1.3. The PI3K Metabolic Pathway.....	8
Figure 1.4. Systematic Analysis of Cellular PIP Generation.....	17
Figure 2.1. Critical Micelle Concentration (CMC) and Kinetic Constants of PIP₂ Derivatives.....	22
Figure 2.2. Fluorescent PI(4,5)P₂ Substrate Competition.....	23
Figure 2.3. In-vitro Membrane Association of Fluorescent PIP₂ Reporters.....	25
Figure 2.4. Competition with Endogenous PI(4,5)P₂ in Liposome Based Assay.....	26
Figure 2.5. Biophysical and Kinetic Analysis of Fluorescent PtdIns Analog.....	27
Figure 3.1. Common Chemical Moieties in Photocaging of Phospholipids.....	56
Figure 3.2. Common Lipids Used in Liposome Formulation for Cellular Transfection,.....	58
Figure 3.3. Carrier Free Delivery of Fluorescent Lipid Reporters.....	61
Figure 3.4. Generation and Uncaging of Compound 54 with MKS-1.....	62
Figure 3.5. Delivery of uncaged 36 and caged 54 to Cells.....	63
Figure 3.6. Histone Delivery of BODIPY-PtdIns-C15 to Cells.....	64
Figure 3.7. Cationic Liposome Delivery of BODIPY-PtdIns-C15 to Cells.....	66
Figure 3.8. Fusogenic Liposome Delivery of BODIPY-PtdIns-C15 to Cells.....	68
Figure 3.9. CE Analysis of Metabolites Generated using Fusogenic Liposome Delivery of BODIPY-PtdIns-C15.....	69
Figure 3.10. Bidentite interaction between guanidine and phosphate.....	70
Figure 3.11. CARTs for the Delivery of BODIPY-PIP₂-C15.....	75

Figure 3.12. Delivery of BODIPY-PIP₂-C15 to cells via CART systems A11 and G7.....	76
Figure 3.13. TLC analysis of Fluorescent Metabolites Generated from BODIPY-PIP₂-C15 in Cells using the CART System.....	77
Figure 4.1. Suite of Fluorescent Reporters to Probe Various PIP Metabolic Pathways.....	95
Figure 4.2. Breast Cancer Cell Lines for PI3K Pathway Metabolic Analysis.....	96
Figure 4.3. Concentration Dependent Increase of PA Production with BODIPY-DAG-C15.....	97
Figure 4.4. Delivery of BODIPY-PIP₂-C15 into MDA-MB-453 cells with CARTs.....	98
Figure 4.5. Analysis of Fluorescent Metabolite Distribution in MDA-MB-436 Cells.....	100
Figure 4.6. Method to ‘Capture’ Fluorescent PIP₃ Produced in MDA-MB-436 Cells.....	101
Figure 4.7. Analysis of Fluorescent Metabolite Distribution in MDA-MB-453 Cells.....	102
Figure 4.8. Structure of AK-PtdIns-C15 and Fluorophore Addition via ‘Click-Chemistry’.....	106

LIST OF ABBREVIATIONS

PIPs	Phosphoinositides
DAG	Diacylglycerol
PtdIns	Phosphatidylinositol
PI(4,5)P ₂ ; PIP ₂	Phosphoinositide 4,5-bisphosphate
PI(4)P	Phosphoinositide 4-phosphate
PI(3,4,5)P ₃ ; PIP ₃	Phosphoinositide 3,4,5-trisphosphate
PI3K	Phosphoinositide 3-kinase
PI4K	Phosphoinositide 4-kinase
PH	Pleckstrin Homology Domain
PTEN	Phosphatase and tensin homolog
PLC	Phospholipase C
DAGK	Diacylglycerol kinase
INPP4	Inositol-3,4-bisphosphate 4-phosphatase
PM	Plasma Membrane
GPCR	G-Protein Coupled Receptor
RTK	Receptor Tyrosine Kinase
EGF	Epidermal Growth Factor
EGFR	Epidermal Growth Factor Receptor
PDGFR	Platelet derived growth factor receptor
HGF	Hepatocyte Growth Factor
HGFR	Hepatocyte Growth Factor Receptor
FOX01	Forkhead Box 01

NfKb	Nuclear Factor Kb
mTOR	Mammalian target of rapamycin
PA	Phosphatidic acid
fMLP	N-Formylmethionyl-leucyl-phenylalanine
MS	Mass spectrometry
GFP	Green fluorescent protein
TLC	Thin layer chromatography
CE-LIF	Capillary Electrophoresis with laser induced fluorescence
DCC	<i>N,N'</i> -Dicyclohexylcarbodiimide
DMAP	Dimethylaminopyridine
DCM	Dichloromethane
DTT	Dithiothreitol
MOPS	3-(N-morpholino)propanesulfonic acid
ATP	Adenosine triphosphate
BODIPY	4,4-Difluoro-5,7-Dimethyl-4-Bora-3a,4a-Diaza-s-Indacene
Cbz	Carboxybenzyl
Bn	Benzyl
Pd/C	Palladium on carbon
MOM	methoxymethyl
NHS	N-Hydroxysuccinimide
Fmoc	Fluorenylmethyloxycarbonyl
BOC	tert-butyloxycarbonyl
PC	Phosphatidylcholine

PE	Phosphatidylethanolamine
PS	Phosphatidylserine
Chol	Cholesterol
DOPE	1,2-dioleoylphosphatidylethanolamine
DOTAP	1,2-dioleoyl-3-trimethylammonium-propane
EDMPC	1,2-dimyristoyl-sn-glycero-3-phosphocholine
EDPPC	1,2-dipalmitoyl-sn-glycero-3-ethylphosphocholine
EDOPC	1,2-dioleoyl-sn-glycero-3-ethylphosphocholine
di-C14 DAB	N,N-Dimethyltetradecylamine
DMTAP	1,2-dimyristoyl-3-trimethylammonium-propane
CART	Charge altering releasable transporter

CHAPTER 1. INTRODUCTION AND IMPORTANCE OF SYSTEMATIC ANALYSIS OF BIOACTIVE LIPIDS

1.1 Importance of Bioactive Lipids

Lipids are responsible for diverse and vital cellular processes with variations in lipid head groups and aliphatic chains allowing for the existence of >1,000 different lipid species [1, 2]. While largely recognized as being important structural components of the cell allowing for compartmentalization of cellular tasks, lipids also serve as critical regulators of a wide array of biological outcomes. Lipids can serve as an energy sources in times of glucose depletion. Fatty acids can be hydrolyzed from phospholipids that enter a stepwise pathway leading to the generation of acetyl CoA, that provides needed carbon atoms to the Krebs's cycle where they can be oxidized for energy production [3]. Lipids can also serve as post-translational modifications of proteins such as the addition of myristoyl group to the N-terminal of the protein leading to membrane association, subcellular localization, and protein-protein interactions [4].

Lipid metabolites are also important signaling metabolites that control a wide array of cellular processes including cell proliferation, migration, and apoptosis [5]. Signaling lipids, such as sphingolipids and phosphoinositides (PIPs), are large networks of metabolites and enzymes that respond uniquely to various extracellular and intracellular stimuli that lead to specific cellular functions [3, 5]. For instance phosphoinositides metabolic enzymes respond to both extracellular stimulation of receptor tyrosine kinases such epidermal growth factor receptor (EGFR) and platelet

derived growth factor receptor (PDGFR) that lead to downstream signaling cascades generally promoting cell survival and growth [6-8]. Likewise, a separate subset of PIP modifying enzymes can also be stimulated by Wnt leading to activation of a separate signaling cascade Wnt [9, 10]. Interestingly, PIP pathways also respond to intracellular production of lipid metabolites possibly as a feedback mechanism to control the ratios of the various metabolites which will be highlighted in the future sections and summarized in **Table 1.1** [11].

1.2 Importance of Systematic Analysis of Lipid metabolites

Because of the broad role of lipid signaling molecules, various enzymes within different pathways control the levels of various lipid metabolites very tightly to maintain cellular homeostasis. Imbalances of these metabolites contribute to a wide variety of human diseases including neuro-degeneration and cancers [5]. For example, mutations in the lipid modifying enzyme phosphoinositides 3-kinase (PI3K) leads to an increase production of signaling metabolite phosphoinositide 3,4,5-trisphosphate (PIP₃). This increased production of PIP₃ is important in cancer onset and progression [12]. Likewise, imbalances resulting from the increased production of another lipid metabolite phosphoinositide 4-phosphate (PI(4)P) by aberrant phosphoinositide 4-kinase (PI4K) has implications in mental health diseases such as bi-polar disorder highlighting the complexity and reach of lipid metabolism in disease [13]. However, due to the complexity of the lipid signaling pathways, areas of aberrant activity have been studied in isolation focusing on a single node of activity separate from the rest of the metabolic network [14-16]. This has most commonly been done using methods such as dominant negative enzymes, siRNA interference, as well as through the development of small molecule chemical probes for biological analysis [15-19]. However, this method of

analysis has raised many questions about the contributions of the total metabolic pathway versus that of just a single metabolite because of the interconnected lipid pathways [20]. Indeed, there are crosstalk and feedback mechanisms among various lipid metabolites within a single pathway as well as interactions between various classes of bioactive lipids [21, 22]. For instance, the sphingolipid and phosphoinositides metabolic pathways have shown to interact through stimulation of diacylglycerol kinase (DAGK) activity. Cells treated with increasing concentrations of sphingosine lead to an increase in phosphatidic acid (PA) production suggesting the pathways are intertwined [21]. Therefore understanding the systems contributions of the various classes of bioactive lipids would be invaluable to understanding their importance in biological processes and diseases [20]. Despite the importance of the lipid signaling metabolic networks, little is known about the interplay between metabolites in cellular processes due to the difficulty in studying multiple metabolic events systematically within the cell [20].

<u>Substrate</u>	<u>Interacting Enzyme</u>	<u>Result</u>
DAG	DAGK	Stimulated
DAG	PKC	Stimulated
Sphingosine	DAGK	Stimulated
PI(3,4,5)P₃ (Increase)	DAGK	Stimulated
PI(3,4,5)P₃ (Depleted)	DAGK	Increased Expression
PI(4,5)P₂	PLC	Stimulated
PI(4)P	PI4P5K	Stimulated

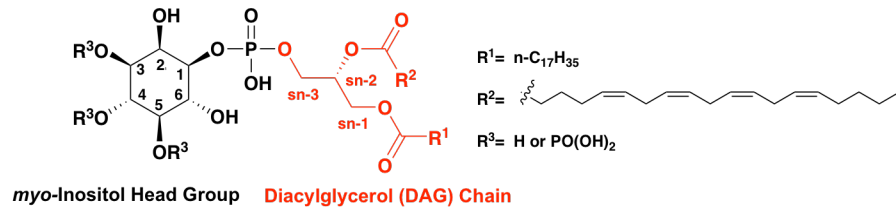
Table 1.1 Summary of Interactions Within Lipid Signaling Networks^{21, 22, 23, 59, 60, 61}

1.3 Importance of Phosphoinositides

1.3.1 Background on Phosphoinositides

Phosphoinositides (PIPs) are a vital class of signaling lipids that also play critical roles in a variety of cellular processes and human diseases, especially cancers [5, 12, 13, 16, 23-28]. PIPs constitute approximately 1% of the phospholipids in the cell membranes and as one of the most versatile family of signaling molecules, PIPs play important roles in numerous facets of cell signaling, cell motility, vesicle transport and development [19, 29-33]. All PIPs are derived from phosphatidylinositol (PtdIns), which can be reversibly phosphorylated on the hydroxyl groups at the C3, C4, and C5 positions to generate seven endogenous PIPs as illustrated in **Figure 1.1A** [34, 35]. PIPs contain a diacylglycerol (DAG) side chain most commonly containing stearic and the polyunsaturated arachidonic acid that anchors them to various subcellular membranes. Because of wide variety of roles that PIPs play in cellular metabolism, there is stringent temporal and spatial control over metabolite generation. Consequently, abnormal levels of PIPs have been associated with development of a wide range of diseases including cancers and neurodegenerative disorders [36-38]

A.



B.

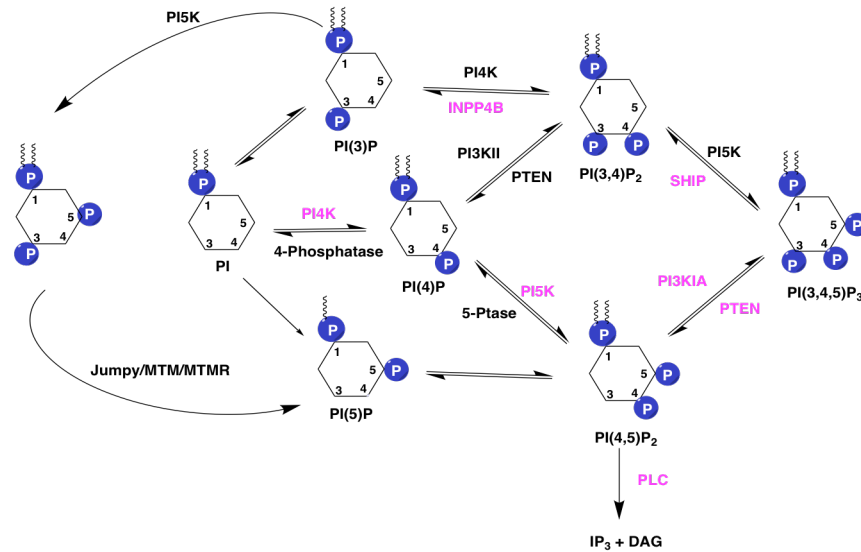


Figure 1.1 Structure and Metabolic Pathway of Phosphoinositides: A. General Structure of Phosphoinositides (PIPs). Phosphoinositides are composed of a myo-inositol head group that can be selectively phosphorylated at the 3,4, and 5 position. It is linked to a DAG chain via a phosphodiester bond with the sn-1 position. The DAG chain most commonly contains arachidonic acid and stearic acid at the sn-2 and sn-3 positions, respectively. B. The PIP Metabolic Network. The PIP metabolic network is a collective of kinases and phosphatases responsible for the generation of 7 distinct phosphorylated PIPs.

1.3.2 Cellular Distribution of PIPs

PIPs are found distributed on specific membranes and the abundance of each lipid is tightly controlled giving great spatial and temporal control of the pathway [2]. As shown in **Figure 1.1B**, PtdIns is modified to generate a pool of 7 PIPs through reversible phosphorylation of the C3, C4, and C5 hydroxyl groups that are distributed

throughout various cell membranes [34, 35]. These lipid metabolites are distributed throughout various membranes as summarized in **Table 1.2**. The most abundant of the PIPs in cells are phosphoinositides 4,5-bisphosphate (PI(4,5)P₂; PIP₂) and phosphoinositide 4-phosphate (PI(4)P) which are important precursors to generate second messenger PI(3,4,5)P₃. Because of the potent signaling functions of PIP₃ it is generally found at only ~2—5% of the levels of PIP₂ at basal conditions [20, 34, 39]. PIP₂ Other low abundance PIPs, such as PI(3)P and PI(3,5)P₂ are found primarily in various endosomes and lysosomes while PI(5)P has been shown to be both a nuclear and cytosolic signaling molecule underscoring the vast diversity amongst distribution and function of PIPs [33, 39].

Metabolite	Location
PI(4)P	Golgi/Vesicles
PI(4,5)P₂	Plasma Membrane
PI(3,4,5)P₃	Plasma Membrane
PI(3,4)P₂	Vesicles
PI(3)P	Early Endosome

Table 1.2 Cellular Distribution of PIPs³⁸:
Metabolites of the PIP metabolic pathway are distributed amongst specific organelles.

1.3.3 Cellular Functions of Phosphoinositides

The various PIPs are generated from a collective of kinases and phosphatases that make up the PIP metabolic network. PIP modifying enzymes can be stimulated through a variety of receptors including G-Protein coupled receptors (GPCRs) and receptor tyrosine kinases (RTKs) by corresponding ligands allowing for temporal control

over the generation of metabolites [33, 35]. PIPs have a wide range of downstream targets and cellular functions through interacting with targets at or recruited to the membrane [34, 35]. Effector proteins are recruited to cellular membranes via stereospecific binding to the phosphorylated inositol head groups enabling spatial organization and control [39]. One such example is the pleckstrin homology (PH) domain, the most abundant lipid-binding domain, which binds to numerous phosphorylated metabolites as seen in **Figure 1.2** [13, 40]. Effector proteins, such as Akt (PKB), contain PH domains that localize the protein to the membrane allowing for activation and downstream signaling effects. This further highlights the importance of stringent control over production of secondary signaling metabolites [33, 34].

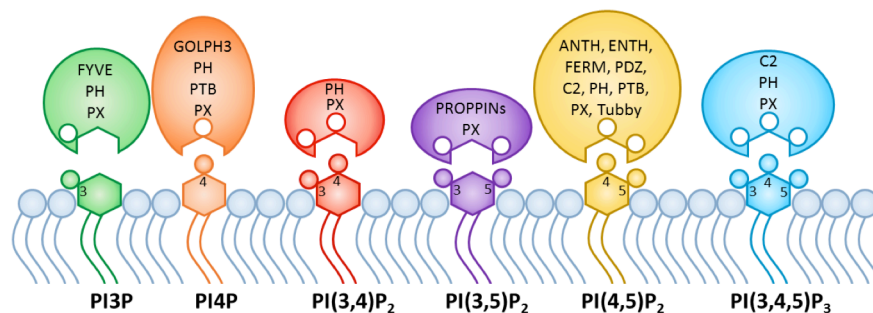


Figure 1.2 PIP Binding Effector Protein Domains: Various protein domains and their PIP target. Effector proteins recognize phosphorylation patterns of PIPs and are recruited to cellular membranes for activation.

1.4 The PI3K Metabolic Pathway

1.4.1 Background

The PI3K pathway is a localized metabolic pathway of 4 enzymes and 4 metabolites within the larger PIP metabolic network and is illustrated in **Figure 1.3** [41, 42]. The central enzyme phosphoinositide 3-kinase (PI3K) is responsible for generation

of potent second messenger $\text{PI}(3,4,5)\text{P}_3$ (PIP_3) from the most abundant PIP metabolite $\text{PI}(4,5)\text{P}_2$. In addition to PI3K, the pathway contains 3 phosphatases responsible for diminishing the pool of PIP_3 : phosphatase and tensin homolog (PTEN), Phosphoinositol-3,4,5-trisphosphate 5-phosphatase 1 (SHIP1), as well as the inositol polyphosphate 4-phosphatase type II (INPP4B) [14, 25, 38]. While the resulting reaction does not generate a PIP, phospholipase C (PLC) is also an important enzyme that is relevant to the PI3K pathway as PLC and PI3K share $\text{PI}(4,5)\text{P}_2$ as a substrate and respond to many of the same stimuli [33]. Other signaling metabolites DAG and inositol 1,4,5-triphosphate (IP_3) that are generated by PLC also serve as important regulators of the PIP metabolic pathway and cellular functions as second messengers [5].

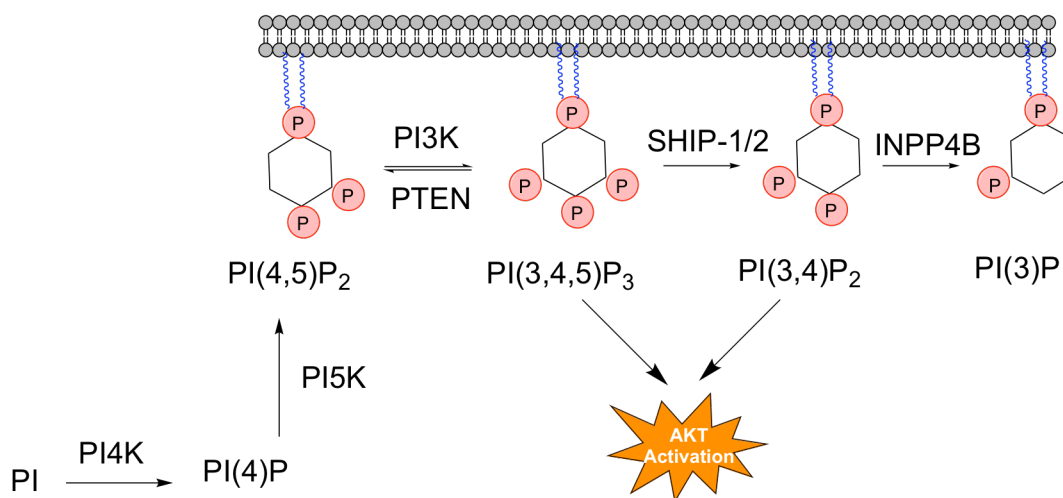


Figure 1.3 The PI3K Metabolic Pathway: The enzymes and metabolites that make up the PI3K metabolic pathway with $\text{PI}(4,5)\text{P}_2$ supplied from PtdIns via $\text{PI}(4)\text{P}$.

1.4.2 The Importance of PI3K in Human Disease

Genes encoding for the PIP modifying enzyme PI3K are found frequently mutated in a variety of cancers summarized in **Table 1.3** [12, 13, 23, 43-45]. Class 1A

PI3Ks are heterodimers composed of a p110 catalytic subunit responsible for generation of PIP_3 , and a p85 regulatory subunit responsible for auto-inhibition of the enzyme [46, 47]. Mutations in the helical and kinase domains of the protein result in increased enzymatic activity through both increased lipid binding and relief of p85 auto-inhibition resulting in an increase in PIP_3 production [23, 46, 47]. Increases in PIP_3 levels drive tumorigenesis due to an increased activation of the PH domain containing effector protein Akt (PKB), which is activated following binding to PIP_3 [25, 38, 48]. The increase in Akt activation results in misregulated downstream signaling of effector proteins including inhibition of transcription factor forkhead box 01 (FOXO1) and increased activity of anti-apoptotic proteins such as nuclear factor κB (NF κB) and mammalian target of rapamycin (mTOR), all important in tumorigenesis [14, 49, 50]. Interestingly the conversion of $\text{PI}(3,4,5)\text{P}_3$ to $\text{PI}(3,4)\text{P}_2$ by the SHIP family of phosphatases does not reduce Akt activation and it has been shown that both metabolites are capable of PH domain binding and Akt activation^[40]. Therefore, both PTEN and INPP4B are responsible for direct termination of PI3K/Akt signaling through depletion of both $\text{PI}(3,4,5)\text{P}_3$ and $\text{PI}(3,4)\text{P}_2$ respectively, suggesting tumor suppressor potential for both of these enzymes. Indeed, knockdowns of both PTEN and INPP4B results in increased Akt activation leading to increased anchorage independent growth and cell motility. Likewise, deletion of PTEN or INPP4B in mice leads to an increase in tumor size in various xenograft models, further validating the tumor suppressor function of these enzymes [24, 28, 40, 45, 51, 52]. Not surprisingly, loss of PTEN expression or activity is common in human cancers and is the second most mutated tumor suppressor gene in

human cancer behind $p53^{[52]}$. Collectively, these findings have made the PI3K pathway an attractive target for pharmaceutical development [14, 16, 38, 49, 50, 53].

Disease	Frequency (%)
Head and Neck Cancer	42
Breast Cancer	25
Lung Cancer (Squamous Cell)	53
Colorectal Cancer	37
Lung Cancer (Small Cell)	27

Table 1.3 Summary of Frequency of *PIK3CA* Alterations in Human Cancer^{6,10,12, 30}

Highlighting this need of expanded analytical techniques, a study⁶ of MCF10A cell populations using flow cytometry revealed heterogeneity in PI3K activity that was previously unknown due to measurement of population averages. In this study, a bimodal distribution of Akt activity was observed following EGF stimulation that correlates with PI3K protein production. Interestingly, the same distribution of PI3K was observed on a single cell level for both wild type and mutant PI3K^{H1047R} suggesting that only a subset of cells classified as having a high levels of PI3K can activate Akt [7]. Because cell-to-cell variability has been demonstrated in multiple systems can lead to unique cellular fates and understanding how this is maintained and regulated could be a powerful tool in basic biology and pharmaceutical targeting of PI3K [54, 55]. For instance, targeting a population of cells are expressing low quantities of mutant PI3K with low Akt activation may be unsuitable for achieving a positive therapeutic effect [16]. Therefore, a simple and effective diagnostic tool to better understand this heterogeneity and PI3K activity in a patient could be effective in better determining a method and time of treatment.

1.4.3 Pharmaceutical Targeting of PI3K Pathway

Attempts at therapeutic intervention against the PI3K pathway have been made by targeting PI3K directly as well as downstream effectors of the pathway. Indeed, the PI3K-d selective inhibitor, idelalisib, has been approved by the FDA to treat chronic lymphocytic leukemia in combination with rituximab though only as a third line treatment following multiple treatment failures [56]. Likewise, the drug was pulled from multiple clinical trials in 2016 due to lack of efficacy. Pan PI3K inhibitors represent the largest class of agents used to regulate aberrant PI3K activity [14, 16, 49, 57, 58]. Unfortunately, such a strategy has proven to be difficult in achieving clinical success and raises questions regarding the possible off-target effects of inhibiting all isoforms of PI3K versus the oncogenic PI3K α mutant [49]. Akt inhibition is the second most common target of pharmacological agent for PI3K aberrant cancers, but this too has seen little positive clinical outcomes [14, 16, 34, 49]. Such failures in the clinic have raised numerous interesting and important biological questions that are essential in understanding the complex nature of the PI3K signaling network, as well as the PI metabolic pathway as a whole. One such goal is understanding the roles of various metabolites within the pathway and possible feedback loops across various cancer types [14, 16, 49, 57]. Likewise, it places an emphasis on achieving a systems understanding of PIP biology within a tumor microenvironment, especially with the previously described cell-to-cell variability of PI3K and Akt activation [3, 7]. It is hypothesized that inhibition of PI3K or Akt is overcome by compensatory lipid signaling pathways over time allowing for the cell to evade deleterious effects of inhibition.

Supporting this hypothesis of compensatory pathways, products of the PI3K pathway have been shown to alter levels of other PI modifying enzymes including

DAGK, which converts DAG to PA [59]. In this study, increased DAGK activity was observed following an increase in PI(3,4,5)P₃ and PI(3,4)P₂ both *in vitro* and *in vivo*. This was an interesting result as it was the first instance of DAGK activation in the absence of receptor-regulated calcium release. Further, it showed that DAGK can be activated and recruited to the plasma membrane as a direct consequence of PI3K activation highlighting the interconnectivity of lipid metabolic pathways [59].

Interestingly, another study showed extended inhibition of PI3K resulted in increased expression level of DAGK, contradictory to the previously described study. DAGK has been shown to activate tyrosine kinase SRC, which canonically is activated through PIP₃/Akt [22, 60]. Dual inhibition of both DAGK and PI3K leads to a decrease in cell growth versus a single agent inhibition alone. These results suggest that understanding pathway heterogeneity and the changes oncogenic mutations confer as well as the relationship between the other enzymes and metabolites within the PI3K pathway are essential to achieving clinical success targeting the PI3K pathway or other members of the PI metabolic network [6, 22, 61]. Likewise, the seemingly contradictory actions of the pathway under different cell stimuli and in different cell types could be vital to understanding the pathway's contributions to disease progression. Thus, an improved understanding of the direct role of PIs in disease progression would further validate this pathway as a drug target and lead to improved understanding of the interplay between the pathway's metabolites, lead to biomarker identification, and serve as a powerful tool in achieving clinical success targeting the pathway.

1.5 Measurement of Lipid Metabolites

1.5.1 Background

To better understand the systems biology of PIP metabolism, sensitive detection methods are needed to analyze the changes of both major and minor metabolites. Such sensitivity is necessary to discern the roles of low-level metabolites in the system and to extend the analysis to a single cell level in order to paint a clear picture of the tumor microenvironment^[34]. PIPs represent less than 1% of total phospholipid content in the cell and at a concentration of 10 mM PIP_2 is 25-fold more abundant than other phosphorylated PI metabolites [21, 23]. Sensitive and robust detection methods are needed for analysis, especially when only a maximum of 10% of this pool of PIP_2 is converted to PIP_3 following stimulation and the metabolite has a short life span [25, 62-64].

1.5.2 Radiolabeled Substrate

Current methods aimed at quantifying PI metabolism is done using radioactivity-based methods through the metabolic labeling of living cells with radiolabeled inorganic phosphate (^{32}Pi or ^{33}Pi) or $[2\text{-}^3\text{H}]\text{myo}$ -inositol. A major downfall of this method is that labeling time and conditions greatly affects signal output and can therefore result in improper analysis of metabolic activity. This method also suffers from the inability to distinguish phosphorylation isomers such as $\text{PI}(4,5)\text{P}_2$ vs. $\text{PI}(3,4)\text{P}_2$ and requires a large number of cells for analysis and therefore is ineffective at analysis of tumor microenvironment heterogeneity through single cell analysis [20, 34, 62, 63]. These methods have been effective at quantifying the average basal levels of multiple metabolites, though such a method takes long incubation (up to >24 h) and again lacks

sensitivity to effectively measure systematic metabolism. Likewise, while it is acceptable for studying steady-state metabolism of PIs it is not effective in accurately capturing short lived metabolic products such as PIP_3 [34]. Because of the drawbacks of this method, it would not be effective in achieving a detailed view of PI metabolism necessary for use in diagnostic applications.

1.5.3 Mass Spectrometry

Mass spectrometry (MS) can also be used to analyze complex mixtures of PtdIns metabolites. Unfortunately MS relies on a large number of cells and can be problematic in identifying low level and highly phosphorylated phospholipid species such as $\text{PI}(4,5)\text{P}_2$ and $\text{PI}(3,4,5)\text{P}_3$ [64-68]. A promising MS method requires chemical manipulation of isolated phospholipids in a reaction with TMS-diazomethane to generate a pool of methylated phosphate esters [64, 67]. This neutralizes the negative charge of the lipid and allows for a more sensitive detection on MS. Following parent ion identification, a MS/MS experiment can be performed to determine the phosphorylation state of the selected mass by fragmentation and analyzing for the mass of the now neutral inositol head group. While this method is successful in determining the relative concentration of lipid metabolites in a cell population, it is unable to distinguish isomers of phosphorylation states and using the endogenous pool of lipids results in a large number of mass signals that must be analyzed. Likewise, the PIs can contain various fatty acids at the *sn*-1 and 2 positions further complicating analysis, though such detailed information may be useful when further analyzing the role of PI metabolites in biological processes [64, 66, 67]. This method is also very technically demanding with complex data analysis following the use of specialized MS equipment and methods [65, 69].

1.5.4 Fluorescent Protein Domains

Another method of studying PI metabolism is the use of engineered fluorescent proteins such as tagged PH domains to analyze enzymatic activities via microscopy and the translocation of the fluorescent domains following cell stimulation. PH domains, such as that from Akt, are engineered to contain a green fluorescent protein (GFP) that can be monitored via fluorescence microscopy. Following a cell stimulation event, the fluorescent domains can be analyzed translocating from the cytosol to the membrane where the lipid messenger is present [70]. Such methods, however, are indirect measurements of enzymatic activity and suffer from the inability to analyze multiple metabolites simultaneously [34, 62, 71, 72]. Likewise, it has been demonstrated that PH domains can bind to multiple lipid metabolites again complicating biological conclusions that could be discerned from using this method. Further, this method cannot be used as diagnostic tool because of the necessity to engineer and express fluorescent-tagged protein domains is not compatible with clinical samples [20, 62, 63].

1.6 Synthetic Tools for Studying PIP Metabolism

1.6.1 Fluorescent Substrates

A promising tool for the advancement of PIs analysis are synthesized reporters that share the core structure of specific PI metabolites while containing unique chemical moieties that allows for sensitive and specific quantification of metabolites [20]. Such an approach is powerful because the reporters can be manipulated to contain various moieties specific to the desired biological question. One of the most widely used chemical biology methods that have been increasingly applied to synthetic PIs is the use of a fluorescent-tagged substrate. This technology allows for visualization of the PI metabolic network by both microscopy as well as monitoring biochemical reactions via

thin layer chromatography (TLC) separation and fluorescent scanning [71]. Such a technology is more advantageous than radiolabeling due to increased sensitivity of fluorescence based analytical platforms. Likewise, a known concentration of a specific metabolite reporter could be loaded into cells versus relying on the steady-state metabolic incorporation of the labeled unit into the pool of phospholipids allowing for the direct dissection of specific nodes of the metabolic pathway and possibly systematic metabolic analysis. Fluorescent PIP reporters have been shown to serve as substrates for various PI modifying enzymes *in-vitro*, but due to the difficulty in their chemical synthesis, there has been little analysis on the effects of reporter structure on enzymatic turnover or cellular localization^[62, 63, 71, 73].

1.6.2 Chemical Cytometry coupled with Fluorescent Substrates

Another trend in PIP systems biology is the use of microanalytical chemical separation, known as chemical cytometry, to separate and analyze complex cellular mixtures. One such technique, capillary electrophoresis with laser-induced fluorescence (CE-LIF), has been validated as an effective platform for analyzing multiple classes of lipid kinases and phosphatase reporters and is capable of single cell metabolic analysis [62, 74-78]. Further, this method has been validated for the separation of the various metabolites found within the PIP metabolic network, including isomers of the same phosphorylation state [62, 63]. In this method, cells are loaded with fluorescent reporters followed by lysis of the cells and the contents are loaded into a capillary and separation is achieved via capillary electrophoresis. This method holds great promise for PIP metabolic analysis as a known concentration of reporter can be delivered to the cell to minimize perturbation of the endogenous pool of metabolites. The level of sensitivity, as low as 10^{-20} mol, and the capability of single-cell analysis also makes this

a powerful technique for developing a lipid profile and could also be applied to patient samples for possible diagnostic applications [62, 63, 77]. Such technology could be applied to PI metabolic analysis and provide a detailed profile of PIP metabolites in various disease states and provide a powerful system to better understand the systems contributions to biology. Ideally, a fluorescent reporter could be delivered to cells where it could undergo in-cell mixture synthesis through the metabolic network followed by analysis of the collective of lipid metabolites by CE-LIF as shown in **Figure 1.5**. In this dissertation, I will describe our efforts in validating a platform utilizing fluorescent lipid reporters for PIP metabolic analysis.

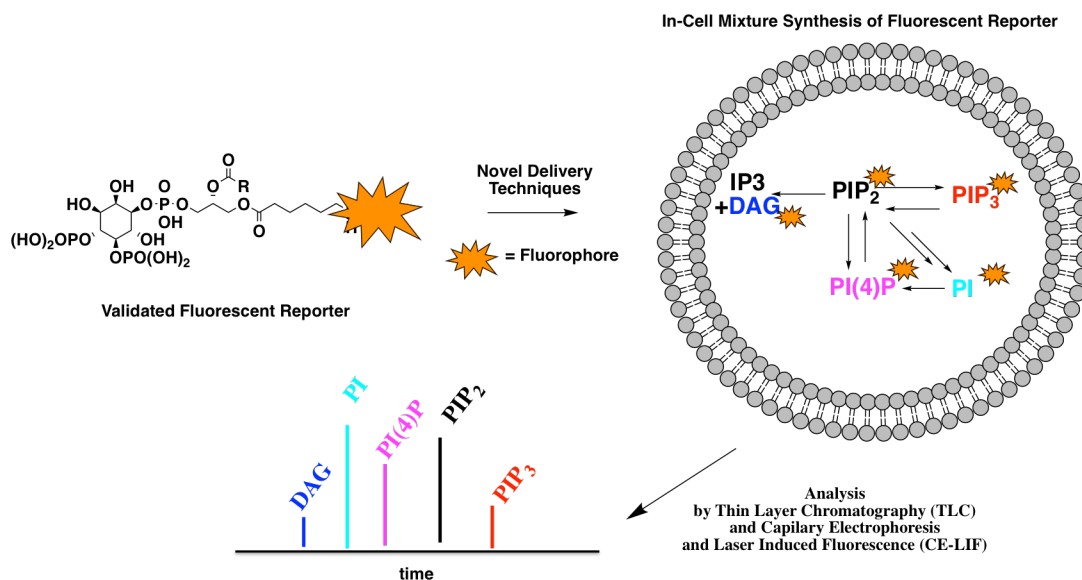


Figure 1.4 Systematic Analysis of Cellular PIP Generation: A system using a validated fluorescent PIP₂ reporter coupled with non-invasive delivery techniques would allow for generation of a variety of fluorescent metabolites that can then be measure via CE-LIF and TLC

CHAPTER 2. THE IMPORTANCE OF HYDROPHOBICITY IN LIPID SIGNALING REPORTERS: SYNTHESIS AND EVALUATION OF FLUORESCENT LIPID REPORTERS

2.1 Introduction to Interfacial Catalysis by PIP Modifying Enzymes

PI3K and other PIP modifying enzymes catalyze reactions at the lipid/water interface in a process known as interfacial catalysis wherein hydrophobic contact between the enzyme and substrate as well as enzyme and membrane are of critical importance to catalytic turnover [46, 79, 80]. Likewise, various cancer causing mutations in the PIP family of enzymes have been shown to cause increased activity through required hydrophobic interaction with the membrane [46, 80]. Consequently, the hydrophobic side chains in fluorescent PIP derivatives will likely play important roles in their capacity as enzyme substrates. Consequently, reporters that cannot undergo efficient metabolism like that of their endogenous counterparts will not be useful tools in monitoring cellular PIP metabolism [20].

Unfortunately PIP synthesis is labor intensive and consequently short chain soluble PIPs are more frequently utilized as they are easier to synthesize, purify and analyze in biochemical assays [81, 82]. However, the effects of the acyl chain in these fluorescent PIPs on their capacity as enzyme substrates have been ignored. The roles of the side chains in non-fluorescent substrates have been previously demonstrated. For example, a study of *B. cereus* phospholipase C (PLC) activity on phosphatidylcholine substrates revealed changes in the kinetic constants for the various substrates with a preference for long acyl chains [83].

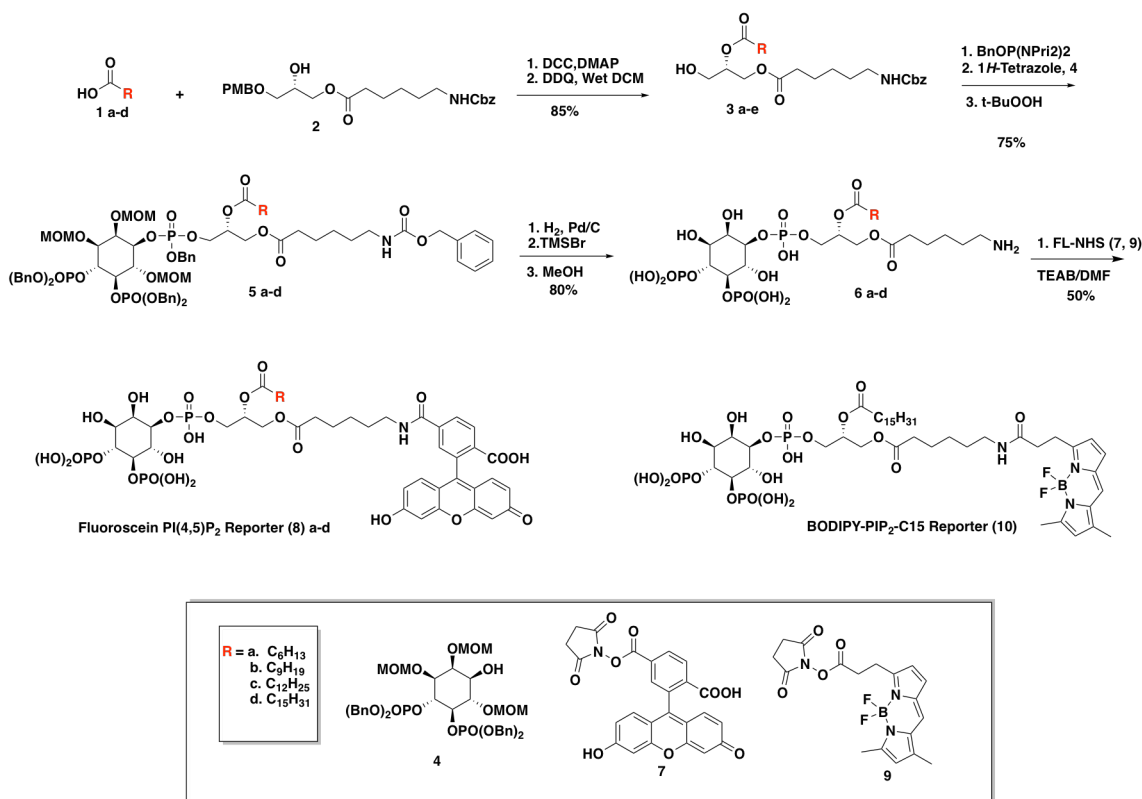
With the goal of using fluorescent PIP reporters to profile cellular metabolism we synthesized fluorescent PIP₂ and PtdIns derivatives that contain varied degrees of hydrophobicity and investigated their ability to serve as reporters of PI3K α and PI4KII α activity, respectively. This chapter describes the synthesis and biochemical evaluation of various PIPs with different degrees of hydrophobicity in their side chains for selection of a suitable reporter for cellular studies. We describe a set of assays that prove useful in reporter selection for lipid signaling enzymes and could be applied to various classes of signaling phospholipids. We further describe the synthesis of various other PIP metabolites based on our findings in these studies to be used as both standards and reporters in future cellular experiments.

2.2 Results and Discussion

2.2.1 Design and synthesis of fluorescent PIP₂ derivatives

To investigate the effects of hydrophobicity on the capacity of fluorescent PIP₂ derivatives as enzyme substrates, we synthesized four PIP₂ analogs **PIP₂-C6**, **PIP₂-C9**, **PIP₂-C12** and **PIP₂-C15** with different alkyl groups C₆H₁₃, C₉H₁₉, C₁₂H₂₅, and C₁₅H₃₁, respectively, at the *sn*-2 position according to **Scheme 2.1**. Fluorescein was chosen as the fluorophore for evaluation of multiple PIP₂ derivatives because of our prior success in separating fluorescein-tagged PIPs by both thin layer chromatography (TLC) and capillary electrophoresis (CE) [62, 71, 76]. A BODIPY tagged C15 PIP₂ was (BODIPY-C15-PIP₂) also synthesized as the fluorophore possesses some chemical characteristics that may make it a more suitable for cellular analysis [84]. Briefly, carboxylic acids **1** with various length of alkyl chain coupled with the alcohol **2**. Subsequently, the *p*-methoxybenzyl (PMB) group was removed to form **3**. The primary alcohol in **3** was then converted to a phosphoramidite, which was coupled to the

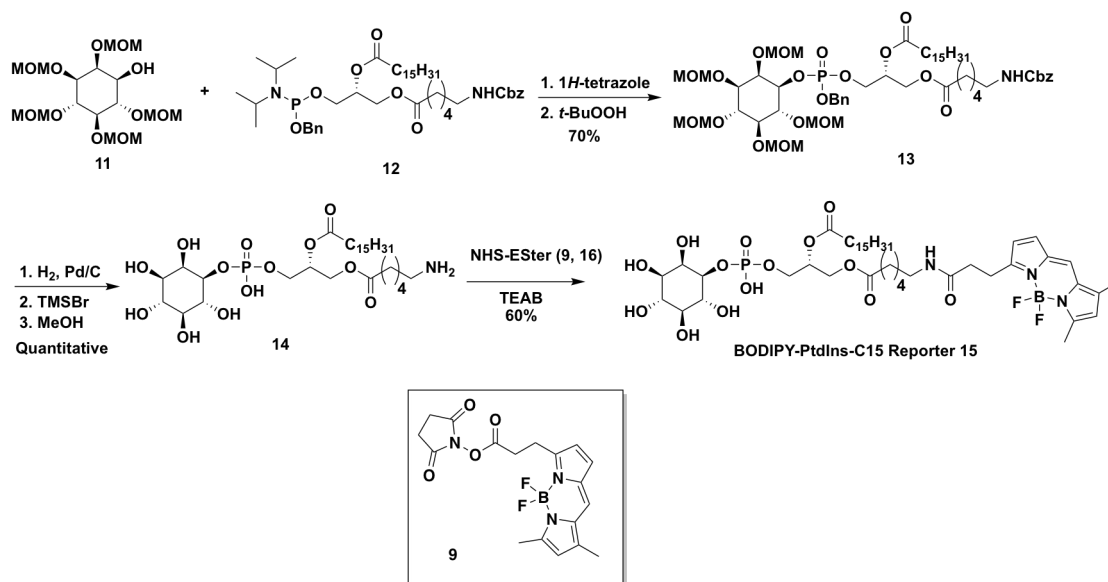
protected inositol **4** previously synthesized according to literature protocols [81]. After oxidation with *t*-butyl hydroperoxide, compound **5** was formed and the carboxybenzyl (Cbz) and benzyl (Bn) groups were removed by hydrogenolysis. Deprotection of the methoxymethyl (MOM) groups then provided the primary amine **6**, which reacted with the NHS ester of fluorescein **7** or BODIPY **9** to yield fluorescent PIP₂ derivatives [81, 82, 85, 86].



Scheme 2.1: Synthesis of Fluorescent PIP₂ Derivatives with Varied Hydrophobicity

BODIPY-PtdIns-C15 was synthesized in a similar manner according to according to **Scheme 2.2** [81]. Briefly, DAG phosphoramidite **12** containing palmitic acid at the sn-2 position was synthesized as described in **Scheme 2.1** and was coupled with protected inositol derivative **11** followed by oxidation with *t*-BuOOH to generate

compound **13**. Removal of all the protective groups resulted in **14**, which reacted with BODIPY-NHS to provide fluorescent **15 (BODIPY-PtdIns-C15)**.



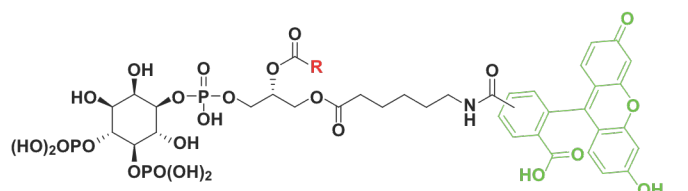
Scheme 2.2: Synthesis of Fluorescent PtdIns Reporter

2.2.2 Biophysical and Biochemical Evaluation of Fluorescent PIP₂ Reporters

The critical micelle concentration (CMC) of the fluorescent PIP₂ derivatives was calculated by measuring light scattering of various concentrations of the reporters in H₂O at 25 °C [71]. As expected, the PIP₂ derivative with a longer acyl chain, and thereby higher hydrophobicity, has lower CMC value than that with a shorter acyl chain. In comparison, the endogenous PI(4,5)P₂ has a reported CMC of 10 μ M [71].

A mixed micelle assay was utilized to compare the kinetic parameters of the substrates [71]. The assay was initiated by the addition of purified PI3K enzyme to assay buffer containing individual fluorescent PIP₂ derivative and ATP and stopped by the addition of a mixture of CHCl₃/MeOH (1:1 v:v). The reaction mixture was analyzed

by TLC or CE for production of fluorescent PI(3,4,5)P₃ as previously described [71]. The concentration of substrate was varied to give a set of initial velocity values and this data was fit to the Michaelis-Menten equation to calculate the relative K_m and V_{max} values of the reporters summarized in **Figure 2.1**. Under these conditions, no detectable amount of the corresponding PIP₃ was formed for the **PIP₂-C6** reporter, suggesting that short chain **PIP₂-C6** was not an effective substrate for PI3K α under the assay conditions examined. Unsurprisingly, the most hydrophobic **PIP₂-C15** was the most efficiently metabolized substrate.



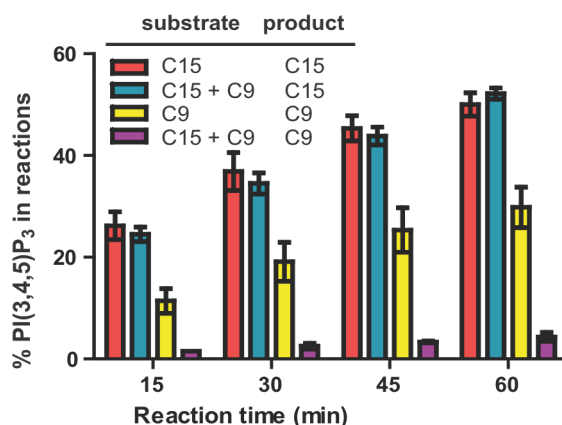
Probe	R	CMC (μ M)	K _m (μ M)	V _{max} (pmol/ng/min)
FL-PIP ₂ -C6	C ₆ H ₁₃	196 \pm 1	n.d.	n.d.
FL-PIP ₂ -C9	C ₉ H ₁₉	124 \pm 4	39.5 \pm 17.8	0.07 \pm .02
FL-PIP ₂ -C12	C ₁₂ H ₂₅	26 \pm 6	34.6 \pm 13.5	0.18 \pm .04
FL-PIP ₂ -C15	C ₁₅ H ₃₁	13 \pm 1	29.4 \pm 7.3	0.34 \pm .04

Figure 2.1: Critical Micelle Concentration (CMC) and Kinetic Constants of PIP₂ Derivatives. The CMC was measured in water using dynamic light scattering (DLS). Mixed micelle PI3K assays were used to calculate the kinetic constant of the various fluorescent derivatives. Kinetic constants for the C6 reporter were not obtained due to the lack of production of the corresponding PIP₃.

To further assess the ability of fluorescent PIP₂ probes as PI3K α substrates, a 1:1 (mol:mol) mixture of **PIP₂-C9** and **PIP₂-C15** was used in a mixture in a soluble PI3K assay, with reactions of equimolar **PIP₂-C9** or **PIP₂-C15** alone under the same assay conditions as controls. **PIP₂-C9**, **PIP₂-C15** and their corresponding PI(3,4,5)P₃ products were efficiently separated by CE (**Fig. 2.2 B**). As shown in **Figure 2.2**, the conversion of **PIP₂-C9** in the presence of **PIP₂-C15** was decreased by approximately 5-fold compared

to when it was the only PI3K substrate. In contrast, the conversion of **PIP₂-C15** remained consistent with or without the presence of **PIP₂-C9**. These results again highlight the importance of hydrophobicity in fluorescent PIP₂ probes, especially when competing substrates were present- a scenario when the probe was used as a reporter in live cells.

A.



B

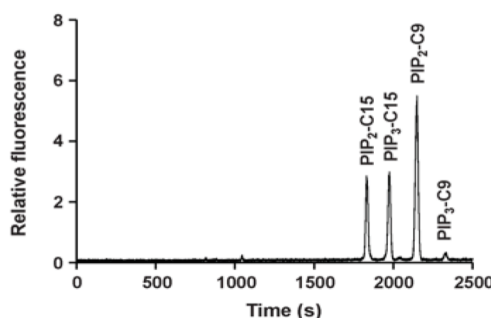
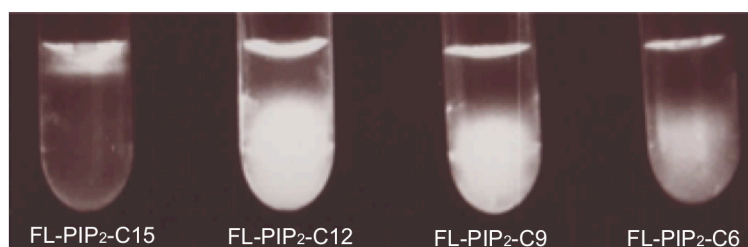


Figure 2.2 Fluorescent PI(4,5)P₂ Substrate Competition. (A) Mixed micelle PI3K assay conditions were used to analyze the effects of multiple reporters in solution. Production of PIP₃ was monitored from reactions that contained a single fluorescent PIP₂ derivative (20 μM), short chain C9 or long chain C15, as well as production of each product in reactions that contained both reporter in equimolar (20 μM) concentrations. (B) Representative chromatogram of separation of PIP₂-C9, PIP₂-C15, PIP₃-C9 and PIP₃-C15 by CE. The CE analysis was carried out by Dr. Angela Proctor in Dr. Nancy Allbritton's lab

2.2.3 In vitro Membrane Association of Fluorescent PIP₂ Reporters

The acyl side chain in a fluorescent PIP₂ probe is vital to cellular localization. However, the non-invasive method of using histone as a carrier protein to deliver fluorescent PIP₂ derivatives into cells resulted in very low efficiency in our hands [87]. Consequently, we utilized a membrane association assay that was developed for protein-lipid interactions to investigate likely membrane localization of fluorescent PIP₂ probes [88]. In this assay, liposomes and the associated cargo are recovered by centrifugation atop a dense sucrose gradient. Liposomes were formulated to mimic mammalian membranes with a final composition of phosphatidylcholine (PC; 45%), phosphatidylethanolamine (PE; 25%), phosphatidylserine (PS; 5%), phosphatidylinositol (PtdIns; 10%), and cholesterol (Chol; 15%). **Figure 2.3** shows representative images of the assay mixtures after centrifugation. The top lipid layer and bottom sucrose layers were then collected and each layer quantified by CE for the presence of fluorescent PIP₂. Approximately 91% of the **PIP₂-C15** probe was incorporated into the liposome layer (Fig. 2A). The percentage of incorporation decreased dramatically to 35% for **PIP₂-C12**. Only 12% and 9% of the probe was incorporated into liposome for **PIP₂-C9** and **PIP₂-C6**, respectively. These results demonstrated that only the **PIP₂-C15** probe with a long acyl side chain could be efficiently incorporated into membrane like structures, which is important for localization if these reporters are to be used in future cellular experiments.



Probe	FL-PIP ₂ -C15	FL-PIP ₂ -C12	FL-PIP ₂ -C9	FL-PIP ₂ -C6
in lipid layer (%)	91 ± 7	35 ± 19	12 ± 4	9 ± 3

Figure 2.3: In-vitro Membrane Association of Fluorescent PIP₂ Reporters: Probes were incubated with liposomes and under a gradient of sucrose. Following centrifugation the samples were visualized using a UV light source. The top liposome containing layer and bottom layer was isolated and total PIP₂ content was determined using CE separation.

2.2.4 Vesicle Based PI3K Analysis

To further assess whether **PIP₂-C15** functions as an effective reporter in the presence of endogenous substrate, the PI3K-catalyzed reaction was run on lipid vesicles, an environment that closely mimic cellular presentation of lipid substrates, in the presence or absence of endogenous PIP₂. Liposomes composed of a carrier lipid, phosphatidylserine (PS) which is the most common anionic lipid in the plasma membrane, **PIP₂-C15** and endogenous PIP₂ at different ratios, were formulated for enzymatic reactions [39, 89]. The total concentration of **PIP₂-C15** and endogenous PIP₂ was 10 μ M, which is close to that of the cellular environment and the conversion of **PIP₂-C15** to its corresponding PIP₃ product was then measured and shown in **Figure 2.4**. The rate of conversion decreased by approximately 27% when the ratio of **PIP₂-C15** to endogenous PIP₂ was 1:1, and approximately 50% when the ratio was 1:9,

compared to 100% **PIP₂-C15**. These results suggested that **PIP₂-C15** was a similar to endogenous substrate and can function as a reporter of PI3K activity.

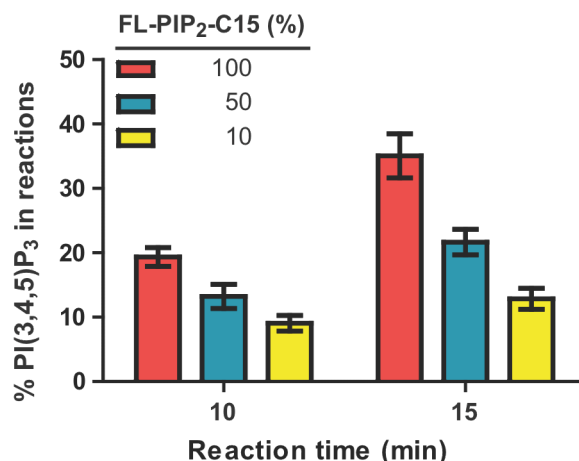


Figure 2.4: Competition with Endogenous PI(4,5)P₂ in Liposome Based Assay: Liposomes were formulated to contain 10 μ M total PI (4,5)P₂ using fluorescent C15 PI(4,5)P₂ derivative or endogenous PI(4,5)P₂ and 10 μ M of PS as a carrier lipid. Production of PI(3,4,5)P₃ was monitored to analyze the ability of the reporter to be metabolized in the presence of endogenous substrate.

2.2.5 Required Hydrophobicity for PI4K Substrate PtdIns

Like PI3K, PI4K catalyzes reactions at the lipid/water interface. Consequently, what was observed for PI3K likely applies to PI4K as well as other enzymes in the pathway. There is only one commercial fluorescent PI derivative, **BODIPY-PtdIns-C7** (Fig. 2.5A) with a short acyl side chain. We thus designed **BODIPY-PtdIns-C15** with a longer acyl side chain to assess its capacity as PI4K substrate. Next, both **BODIPY-PtdIns-C15** were **BODIPY-PtdIns-C7** tested as substrates of PI4KII α under soluble assay conditions. Consistent with what we observed with fluorescent PIP₂ derivatives, the PI(4)P product of the fluorescent PI with a longer acyl side chain **BODIPY-PtdIns-C15** was efficiently generated shown in . In contrast, no detectable amount of product was formed for **BODIPY-PtdIns-C7** containing a shorter acyl side chain shown in

Figure 2.5B. Likewise, over 99% of **BODIPY-PtdIns-C15** (not detectable in the aqueous layer) but only approximately 15% of **BODIPY-PtdIns-C7** participated into the lipid layer in the *in vitro* membrane association assay as seen in **Figure 2.5C**.

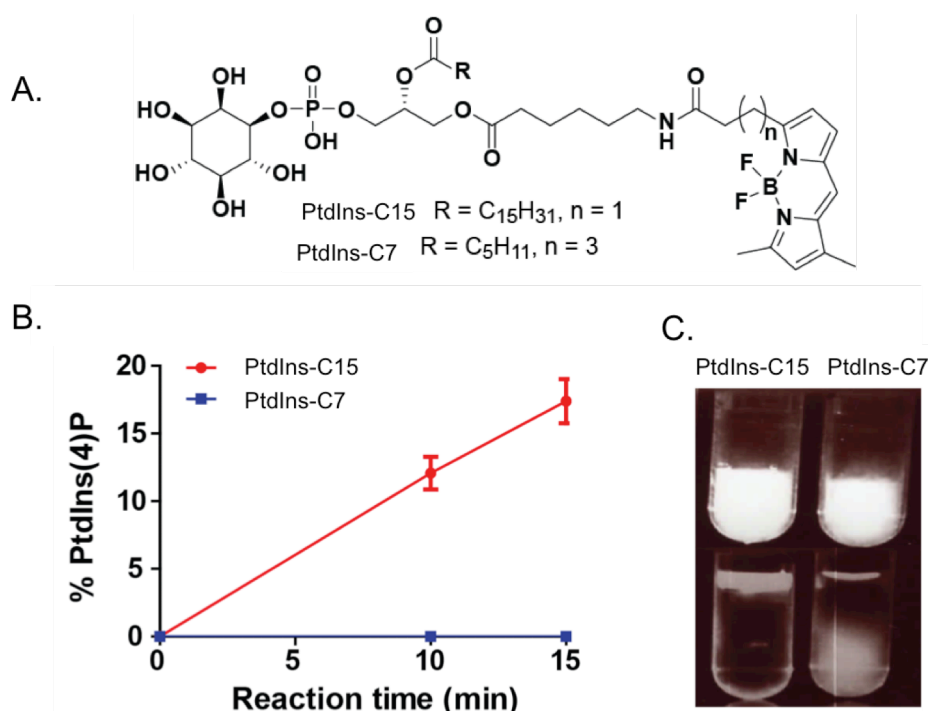
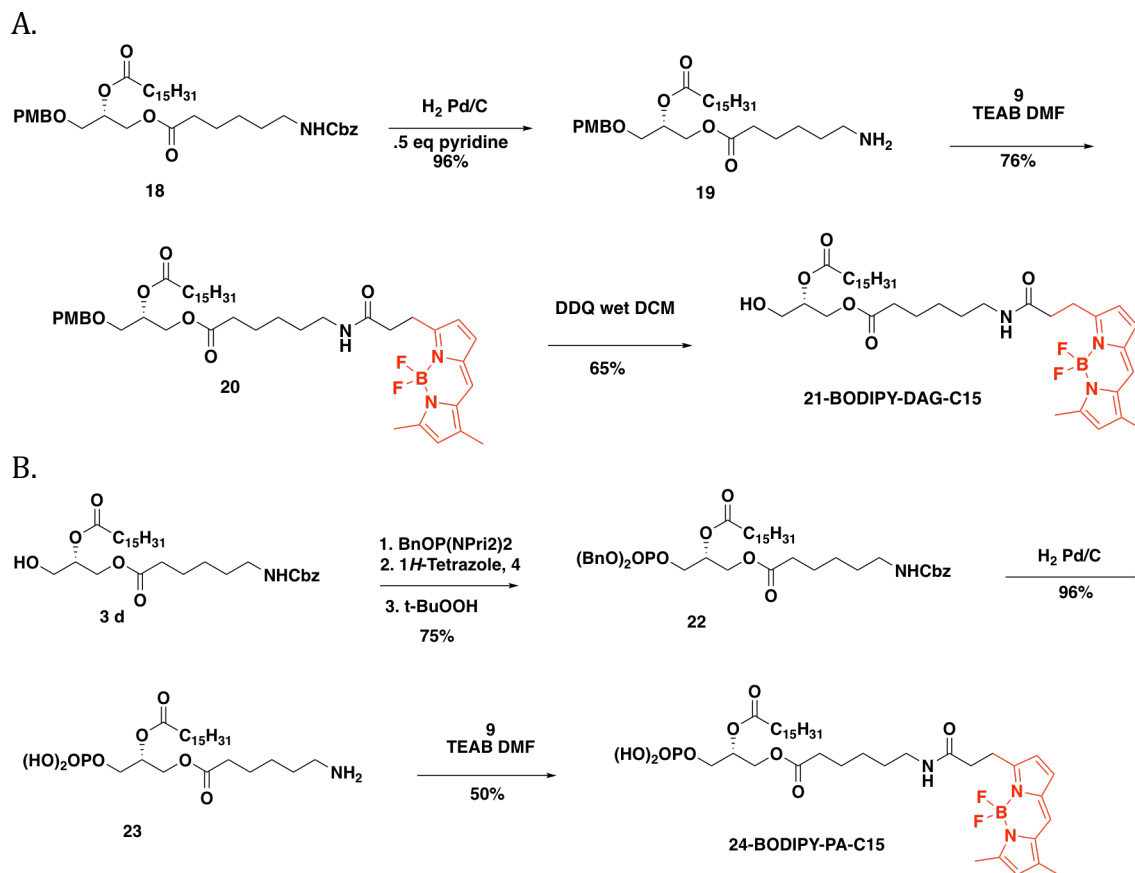


Figure 2.5: Biophysical and Kinetic Analysis of Fluorescent PtdIns Analogs: **A.** Chemical structures of fluorescent PtdIns derivatives. **B.** Mixed micelle PI4K assay with fluorescent PtdIns derivatives monitoring production of PtdIns(4)P. **C.** Representative images of fluorescent PtdIns derivatives interacting with liposome with fluorescent PtdIns quantified by CE separation.

2.2.6 Synthesis of BODIPY-DAG-C15 and BODIPY-PA-C15

With the goal of using these reporters for future cellular studies, multiple lipid metabolites of the PIP pathway for were also synthesized as standards for metabolite identification. **BODIPY-DAG-C15** and **BODIPY-PA-C15** were synthesized to contain the C15 acyl chain to be used as standards for CE and TLC analysis of cellular experiments as well as chemical reporters. In addition to the C15 alkyl chain, the

metabolites were synthesized also contain the same N-caproic acid tagged with a BODIPY fluorophore was kept constant to ensure the standards will chemically match the metabolites produced from our reporter in cellular experiments. When synthesizing fluorescent DAG, great care must be taken to avoid acyl migration from the secondary sn-2 position to the primary sn-3 position of DAG. If the primary hydroxyl is free under hydrogenolysis and basic conditions the side chain will migrate. To alleviate this, the hydroxyl was left protected with a PMB group until the final deprotection with DDQ. Under these conditions acyl migration does not occur as judged by NMR analysis of products from each synthetic step. Briefly, the Cbz group is selectively deprotected via hydrogenolysis in the presence of pyridine leaving the PMB group intact [90, 91]. Addition of BODIPY via the corresponding NHS ester followed by DDQ oxidation of the PMB protecting group resulted in final fluorescent DAG (**Scheme 2.3A**). Fluorescent PA was synthesized in a scheme similar to PIP₂ and PtdIns synthesis because the hydroxyl is phosphorylated in acidic conditions there is much less concern for acyl migrations. Briefly, compound **3d** was phosphorylated using commercial phosphoramidite as previously described. Hydrogenolysis of the Cbz and Bn protecting groups and subsequent addition of NHS-BODIPY resulted in pure fluorescent PA (**Scheme 2.3B**).



Scheme 2.3: Synthesis of PIP Metabolites. **A.** Synthetic scheme for the synthesis of fluorescent diacylglycerol (DAG). **B.** Synthetic scheme for the synthesis of fluorescent phosphatidic acid (PA)

2.3 Conclusions and Future Directions

In summary, we have synthesized a series of fluorescent PIP₂ derivatives with varied levels of hydrophobicity and investigated their capacity as PI3K substrates. The probe with a longer acyl side chain functions as a better substrate for PI3K and has a higher affinity with liposome compared to that with a shorter acyl side chain. Strikingly, when the side chain is sufficiently short and thereby has low hydrophobicity, the fluorescent PIP₂ is no longer an effective PI3K substrate to generate detectable amount

of enzymatic product, highlighting the required hydrophobicity of fluorescent PIP₂ derivatives. Likewise, the fluorescent PtdIns derivative with a long acyl side chain functions as an effective PI4K substrate, while that with a short acyl side chain does not generate detectable amount of enzymatic product. These results suggest that the required hydrophobicity of a fluorescent probe, which can be assessed through its interaction with liposomes, is likely essential for phosphatidylinositide metabolic enzymes.

PIP₂-C15 has shown similar properties as the endogenous PIP₂ in regard to CMC, kinetic parameters and tendency for membrane association. Unlike the endogenous PIP₂, **PIP₂-C15** is easy to handle both in chemical synthesis and CE separation. Similarly, **BODIPY-PtdIns-C15** has also been efficiently synthesized and separated from its enzymatic products. These results demonstrate that fluorescent **PIP₂-C15** and **PtdIns-C15** may strike the right balance between required hydrophobicity and practical handling during chemical synthesis and separation. Consequently, they are likely effective fluorescent probes that can be used to profile metabolism of PIPs when coupled with CE separation. Likewise, fluorescent **PI**, **DAG** and **PA** will serve as valuable standards for analyzing PI metabolism as well as serve as functional tools for dissecting distinct nodes of the PI metabolic pathway. When coupled with an effective cellular delivery method, and CE separation, we predict these reporters will be capable of monitoring changes in dynamic PI metabolism.

With the ultimate goal of the work being cellular analysis of PIs, the cellular efficacy of the lipid reporters must be confirmed using an effective delivery method and analysis for metabolic distribution of metabolites. Ideally, our system will mimic closely

what has been previously described using radiolabeled substrates, though with increased sensitivity for minor metabolites. Despite our best efforts at analyzing membrane association via a liposomal flotation experiment, it is still possible we will see non-specific and cytosolic localization of our lipid reporters. Therefore, it may be beneficial to further increase the hydrophobicity at the sn-2 position of the PI reporters. One such modification would be the addition of stearic, nonadecylic, or arachidic acids at this position to further increase hydrophobicity and better mimic the endogenous substrate. Likewise, removal of the fluorophore for an alkyne tag on all substrates would make the reporters more suitable for cellular delivery and could lend well to future analytical platforms of single cell analysis. Further, the fluorophores of various PI metabolites could be altered to allow multiple pools of metabolites to be tracked distinctly by using dual fluorophores with unique and non-overlapping excitation wavelengths.

2.4 Experimental

PIP₂-C12 and related intermediates were synthesized and characterized by Dr. Weigang Huang. Purified PI3K1 α enzyme was purchased from Invitrogen-Life Technologies. Purified PI4K1 α was purchased from Creative Biomart. Dynamic light scattering data were recorded on a Wyatt DynaPro dynamic light scattering plate reader. Endogenous PI(4,5)P₂ (brain, porcine) was purchased from Avanti Polar Lipids. PtdIns-C7 was purchased from Echelon Biosciences and confirmed via ES-HRMS (Appendix). ATP and TLC plates with silica gel 60 were purchased from Sigma. All solvents were purchased from Fischer Scientific. NMR analysis was done on an Inova 400 MHz spectrometer in the indicated solvent- spectra are available in the Appendix. All compounds were further confirmed by ESI mass spectrometry.

2.4.1 Soluble PI3K Assay Conditions

Fluorescent PIP₂ derivatives were added to assay buffer composed of MOPS (50 mM, pH 6.7), NaCl (100 mM), MgCl₂ (10 mM), sodium cholate (0.5 mM), DTT (1 mM), followed by the addition of ATP (2 mM). The reaction was initiated by the addition of purified PI3K α enzyme to a final concentration of 1.2 ng/ μ L or 2.4 ng/ μ L and incubated at 37 °C. At the indicated time point, an aliquot of the reaction was removed and diluted to 0.2 μ M in CHCl₃/MeOH (1:1) for analysis. All assays were performed in duplicate 3 times.

2.4.2 Soluble PI4K Assay Conditions

Fluorescent PtdIns derivatives were added to assay buffer composed of MOPS (50 mM, pH 6.7), NaCl (100 mM), MgCl₂ (10 mM), sodium cholate (0.5 mM), DTT (1 mM), followed by the addition of ATP (2 mM). The reaction was initiated by the addition of purified PI4KII α enzyme to a final concentration of 1.0 ng/ μ L and incubated at 37 °C. At the indicated time point, an aliquot of the reaction was removed and diluted to 0.2 μ M in CHCl₃/MeOH (1:1) for analysis. All assays were performed in duplicate for 3 times.

2.4.3 Vesicle Based PI3K Assay Conditions

Liposomes were prepared to contain 10 μ M total PIP₂ composed of PIP₂-C15 and endogenous substrate with 10 μ M phosphatidylserine (PS) as a carrier lipid in final assay conditions. Lipid stocks in CHCl₃ or water were added to a 1:1 MeOH/H₂O mixture followed by solvent removal by speed-vac and drying under vacuum for at least 1 h. The lipids were then re-suspended in 5X MOPS (250 mM, pH 6.7) and 5X NaCl (500 mM) followed by sonication in a bath for 5 min to form lipid vesicles. The vesicles were then used to prepare a mixture containing a final PtdIns(4,5)P₂ concentration of 10 μ M in MOPS (50 mM, pH 6.7), NaCl (100 mM), DTT (1 mM), MgCl₂ (10 mM) and ATP

(2 mM). The reaction was initiated by adding purified PI3K enzyme (0.6 ng/ μ L) and then incubated at 37 °C. At the indicated time point, an aliquot of the reaction mixture was removed and diluted to 0.2 μ M in 1:1 $\text{CHCl}_3/\text{MeOH}$ for TLC analysis. In the case of the 10% $\text{PIP}_2\text{-C15}$ liposome, the reaction was first stopped by the addition to methanol, followed by concentration and addition of $\text{CHCl}_3/\text{MeOH}$ to achieve the desired concentration of 0.2 μ M FL-PtdIns(4,5) P_2 substrate as direct dilution results in phase separation. All experiments were performed using a single batch of liposome in duplicate for three times.

2.4.4 TLC Analysis of Fluorescent Lipid Metabolites

TLC plates (Merck, Silica Gel-60) were pre-treated with a solution of 1.2% potassium oxalate and 1.2 mM EGTA in MeOH/water ($v:v = 2:3$) and heated at 110 °C for 20 min before use. Reaction mixture was diluted in $\text{CHCl}_3/\text{MeOH}$ ($v:v = 1:1$) and spotted on a TLC plate directly. The TLC plate was then developed in $\text{CHCl}_3\text{:Acetone:MeOH:AcOH:water}$ ($v:v:v:v:v = 80:30:26:24:14$) and scanned on a Typhoon 9400 Variable Mode Imager ($\lambda_{\text{ex}}/\lambda_{\text{em}} = 488 \text{ nm}/520 \text{ nm}$). The fluorescence intensity of various spots on the TLC plate was quantified with ImageQuant software (V.5.0).

2.4.5 CE Analysis of Fluorescent Lipid Metabolites

Capillary electrophoresis coupled with laser induced fluorescence detection (CE-LIF, 488 nm excitation) was performed on a custom-built system mounted to the stage of an inverted microscope, described previously in detail[75]. Fused silica capillaries were 38 cm long with a 20.5 cm effective length [30 μ m inner diameter and 360 μ m outer diameter (Polymicro Technologies; Phoenix, AZ)] and were conditioned prior to use by rinsing for 1 h in DI H_2O , 12 h in 0.1 M NaOH, 1 h in DI H_2O , 6 h in 0.1 M HCl, and 12 h

in DI H₂O. Prior to each run, capillaries were rinsed with 1 M NaOH and DI H₂O for 5 min each and with electrophoretic buffer for 10 min by application of pressure to the capillary outlet. Buffer at the capillary inlet and outlet was completely refreshed prior to each electrophoretic run. The composition of the electrophoretic buffer was 80 mM NaH₂PO₄, pH 6.8 containing 15% 2-propanol and a field strength of 210 V cm⁻¹ was used for all separations. Internal standards and samples were hydrodynamically loaded by raising the inlet 3 cm relative to the outlet and holding the capillary inlet in the sample for 10 sec. The inlet was then lowered to the height of the outlet and electrophoresis was initiated by application of a negative voltage to the outlet while grounding the inlet. Electropherograms were plotted and analyzed utilizing OriginLab 9.0 (OriginLab Corporation; Northampton, MA).

2.4.6 Fluorescent lipids/liposome interaction

The liposome mixture was prepared from stock solutions of lipids in CHCl₃ for a final composition of 45% PC, 25% PE, 15% cholesterol, 10% PI, and 5% PS. The solvent was blown off under a stream of N₂ followed by drying under vacuum for at least 1 h. The lipid film was then suspended in buffer composed of MOPS (50 mM, pH 6.7), NaCl (100 mM), DTT (1 mM), and MgCl₂ (10 mM) to a concentration of 2 mM. Liposomes were extruded through a 0.03 µm pore size polycarbonate filter membrane for at least 11 times back and forth. Fluorescent PIP₂ or PI (10 µM) and liposomes (1 mM) were incubated in buffer at room temperature for 5 min in a total volume of 150 µL. The suspension was adjusted to 30% sucrose by the addition of 100 µL of 75% w/v sucrose in buffer followed by mixing. Buffer (200 µL) containing 25% w/v sucrose was then overlaid on the high-sucrose suspension followed by 50 µL of buffer containing no sucrose. The sample was centrifuged at 55,000 r.p.m in a Beckman swing rotor (TLS

55) for 1 h at 4 °C. The bottom 350 μ L and top 150 μ L were manually collected using a syringe and analyzed for fluorescent PI or PIP₂ content by both TLC and CE. A fluorescence image of the tubes was also taken prior and following centrifugation using a UV light source below the samples and a CCD camera.

2.4.7 Chemical Synthesis

Synthesis of (S)-1-((6-(((benzyloxy)carbonyl)amino)hexanoyl)oxy)-3-hydroxypropan-2-yl palmitate 3d A mixture of compound **2** (350 mg, 0.76 mmol), **1d** (234.5 mg, 0.91 mmol), DCC (189 mg, 0.91 mmol), and DMAP (51 mg, 0.42 mmol) in anhydrous CH₂Cl₂ (6 mL) was stirred at room temperature overnight. The reaction mixture was concentrated and purified by flash chromatography (hexane-ethyl acetate = 2:1) over silica (407 mg, 89%). The so-formed intermediate (407 mg, 0.58 mmol) was dissolved in wet CH₂Cl₂ (20 mL) followed by addition of DDQ (278 mg, 1.2 mmol) and the mixture was stirred at room temperature for 4 h. The reaction mixture was then by washed with 10% NaHCO₃ and saturated NaCl, dried over MgSO₄, and concentrated under vacuum. The residue was then purified by flash chromatography (hexane-ethyl acetate =2:1) over silica to generate **3d** (281 mg, 83%) as a colorless oil. ¹H NMR (400 MHz, CDCl₃) δ 7.26-7.38 (m, 5H), 5.06-5.11 (m, 3H), 4.83 (brs, 1H), 4.33 (dd, J = 11.9, 4.5 Hz, 1H), 4.21 (dd, J = 11.9, 5.7 Hz, 1H), 3.72 (d, J = 4.9 Hz, 1H), 3.19 (q, J = 13.1, 6.7 Hz, 1H), 2.24-2.30 (m, 4H), 1.58-1.68 (m, 4H), 1.48-1.55(m, 2H), 1.25-1.38 (m, 26H), 0.88 (t, J = 6.9 Hz, 3H). ¹³C NMR (101 MHz, CDCl₃) δ 173.55, 156.58, 136.71, 128.63, 128.21, 72.20, 72.12, 66.75, 62.30, 61.55, 40.94, 34.40, 33.99, 32.04, 29.82, 29.78, 29.74, 29.60, 29.48, 29.39, 29.21. 26.23, 25.05, 24.55, 22.81, 14.24. ESMS 577.8 [M]⁺

Synthesis of (S)-1-((6-(((benzyloxy)carbonyl)amino)hexanoyl)oxy)-3-hydroxypropan-2-yl tridecanoate (3c) Compound **3c** (80 mg, 75%). was prepared in a similar manner to compound **3d**. ¹H NMR (CDCl₃, 400 MHz) δ 7.26-7.36 (m, 5H), 5.02-5.15 (m, 3H), 4.96 (brs, 1H), 4.32 (dd, *J* = 11.9, 4.3 Hz, 1H), 4.18 (dd, *J* = 11.9, 5.9 Hz, 1H), 3.69 (d, *J* = 5.2 Hz, 2H), 3.16 (q, *J* = 6.5 Hz, 2H), 2.26-2.36 (m, 4H), 1.43-1.66 (m, 6H), 1.18-1.40 (m, 20H), 0.86 (t, *J* = 7.1 Hz, 3H); ¹³C NMR (CDCl₃, 101 MHz) δ 173.41, 173.37, 156.47, 136.57, 128.45, 128.03, 72.00, 66.56, 62.25, 61.27, 40.77, 34.24, 33.82, 31.87, 29.61, 29.59, 29.57, 29.54, 29.30, 29.23, 29.05, 26.07, 24.89, 24.39, 22.64, 14.08. ESMS 535.7 [M]⁺

Synthesis of (S)-1-((6-(((benzyloxy)carbonyl)amino)hexanoyl)oxy)-3-hydroxypropan-2-yl decanoate (3b) Compound **3b** (170 mg, 89%) was prepared in a similar manner to compound **3d** as a colorless oil. ¹H NMR (400 MHz, CDCl₃) δ 7.26-7.38 (m, 5H), 5.05-5.12 (m, 3H), 4.99 (brs, 1H) 4.33 (dd, *J* = 11.9, 4.2 Hz, 1H), 4.19 (dd, *J* = 11.9, 5.9 Hz, 1H), 3.70 (d, *J* = 5.1 Hz, 1H), 3.18 (q, *J* = 13.0, 6.5 Hz, 1H), 2.25-2.30 (m, 4H), 1.46-1.56 (m, 6H), 1.20-1.39 (m, 14H), 0.88 (t, *J* = 6.8 Hz, 3H). ¹³C NMR (101 MHz, cdcl₃) δ 173.11, 173.06, 159.29, 156.39, 136.65, 129.73, 129.28, 128.46, 128.04, 128.02, 114.50, 113.79, 77.40, 77.08, 76.77, 72.92, 70.00, 67.86, 66.52, 62.81, 62.58, 55.22, 55.11, 49.02, 40.81, 34.30, 34.08, 33.90, 33.84, 31.84, 29.67, 29.57, 29.41, 29.25, 29.05, 26.13, 25.62, 24.93, 24.39, 22.64, 14.09. ESMS 493.2 [M]⁺

Synthesis of (S)-1-((6-(((benzyloxy)carbonyl)amino)hexanoyl)oxy)-3-hydroxypropan-2-yl heptanoate (3a). Compound **3a** was prepared in a similar manner

to compound **3d** (336 mg, 0.73 mmol, 96%) as a colorless oil. ^1H NMR (400 MHz, CDCl_3) δ 7.26-7.38 (m, 5H), 5.02-5.20 (m, 3H), 4.95 (brs, 1H), δ 4.33 (dd, J = 11.9, 4.3 Hz, 1H), 4.20 (dd, J = 11.9, 5.8 Hz, 1H), 3.71 (d, J = 5.1 Hz, 2H), 3.18 (q, J = 6.5 Hz, 2H), 2.25-2.38 (m, 4H), 1.40-1.75 (m, 6H), 1.19-1.40 (m, 8H), 0.88 (t, J = 6.8 Hz, 3H). ^{13}C NMR (101 MHz, CDCl_3) δ 173.12, 173.06, 159.29, 156.38, 154.12, 136.62, 129.73, 129.28, 128.47, 128.06, 128.04, 113.80, 77.35, 77.03, 76.72, 72.93, 70.14, 69.99, 67.86, 66.55, 62.82, 62.59, 55.24, 49.65, 49.18, 40.81, 35.93, 34.30, 33.84, 32.74, 31.57, 31.42, 30.90, 29.67, 29.58, 28.93, 28.77, 28.70, 26.38, 26.13, 25.58, 25.50, 25.42, 25.32, 24.88, 24.80, 24.70, 24.39, 22.47, 22.45, 14.01. ESMS 451.3 $[\text{M}]^+$

Synthesis of tetrabenzyl ((1*R*,2*R*,3*S*,4*R*,5*S*,6*S*)-4-hydroxy-3,5,6-tris(methoxymethoxy)cyclohexane-1,2-diyl) bis(phosphate) (4). **4** was synthesized as previously described from *myo*-inositol [81]. ^1H NMR (400 MHz, CDCl_3) δ 7.40 – 7.19 (m, 19H), 5.15 – 4.87 (m, 11H), 4.84 (dd, J = 6.7, 0.9 Hz, 1H), 4.74 (dd, J = 6.6, 0.9 Hz, 1H), 4.57 (dd, J = 7.1, 0.9 Hz, 1H), 4.53 – 4.34 (m, 4H), 4.16 – 4.12 (m, 1H), 3.74 (t, J = 9.3 Hz, 1H), 3.64 – 3.54 (m, 1H), 3.50 – 3.44 (m, 1H), 3.42 – 3.39 (m, 3H), 3.30 – 3.28 (m, 3H), 3.28 – 3.26 (m, 3H). ^{13}C NMR (101 MHz, CDCl_3) δ 136.07, 136.04, 136.00, 135.96, 135.93, 135.86, 128.51, 128.51, 128.49, 128.45, 128.41, 128.38, 128.32, 128.27, 128.23, 128.15, 128.05, 128.00, 127.97, 127.89, 127.85, 127.77, 127.72, 99.00, 97.65, 96.82, 83.27, 79.37, 79.32, 79.30, 79.26, 77.99, 77.94, 77.88, 77.48, 77.36, 77.16, 76.84, 75.60, 75.09, 75.07, 75.05, 70.41, 69.58, 69.52, 69.49, 69.43, 69.24, 69.19, 69.10, 69.01, 55.98, 55.78, 55.65, 55.55, 29.88, 29.85, 29.83, 29.81, 29.79. ^{31}P NMR (162 MHz, CDCl_3) δ -1.37 (1P), -1.69 (1P). ESMS 832.3 $[\text{M}]^+$

Synthesis of (2R)-1-(((benzyloxy)(((1R,2S,3R,4R,5S,6R)-3,4-bis((bis(benzyloxy)phosphoryl)oxy)-2,5,6-tris(methoxymethoxy)cyclohexyl)oxy)phosphoryl)oxy)-3-((6-(((benzyloxy)carbonyl)amino)hexanoyl)oxy)propan-2-yl palmitate (5d).

A solution of **3d** (100 mg, 0.17 mmol) in anhydrous CH₂Cl₂ (1 mL) was added drop-wise under argon to a flask that contained 1-(benzyloxy)-*N,N,N',N'*-tetraisopropylphosphodiamine (360 mg, 0.43 mmol) and 1*H*-tetrazole (170 mg, 0.19 mmol) in anhydrous CH₂Cl₂ (2 mL). The mixture was stirred at room temperature for 2 h and concentrated under vacuum. The resulting residue was purified by column chromatography (hexane:ethyl acetate:triethylamine = 100:20:3) to give a phosphoramidite intermediate as a colorless oil. The so-formed phosphoramidite (125 mg, 0.15 mmol) in anhydrous CH₂Cl₂ (1.5 mL) was added to a solution of **4** (102mg, 0.12 mmol) and 1*H*-tetrazole (82 mg, 0.30 mmol) in anhydrous CH₂Cl₂ (1.5 mL) under argon. The reaction mixture was stirred at room temperature overnight, followed by the addition of *t*-BuOOH (5.5 M, 138 μ L) at -40°C. The reaction was allowed to come to room temperature and stirred for 1 h followed by removal of solvents under vacuum and purified by flash chromatography (2:1 Hex:Acetone) to yield 85 mg of pure product and impure fractions. The impure fractions were then purified by HPLC (BETASIL C18 150 X 21.2 mm water-acetonitrile 30 to 100% over 20 minutes 10 mL/min) to yield pure compound **5d** (150 mg total, 70% combined from compound **3d**) as a clear viscous oil. ¹H NMR (400 MHz, CDCl₃) δ 7.38-7.26 (m, 30H), 4.80-5.21 (m, 14H), 4.80-4.60 (m, 4H), 4.55 (d, *J* = 6.1 Hz, 1H), 4.05-4.49 (m, 9H), 3.53 (dd, *J* = 9.9, 10.1 Hz, 1H), 3.39 (conformation 1) and 3.36 (conformation 2) (s, 3H), 3.32 (conformation 1) and 3.28

(conformation 2) (s, 3H), 3.24 (conformation 1) and 3.23 (conformation 2) (s, 3H), 3.17 (q, J = 6.4 Hz, 2H), 2.24-2.30 (m, 4H), 1.48-1.68 (m, 6H), 1.25-1.38 (m, 26H), 0.88 (t, J = 6.7 Hz, 3H). ^{13}C NMR (101 MHz, CDCl_3) δ 173, 172.94, and 172.89 (1C), 156.55, 136.80, 136.22, 136.17, 136.16, 136.09, 136.04, 135.64, 135.57, 128.83, 128.58, 128.53, 128.15, 128.03, 98.96, 98.90, 97.66, 97.04, 78.91, 76.52, 75.90, 74.69, 69.68, 69.62, 69.57, 69.52, 69.37, 69.32, 66.65, 66.55, 65.72, 65.54, 61.67, 56.80 and 56.74 and 56.68 (1C), 56.02 and 55.93 (1C), 40.94, 34.18 and 33.84 (1C), 32.04, 29.81, 29.61, 29.47, 29.41, 29.21, 26.27, 24.91, 24.49, 22.80, 14.24. ^{31}P NMR (CDCl_3 , 162 MHz) δ -1.31 (2P), -1.65 and -1.70 (1P) ESMS 1561.7 $[\text{M}]^+$

Synthesis of (2R)-1-(((benzyloxy)(((1R,2S,3R,4R,5S,6R)-3,4-bis((bis(benzyloxy)phosphoryl)oxy)-2,5,6-tris(methoxymethoxy)cyclohexyl)oxy)phosphoryl)oxy)-3-((6-(((benzyloxy)carbonyl)amino)hexanoyl)oxy)propan-2-yl tridecanoate (5c)

Compound **5c** (138 mg, 61%) was prepared in a similar manner to compound **5d** from **3c** (80 mg, 0.15 mmol) as a colorless oil. ^1H NMR (CDCl_3 , 400 MHz) δ 7.18-7.40 (m, 30 H), 4.80-5.22 (m, 14 H), 4.56-4.80 (m, 4H), 4.53 (d, J = 7.0 Hz, 1H), 4.02-4.46 (m, 9H), 3.53 (dd, J = 10.0, 10.2 Hz, 1H), 3.37 (conformation 1) and 3.34 (conformation 2) (s, 3H), 3.31 (conformation 1) and 3.27 (conformation 2) (s, 3H), 3.22 (s, 3H), 3.15 (q, J = 6.3 Hz, 2H), 2.20-2.32 (m, 4H), 1.10-1.66 (m, 26H), 0.86 (t, J = 7.0 Hz, 3H); ^{13}C NMR (CDCl_3 , 101 MHz) δ 172.83, 172.77 and 172.72 (1C), 156.41, 136.66, 136.07, 135.95, 135.82, 135.57, 135.50, 135.43, 128.67, 128.43, 128.37, 128.28, 128.24, 128.18, 128.00, 127.88, 98.81, 98.74, 97.61, 97.51, 97.42, 96.88, 78.76, 77.37, 77.24, 77.06, 76.74, 76.35, 75.78, 74.53, 69.86, 69.81, 69.71, 69.64, 69.59, 69.53, 69.47, 69.42,

69.36, 69.26, 69.21, 69.16, 66.48, 65.43, 61.52, 56.65 and 56.59 and 56.53 (1C), 55.85 and 55.80 (1C), 55.76 and 55.69 (1C), 40.79, 34.03 and 33.69 (1C), 33.42, 31.89, 29.66, 29.61, 29.60, 29.56, 29.45, 29.36, 29.32, 29.25, 29.05, 26.12, 24.76, 24.34, 23.16, 22.65, 14.09; ^{31}P NMR (CDCl_3 , 162 MHz) δ -1.37 (2P), -1.73 (1P). ESMS 1519.6 $[\text{M}]^+$

Synthesis of (2R)-1-(((benzyloxy)(((1R,2S,3R,4R,5S,6R)-3,4-bis((bis(benzyloxy)phosphoryl)oxy)-2,5,6-

tris(methoxymethoxy)cyclohexyl)oxy)phosphoryl)oxy)-3-((6-

(((benzyloxy)carbonyl)amino)hexanoyl)oxy)propan-2-yl decanoate (5b) Compound

5b (55 mg, 30% combined from **3b**) was prepared in a similar manner to **compound 5d** from **3b** (77 mg, 0.16 mmol) as a colorless oil. ^1H NMR (400 MHz, CDCl_3) δ 7.38-7.26 (m, 30H), 4.81-5.21 (m, 14H), 4.60-4.79 (m, 4H), 4.55 (d, J = 6.1 Hz, 1H), 4.00-4.50 (m, 9H), 3.50-3.58 (m 1H), 3.39 (conformation 1) and 3.36 (conformation 2) (s, 3H), 3.32 (conformation 1) and 3.28 (conformation 2) (s, 3H), 3.24 (conformation 1) and 3.23 (conformation 2) (s, 3H), 3.18 (q, J = 6.5 Hz, 2H), 2.18-2.34 (m, 4H), 1.40-1.70 (m, 6H), 1.17-1.39 (m, 14H), 0.87 (t, J = 6.8 Hz, 3H). ^{31}P NMR (CDCl_3 , 162 MHz) δ -1.31 (2P), -1.66 and -1.71 (1P). ^{13}C NMR (101 MHz, CDCl_3) δ 172.82, 172.77, 172.72, 156.39, 136.67, 136.13, 136.09, 136.05, 136.03, 136.01, 135.96, 135.91, 135.83, 135.58, 135.51, 128.70, 128.67, 128.45, 128.43, 128.38, 128.35, 128.29, 128.24, 128.19, 128.04, 128.00, 127.98, 127.93, 127.88, 98.81, 98.75, 97.52, 96.87, 77.34, 77.23, 77.02, 76.71, 74.53, 69.85, 69.80, 69.71, 69.64, 69.58, 69.53, 69.47, 69.41, 69.36, 69.28, 69.25, 69.21, 69.16, 66.49, 65.62, 65.38, 61.53, 56.62, 56.57, 55.85, 55.83,

55.74, 40.80, 34.04, 34.02, 33.70, 31.82, 29.66, 29.57, 29.39, 29.23, 29.04, 26.13, 24.75, 24.35, 22.63, 14.08. ESMS 1477.5 [M]⁺

Synthesis of (2*R*)-1-(((benzyloxy)(((1*R*,2*S*,3*R*,4*R*,5*S*,6*R*)-3,4-bis((bis(benzyloxy)phosphoryl)oxy)-2,5,6-

tris(methoxymethoxy)cyclohexyl)oxy)phosphoryl)oxy)-3-((6-

(((benzyloxy)carbonyl)amino)hexanoyl)oxy)propan-2-yl heptanoate (5a) Compound

5a (20 mg, 20% combined from **3b**) was prepared in a similar manner to compound **5d** from **3a** (80 mg, 0.18 mmol) as a colorless oil. ¹H NMR (400 MHz, CDCl₃) δ 7.38-7.20 (m, 30H), 4.80-5.20 (m, 14H), 4.60-4.79 (m, 4H), 4.54 (d, *J* = 7.0 Hz, 1H), 3.99-4.50 (m, 9H), 3.55 (t, *J* = 9.9, 10.0 Hz, 1H), 3.39 (conformation 1) and 3.36 (conformation 2) (s, 3H), 3.32 (conformation 1) and 3.28 (conformation 2) (s, 3H), 3.24 (conformation 1) and 3.23 (conformation 2) (s, 3H), 3.18 (q, *J* = 6.5 Hz, 2H), 2.20-2.35 (m, 4H), 1.37-1.81 (m, 6H), 1.21-1.36 (m, 8H), 0.87 (t, *J* = 6.8 Hz, 3H). ¹³C NMR (101 MHz, CDCl₃) δ 172.83, 172.77, 172.72, 156.39, 136.12, 136.02, 135.95, 135.82, 128.71, 128.68, 128.66, 128.45, 128.43, 128.38, 128.34, 128.29, 128.24, 128.19, 128.04, 128.00, 127.98, 127.93, 127.88, 98.81, 98.75, 97.51, 96.87, 77.32, 77.00, 76.68, 74.53, 69.86, 69.80, 69.71, 69.64, 69.52, 69.47, 69.41, 69.36, 69.21, 69.16, 66.51, 61.54, 56.62, 56.56, 55.85, 55.83, 55.74, 40.80, 34.03, 34.01, 33.69, 31.89, 31.38, 30.89, 29.66, 29.57, 28.67, 26.13, 24.70, 24.34, 22.42, 13.99. ³¹P NMR (CDCl₃, 162 MHz) δ -1.32 (2P), -1.67 and -1.72 (1P) ESMS 1435.5 [M]⁺

Synthesis of (2*R*)-1-((6-aminohexanoyl)oxy)-3-((hydroxy(((1*R*,2*R*,3*S*,4*R*,5*R*,6*S*)-2,3,6-trihydroxy-4,5-bis(phosphonooxy)cyclohexyl)oxy)phosphoryl)oxy)propan-2-yl palmitate (6d) To a solution of compound **5d** (6 mg, 4 μ mol) in MeOH (3 mL) was added 10% Pd/C (10 mg). The mixture was stirred overnight under a balloon of H₂ at room temperature. The reaction mixture was filtered and concentrated under vacuum. The residue was dried under vacuum for 1 h upon which the residue was dissolved in anhydrous CH₂Cl₂ (0.5 mL) and freshly distilled TMSBr (0.5 mL) was added at 0 °C under argon. The mixture was stirred at room temperature for 1 h followed by removal of solvents under vacuum. The resulting residue was then dissolved in MeOH (3 mL) and stirred for 1 h followed by removal of solvent to yield **6d** (3.3 mg, 100%) as a clear oil. ¹H NMR (400 MHz, CD₃OD) δ 5.24-5.27 (m, 1H), 4.50 (dd, *J* = 18.4, 6.3 Hz, 1H), 4.42 (dd, *J* = 11.9, 4.2 Hz, 1H), 3.95-4.30 (m, 7H), 3.63-3.70 (m, 1H), 2.90-2.97 (m, 2H), 2.23-2.43 (m, 4H), 1.6-1.74 (m, 6H), 1.30-1.37 (m, 26H), 0.90 (t, *J* = 6.8 Hz, 3H). ³¹P NMR (CD₃OD, 162 MHz) 0.60 (1P), 0.28 (1P), -1.45 (1P). ESMS 846.4 [M+H]⁺

Synthesis of (2*R*)-1-((6-aminohexanoyl)oxy)-3-((hydroxy(((1*R*,2*R*,3*S*,4*R*,5*R*,6*S*)-2,3,6-trihydroxy-4,5-bis(phosphonooxy)cyclohexyl)oxy)phosphoryl)oxy)propan-2-yl tridecanoate (6c) Compound **6c** was prepared in a similar manner to compound **6d** (10 mg, 80%) as a colorless oil from **5c** (**25 mg, 0.16 mmol**). ¹H NMR (CD₃OD, 400 MHz) δ 5.23 (m, 1H), 4.48 (dd, *J* = 18.5, 6.3 Hz, 1H), 4.40 (dd, *J* = 11.9, 4.2 Hz, 1H), 4.04-4.28 (m, 6H), 3.97 (dd, *J* = 9.4, 9.3 Hz, 1H), 3.64 (m, 1H), 2.92 (t, *J* = 7.3 Hz, 2H), 2.3-2.42 (m, 4H), 1.54-1.74 (m, 4H), 1.20-1.50 (m, 22H), 0.88 (t, *J* = 7.1 Hz, 1H); ¹³C NMR (CD₃OD, 101 MHz) δ 173.14 (2C), 79.67, 78.49, 77.48, 70.93, 70.03, 69.84 and 69.76 (1C), 64.68, 61.62, 39.16, 33.56, 32.97, 31.63, 29.34, 29.31, 29.30, 29.18, 29.03,

28.99, 28.72, 26.77, 25.39, 24.52, 23.85, 22.28, 12.99; ^{31}P NMR (CD_3OD , 162 MHz) δ 0.64 (1P), 0.32 (1P), -1.33 (1P). ESMS 804.3 $[\text{M}+\text{H}]^+$

Synthesis of (2*R*)-1-((6-aminohexanoyl)oxy)-3-((hydroxy(((1*R*,2*R*,3*S*,4*R*,5*R*,6*S*)-2,3,6-trihydroxy-4,5-bis(phosphonooxy)cyclohexyl)oxy)phosphoryl)oxy)propan-2-yl decanoate (6b) Compound **6b** (6.2 mg, 100%) was prepared in a similar manner to compound **6d** from compound **5b** (11 mg, 7 μmol) as a colorless oil. ^1H NMR (400 MHz, CD_3OD) δ 5.20-5.31 (m, 1H), 4.51 (dd, J = 18.5, 6.3 Hz, 1H), 4.43 (dd, J = 11.9, 4.3 Hz, 1H), 3.90-4.23 (m, 7H), 3.65-3.68 (m, 1H), 2.90-3.00 (m, 2H), 2.28-2.50 (m, 4H), 1.42-1.74 (m, 6H), 1.25-1.39 (m, 14H), 0.91 (t, J = 6.7 Hz, 3H). ^{31}P NMR (CD_3OD , 162 MHz) δ 0.75 (1P), 0.40 (1P), -1.16 (1P). ESMS 761.3 $[\text{M}+\text{H}]^+$

Synthesis of (2*R*)-1-((6-aminohexanoyl)oxy)-3-((hydroxy(((1*R*,2*R*,3*S*,4*R*,5*R*,6*S*)-2,3,6-trihydroxy-4,5-bis(phosphonooxy)cyclohexyl)oxy)phosphoryl)oxy)propan-2-yl heptanoate (6a) Compound **6a** (1.9 mg, 100%) was prepared in a similar manner to compound **6d** from compound **5a** (3.9 mg, 3 μmol) as a colorless oil. ^1H NMR (400 MHz, CD_3OD) δ 5.22-5.31 (m, 1H), 4.47-4.57 (m, 1H), 4.42 (dd, J = 18.4, 6.3 Hz, 1H), 3.8-4.24 (m, 7H), 2.91-2.96 (m, 1H), 2.35-2.42 (m, 2H), 1.30-1.64 (m, 6H), 1.20-1.29 (m, 8H), 0.81 (t, J = 6.8 Hz, 3H). ^{31}P NMR (CD_3OD , 162 MHz) δ 0.59 (1P), 0.26 (1P), -1.48 (1P). ESMS 720.2 $[\text{M} + \text{H}]^+$

Synthesis of 4-((6-((2*R*)-3-((hydroxy(((1*R*,2*R*,3*S*,4*R*,5*R*,6*S*)-2,3,6-trihydroxy-4,5-bis(phosphonooxy)cyclohexyl)oxy)phosphoryl)oxy)-2-(palmitoyloxy)propoxy)-6-oxohexyl)carbamoyl)-2-(6-hydroxy-3-oxo-3*H*-xanthen-9-yl)benzoic acid (FI-PIP₂-C15) To a solution of compound **6d** (3.3 mg, 4 μmol) in TEAB buffer (0.5 M, 1.8 mL) was added a solution of NHS ester **7** (3.7 mg, 8 μmol) in DMF (1.85 mL). The reaction

was stirred in the dark at room temperature overnight before the solvents were removed under vacuum. Purification via HPLC (BETASIL C18 150 x 10 mm, a gradient starting with water and ending with 100% MeOH over 30 min with the flow rate at 5 mL/min) yielded **PIP₂-C15** as a red-orange solid (2.5 mg, 53% from compound **5a**). ¹H NMR (400 MHz, CD₃OD) δ 6.50-8.56 (m, 9H), 5.14-5.29 (m, 1H), 4.34-4.49 (m, 1H), 4.26-4.29 (m, 1H), 3.96- 4.26 (m, 6H), 3.62-3.67 (m, 1H), 3.48-3.51 (m, 2H), 2.24-2.41 (m, 4H), 1.49-1.70 (m, 6H), 1.21-1.34 (m, 26H), 0.90 (t, *J* = 6.3 Hz, 3H). ³¹P NMR (CD₃OD), 162 MHz) δ 2.45 (1P), 1.71 (1P), -0.55 (1P). ESI-HRMS for [M + H]⁺ calcd 1204.36, found 1204.3636

Synthesis of 4-((6-((2*R*)-3-((hydroxy(((1*R*,2*R*,3*S*,4*R*,5*R*,6*S*)-2,3,6-trihydroxy-4,5-bis(phosphonooxy)cyclohexyl)oxy)phosphoryl)oxy)-2-(tridecanoyloxy)propoxy)-6-oxohexyl)carbamoyl)-2-(6-hydroxy-3-oxo-3*H*-xanthen-9-yl)benzoic acid (FI-PIP₂-C12). FI-PIP₂-C12 was synthesized in a similar manner to **PIP₂-C15** as a red-orange solid (55%). ¹H NMR (CD₃OD, 400 MHz) δ 6.50-8.20 (m, 9H), 5.18-5.24 (m, 1H), 4.30-4.44 (m, 1H), 4.24 (m, 1H), 3.92-4.18 (m, 6H), 3.61 (m, 1H), 3.34 (m, 2H), 2.22-2.36 (m, 4H), 1.45-1.65 (m, 6H), 1.14-1.40 (m, 20H), 0.85 (t, *J* = 7.1 Hz, 3H); ³¹P NMR (CD₃OD, 162 MHz) δ 2.43 (1P), 1.70 (1P), -0.54 (1P); ESI-HRMS for [M + H]⁺ : calcd 1162.3215, found 1162.3195.

Synthesis of 4-((6-((2*R*)-2-(decanoyloxy)-3-((hydroxy(((1*R*,2*R*,3*S*,4*R*,5*R*,6*S*)-2,3,6-trihydroxy-4,5-bis(phosphonooxy)cyclohexyl)oxy)phosphoryl)oxy)propoxy)-6-oxohexyl)carbamoyl)-2-(6-hydroxy-3-oxo-3*H*-xanthen-9-yl)benzoic acid (FI-PIP₂-C9) FI-PIP₂-C9 (2.1 mg, 64%) was prepared from compound **6b** (2.6 mg, 3 μmol) in a similar manner to **PIP₂-C15** as a red-orange solid. ¹H NMR (400 MHz, CD₃OD) δ 6.50-

8.56 (m, 9H), 5.20-5.28 (m, 1H), 4.43-4.49 (m, 1H), 4.20-4.27 (m, 1H), 3.90-4.20 (m, 6H) 3.58-3.65 (m 1H), 3.30-3.40 (m, 2H), 2.25-2.36 (m, 4H), 1.30-1.70 (m, 6H), 1.20-1.30 (m, 14H), 0.84 (t, $J = 6.8$ Hz, 3H). ^{31}P NMR (CD_3OD , 162 MHz) δ 2.79 (1P), 1.92 (1P), -0.62 (1P). ESI-HRMS for $[\text{M} + \text{H}]^+$: calcd 1120.27, found 1120.2727

Synthesis of 4-((6-((2*R*)-2-(heptanoyloxy)-3-((hydroxy(((1*R*,2*R*,3*S*,4*R*,5*R*,6*S*)-2,3,6-trihydroxy-4,5-bis(phosphonooxy)cyclohexyl)oxy)phosphoryl)oxy)propoxy)-6-oxohexyl)carbamoyl)-2-(6-hydroxy-3-oxo-3*H*-xanthen-9-yl)benzoic acid (FI-PIP₂-C6). FI-PIP₂-C6 (2.0 mg, 67%) was prepared from compound **6a** (1.9 mg, 3 μmol) in a similar manner to **PIP₂-C15** as a red-orange solid. ^1H NMR (400 MHz, CD_3OD) δ 6.40-8.20 (m, 9H), 5.20-5.24 (m, 1H), 4.31-4.45 (m, 1H), 4.21-4.24 (m, 1H), 3.90-4.27 (m, 6H), 3.60-3.67 (m, 1H), 3.34-3.40 (m, 2H), 2.30-2.40 (m, 4H), 1.35-1.70 (m, 6H), 1.20-1.36 (m, 8H), 0.89 (t, $J = 6.9$ Hz, 3H). ^{31}P NMR (CD_3OD , 162 MHz) δ 2.72 (1P), 1.83 (1P), -0.64 (1P). ESI-HRMS for $[\text{M} + \text{H}]^+$: calcd 1078.22 found 1078.2262

Synthesis of (2*R*)-1-((6-(3-(5,5-difluoro-7,9-dimethyl-5*H*-4 E^4 ,5 E^4 -dipyrrolo[1,2-*c*:2',1'-*f*][1,3,2]diazaborinin-3-yl)propanamido)hexanoyl)oxy)-3-((hydroxy(((1*R*,2*R*,3*S*,4*R*,5*R*,6*S*)-2,3,6-trihydroxy-4,5-bis(phosphonooxy)cyclohexyl)oxy)phosphoryl)oxy)propan-2-yl palmitate (BODIPY-PIP₂-C15; 10) Boodipy-PIP₂-C15 (5.4 mg, 65%) Was prepared from compound **6d** (7.2 mg, .007 mmol) in similar conditions to **FI-PIP₂-C15** ^1H NMR (400 MHz, CD_3OD) δ 7.43 (s, 1H), 7.01 (d, $J = 4.1$ Hz, 1H), 6.32 (d, $J = 4.0$ Hz, 1H), 6.21 (s, 1H), 5.22-5.27 (m, 1H), 4.50 (q, $J = 9.2$ Hz, 1H), 4.41 (dd, $J = 12.0, 3.6$ Hz, 1H), 4.25 – 3.94 (m, 6H), 3.63 (dd, $J = 9.8, 2.7$ Hz, 1H), 3.24 – 3.07 (m, 4H), 2.60 (t, $J = 7.6$ Hz, 2H), 2.51 (s, 3H), 2.45 – 2.22 (m, 7H), 1.58-1.62 (m, 4H), 1.53 – 1.45 (m, 2H), 1.30-1.25

(m 26H), 0.89 (t, $J=7.0$ Hz, 3H). ^{31}P NMR (162 MHz, CD_3OD) δ 0.99, 0.50, -0.87. ESMS: 1111.8 $[\text{M}]^+$

Synthesis of (1*S*,2*S*,3*R*,4*S*,5*S*,6*S*)-2,3,4,5,6-pentakis(methoxymethoxy)cyclohexan-1-ol (11).

Compound **11** was synthesized as previously described from *myo*-inositol [81]. ^1H NMR (400 MHz, CDCl_3) δ 4.92 – 4.76 (m, 6H), 4.76 – 4.70 (m, 4H), 4.08 (t, $J = 2.6$ Hz, 1H), 4.00 (d, $J = 4.6$ Hz, 1H), 3.93 (t, $J = 9.7$ Hz, 1H), 3.67 (t, $J = 9.4$ Hz, 1H), 3.50 (dd, $J = 10.1, 2.5$ Hz, 1H), 3.47 – 3.39 (m, 15H); ^{13}C NMR (101 MHz, CDCl_3) δ 98.67, 98.43, 97.94, 96.16, 83.07, 79.61, 77.80, 77.31, 77.19, 76.99, 76.67, 76.38, 70.95, 56.35, 56.28, 56.07, 55.69, 55.66, 28.57. ESMS: 400.2 $[\text{M}]^+$

Synthesis of (2*R*)-1-(((benzyloxy)(diisopropylamino)phosphaneyl)oxy)-3-(((3-(((benzyloxy)carbonyl)amino)propanoyl)oxy)propan-2-yl palmitate (12).

Phosphoramidite **12** (75 mg, 85%) was synthesized from **3d** (64 mg, 0.11 mmol) as previously described [81]. ^1H NMR (400 MHz, CDCl_3) δ 7.37 – 7.28 (m, 10H), 5.23-5.16 (m, 1H), 5.09 (s, 2H), 4.81 – 3.34 (m, 15H), 3.18 (q, $J = 6.7$ Hz, 2H), 2.29 (t, $J = 7.6$ Hz, 4H), 1.61 (d, $J = 5.1$ Hz, 4H), 1.49 (q, $J = 7.5$ Hz, 2H), 1.37 – 1.22 (m, 26H), 1.19 – 1.12 (m, 12H), 0.94 – 0.80 (t, $J=6.9$ hz, 3H). ^{13}C NMR (101 MHz, CDCl_3) δ 173.01, 156.34, 136.61, 128.46, 128.22, 128.04, 127.26, 126.90, 77.31, 76.99, 76.67, 66.55, 65.44, 65.41, 65.23, 62.61, 61.82, 43.17, 43.06, 42.94, 40.81, 34.30, 33.84, 31.89, 29.67, 29.63, 29.60, 29.46, 29.33, 29.26, 29.08, 26.15, 24.89, 24.40, 22.66, 14.10. ^{31}P NMR (162 MHz, CDCl_3) δ 148.79 (0.5 P), 148.64 (0.5P).

Synthesis of (2*R*)-1-(((benzyloxy)(((1*S*,2*R*,3*R*,4*S*,5*S*,6*R*)-2,3,4,5,6-pentakis(methoxymethoxy)cyclohexyl)oxy)phosphoryl)oxy)-3-((3-

(((benzyloxy)carbonyl)amino)propanoyl)oxy)propan-2-yl palmitate (13) Compound **13** (48mg, 70%) was prepared in a similar manner to **compound 5d** from compound **11** (30 mg, 0.078 mmol) and phosphoramidite **12** (70 mg, .085 mmol) as a colorless oil. ^1H NMR (400 MHz, CDCl_3), δ 7.28-7.39 (m, 10H), 5.16-5.22 (m, 1H), 5.07-5.15 (m, 4H), 4.65-4.88 (M, 10H), 4.26-4.33 (m, 1H), 4.24 (t, $J = 2.2$ Hz, 1H) 4.06-4.20 (m, 4H), 3.86-4.00 (m, 2H), 3.32-3.50 (m, 17H), 3.17 (q, $J = 6.4$ Hz, 2H), 2.24-2.30 (m, 4H), 1.48-1.68 (m, 8H), 1.25-1.38 (m, 25H), 0.88 (t, $J = 6.7$ Hz, 3H). ^{13}C NMR (101 MHz, CDCl_3) δ 172.85, 172.80, 172.76, 136.62, 128.72, 128.68, 128.66, 128.48, 128.05, 127.90, 127.88, 98.80, 98.52, 98.49, 97.48, 96.02, 79.44, 77.32, 77.01, 76.69, 75.68, 74.62, 69.55, 66.56, 61.59, 56.68, 56.58, 56.53, 56.46, 55.78, 55.63, 40.81, 34.04, 33.70, 31.90, 29.68, 29.65, 29.63, 29.62, 29.47, 29.34, 29.27, 29.07, 26.13, 24.78, 24.34, 22.67, 14.10. ^{31}P NMR (162 MHz, CDCl_3) δ -1.52 (0.5P), -1.59(0.5P). ESMS: 1087.55 $[\text{M}]^+$

Synthesis of (2R)-1-((3-aminopropanoyl)oxy)-3-((hydroxy(((1S,2R,3R,4S,5S,6R)-2,3,4,5,6-pentahydroxycyclohexyl)oxy)phosphoryl)oxy)propan-2-yl palmitate (14)
Protected PI intermediate **13** (11 mg, .010 mmol) was de-protected using the same conditions previously described for compound **6d** yielding compound **11** (6.7 mg, quantitative) as a colorless oil. ^1H NMR (400 MHz, CD_3OD) δ 4.41 (dd, $J = 12.0, 4.0$ Hz, 1H), 4.02 (t, $J = 9.0$ Hz, 1H), 3.78 (t, $J = 9.5$ Hz, 1H), 3.62 (t, $J = 9.5$ Hz, 1H), 3.37 (dd, $J = 12.0, 4$ Hz, 1H), 3.18 (t, $J=8.0$, 1H), 2.93 (t, $J = 8.0$ Hz, 1H), 2.30-2.40 (m, 4H), 1.39-1.72 (m, 6H), 1.25-1.36 (m, 26H), 0.89 (t, $J = 6.9$ Hz, 3H). ^{31}P NMR (162 MHz, CD_3OD) δ -1.46 (1P). ESMS:644.3 $[\text{M}+\text{H}]^+$

Synthesis of (2*R*)-1-((3-(3-(5,5-difluoro-7,9-dimethyl-5*H*-4 β ,5 β -dipyrrolo[1,2-*c*:2',1'-*f*][1,3,2]diazaborinin-3-yl)propanamido)propanoyl)oxy)-3-

((hydroxy(((1*S*,2*R*,3*R*,4*S*,5*S*,6*R*)-2,3,4,5,6-

pentahydroxycyclohexyl)oxy)phosphoryl)oxy)propan-2-yl palmitate (BODIPY-PI-

C15; 15) To a solution of compound **11** (6.7 mg, 9 μ mol) in TEAB buffer (0.5 M 160 μ L)

was added a solution of NHS-BODIPY (30 mg/mL 160 μ L) in DMF. The reaction was

stirred in the dark at room temperature before removal of solvents by vacuum.

Purification by HPLC (BETASIL C18 150 x 10 mm water-methanol 0-100% over 30

minutes 5 mL/min) yielded fluorescent **PI-C15** (5.3 mg, 60%) as a deep red solid. ^1H

NMR (400 MHz, CD_3OD) δ 7.43 (s, 1H), 7.01 (d, J = 4.0 Hz, 1H), 6.32 (d, J = 4.1 Hz,

1H), 6.21 (s, 1H), 5.20-5.30 (m, 1H), 4.05-4.25 (m, 5H), 4.44 (dd, J = 12.0, 4 Hz, 1H),

3.93 (t, J = 8.1 Hz, 1H), 3.77 (t, J = 8.1Hz, 1H), 3.62 (t, J = 8.1 Hz, 1H), 3.37 (dd, J =

9.7, 2.6 Hz, 1H), 3.10-3.25 (m, 5H), 2.60 (t, J = 8.0 Hz, 1H), 2.51 (s, 3H), 2.29-2.40 (m,

4H), 2.28 (s, 3H), 1.37-1.65 (m, 6H), 1.29-1.40 (m, 26H), 0.88 (t, J = 7.1 Hz, 3H). ^{31}P

NMR (CD_3OD , 162 MHz) δ 0.17 (1P). ESI-HRMS for $[\text{M}]^{+}$ calcd 847.36, found 847.3586

Synthesis of 2,5-dioxopyrrolidin-1-yl hept-6-ynoate (16). N-hydroxysuccinimide (100

mg, .87 mmol) and EDAC-HCl (125 mg, .87mmol) were added to a solution of 6-

heptynoic acid (100 mg, 0.79 mmol) in DCM (5 mL) containing 0.5 mL of DMF and

stirred overnight. To this mixture was added ethyl acetate and the organic layer was

washed with water and brine. The organic layer was dried over sodium sulfate and then

concentrated under vacuum. The crude residue was purified by flash chromatography

(2:1 Hex:EtOAc) to yield pure NHS-ESTer **16** as a waxy solid (140 mg, 80%). ^1H NMR

(400 MHz, CDCl_3) δ 2.89 – 2.77 (m, 4H), 2.64 (t, J = 7.4 Hz, 2H), 2.24 (td, J = 6.9, 2.7

Hz, 2H), 1.96 (t, J = 2.7 Hz, 1H), 1.88 (dt, J = 15.3, 7.4 Hz, 2H), 1.72 – 1.54 (m, 2H). ^{13}C NMR (101 MHz, CDCl_3) δ 169.10, 168.31, 83.46, 68.94, 30.40, 27.30, 25.57, 23.51, 17.95. ESMS: 223.1 $[\text{M}]^+$

Synthesis of (2*R*)-1-((6-(hept-6-ynamido)hexanoyl)oxy)-3-((hydroxy(((1*S*,2*R*,3*R*,4*S*,5*S*,6*R*)-2,3,4,5,6-pentahydroxycyclohexyl)oxy)phosphoryl)oxy)propan-2-yl palmitate (Alkyne-PI; 17) **17 (4.5 mg, 78%)** was synthesized in a similar manner to PI-C15 from **14 (5 mg, .007 mmol)** and NHS ester **16 (1.8 mg, 0.008 mmol)**. ^1H NMR (400 MHz, CD_3OD) δ 5.26-5.18 (sm, 1H), 4.45 (dd, J = 11.9, 3.5 Hz, 1H), 4.22 – 4.15 (m, 1H), 4.07 (q, J = 5.1 Hz, 1H), 3.88 (td, J = 9.0, 8.1, 2.7 Hz, 1H), 3.76 (t, J = 9.5 Hz, 1H), 3.72 – 3.56 (m, 1H), 2.34 (td, J = 7.4, 1.7 Hz, 4H), 2.24 – 2.14 (m, 6H), 1.74 – 1.68 (m, 2H), 1.66 – 1.55 (m, 4H), 1.56 – 1.45 (m, 4H), 1.38 – 1.27 (m, 26H), 0.89 (t, J = 6.5 Hz, 4H). ^{31}P NMR (162 MHz, CD_3OD) δ 0.15 (1P). ESMS: 794.4 $[\text{M}+\text{H}]^+$

Synthesis of (S)-16-(4-methoxyphenyl)-3,10-dioxo-1-phenyl-2,11,15-trioxa-4-azahexadecan-13-yl palmitate (18). A mixture of **2** (350 mg, 0.76 mmol), **1d** (234.5 mg, 0.91 mmol), DCC (189 mg, 0.91 mmol), and DMAP (51 mg, 0.42 mmol) in anhydrous CH_2Cl_2 (6 mL) was stirred at room temperature overnight. The reaction mixture was concentrated and purified by flash chromatography (hexane-ethyl acetate = 2:1) over silica (407 mg, 89%). ^1H NMR (400 MHz, CDCl_3) δ 7.37 – 7.25 (m, 5H), 7.22 (d, J = 8.5 Hz, 2H), 6.86 (d, J = 8.6 Hz, 2H), 5.27 – 5.17 (m, 1H), 5.08 (s, 2H), 4.94 – 4.82 (m, 1H), 4.52 – 4.39 (m, 2H), 4.33 (dd, J = 11.9, 3.8 Hz, 1H), 4.15 (dd, J = 11.9, 6.5 Hz, 1H), 3.78 (s, 3H), 3.54 (dd, J = 5.1, 1.4 Hz, 2H), 3.17 (q, J = 6.7 Hz, 2H), 2.35 – 2.22 (m, 4H), 1.66 – 1.55 (m, 4H), 1.55 – 1.43 (m, 2H), 1.38 – 1.22 (m, 26H), 0.87 (t, J =

6.9 Hz, 3H). ^{13}C NMR (101 MHz, CDCl_3) δ 173.11, 173.05, 159.29, 156.38, 136.64, 129.73, 129.28, 128.47, 128.05, 128.03, 113.80, 77.38, 77.06, 76.74, 72.92, 70.00, 67.87, 66.54, 62.81, 55.33, 55.23, 55.11, 40.81, 34.30, 33.84, 31.91, 29.68, 29.64, 29.61, 29.58, 29.47, 29.34, 29.27, 29.07, 26.13, 24.94, 24.86, 24.39, 22.67, 14.11. ESMS: 720.5 $[\text{M}+\text{Na}]^+$

Synthesis of (S)-1-((6-aminohexanoyl)oxy)-3-((4-methoxybenzyl)oxy)propan-2-yl palmitate (19). Protected precursor **18** (7 mg, 0.01 mmol) was dissolved in methanol (7 mL). Pyridine (1 μL) and Pd/C (10 mol %) were added to the mixture. The mixture was stirred under a balloon of hydrogen gas for 30 minutes followed by filtration of the metal catalyst through celite. The filtrate was collected and concentrated under vacuum to yield free amine. The free amine was used directly in the next reaction with no further purification (5.4 mg, 96%). ^1H NMR (400 MHz, CDCl_3) δ 7.23 (d, J = 8.6 Hz, 2H), 6.87 (d, J = 8.6 Hz, 2H), 5.21 (ddd, J = 5.3, 3.4, 1.4 Hz, 1H), 4.46 (d, J = 6.6 Hz, 2H), 4.32 (dd, J = 11.8, 3.9 Hz, 1H), 4.15 (dd, J = 11.8, 6.4 Hz, 1H), 3.80 (s, 3H), 3.55 (dd, J = 5.0, 1.1 Hz, 2H), 3.06 – 2.86 (m, 2H), 2.37 – 2.20 (m, 4H), 1.69 – 1.51 (m, 4H), 1.50 – 1.36 (m, 2H), 1.34 – 1.16 (m, 26H), 0.87 (t, J = 6.9 Hz, 3H). ^{13}C NMR (101 MHz, CDCl_3) δ 173.16, 172.90, 159.28, 129.75, 129.29, 113.80, 77.32, 77.00, 76.68, 72.94, 69.99, 67.92, 62.91, 55.26, 39.67, 34.31, 33.53, 31.91, 29.69, 29.66, 29.64, 29.63, 29.49, 29.35, 29.28, 29.09, 27.27, 25.84, 24.94, 24.00, 22.68, 14.11. ESMS: 564.4 $[\text{M}+\text{H}]^+$

Synthesis of (S)-1-((6-(3-(5,5-difluoro-7,9-dimethyl-5*H*-4 β ,5 β -dipyrrolo[1,2-*c*:2',1'-*f*][1,3,2]diazaborinin-3-yl)propanamido)hexanoyl)oxy)-3-((4-methoxybenzyl)oxy)propan-2-yl palmitate (20). Free amine **19** (5 mg, 0.009 mmol) was dissolved in anhydrous DMF (150 μL) followed by the addition of 5 μL TEA. After

spinning for 10 minutes under argon, BODIPY-NHS (5.2 mg, 0.013 mmol) in 200 μ L of DMF was added slowly. The reaction proceeded overnight in the dark followed by concentration under a stream of nitrogen. The crude mixture was then purified on silica gel (2:1 EtOAc:Hex, R_f ~0.45) to yield protected fluorescent intermediate (5.6 mg, 76%) ^1H NMR (400 MHz, CDCl_3) δ 7.24 – 7.18 (m, 2H), 7.09 (s, 1H), 6.91 – 6.81 (m, 3H), 6.29 (d, J = 4.0 Hz, 1H), 6.12 (s, 1H), 5.70-5.75 (m, 1H), 5.30–5.16 (m, 1H), 4.45 (d, J = 6.8 Hz, 2H), 4.32 (dd, J = 11.9, 3.8 Hz, 1H), 4.15 (dd, J = 11.9, 6.5 Hz, 1H), 3.80 (s, 3H), 3.54 (d, J = 5.1, 1.2 Hz, 2H), 3.26 (t, J = 7.5 Hz, 2H), 3.23 – 3.11 (m, 2H), 2.62 (t, J = 7.4 Hz, 2H), 2.56 (s, 3H), 2.35 – 2.18 (m, 7H), 1.67 – 1.56 (m, 4H), 1.46 – 1.35 (m, 2H), 1.34-1.22 (m, 26H), 0.87 (t, J = 6.9 Hz, 3H); ^{13}C NMR (101 MHz, CDCl_3) δ 173.14, 173.10, 171.57, 168.98, 167.79, 159.28, 129.73, 129.28, 128.28, 127.85, 124.01, 123.78, 120.72, 120.39, 117.56, 116.75, 113.79, 72.93, 70.00, 67.89, 62.80, 55.25, 39.19, 36.00, 34.31, 33.84, 31.91, 30.32, 29.68, 29.65, 29.62, 29.48, 29.34, 29.28, 29.11, 29.08, 26.21, 25.57, 24.94, 24.43, 23.35, 22.67, 14.91, 14.18, 14.11, 11.31, 11.29. ESMS: 838.8 $[\text{M}+\text{H}]^+$

Synthesis of (S)-1-((6-(3-(5,5-difluoro-7,9-dimethyl-5*H*-4*H*,5*H*-dipyrrolo[1,2-*c*:2',1'-*f*][1,3,2]diazaborinin-3-yl)propanamido)hexanoyl)oxy)-3-hydroxypropan-2-yl palmitate (Boidpy-DAG; **21)** Protected intermediate **20** (6 mg, 0.007 mmol) was dissolved in DCM (10 mL) containing 5% water followed by the addition of DDQ (3.5 mg, 0.015 mmol). The reaction proceeded for 4 hours and was monitored by TLC (2:1 EtOAc:Hex, R_f ~0.25) for completion. DCM (25 mL) were then added and the reaction mixture was washed with 10% NaHCO_3 and brine. The mixture was then purified by column chromatography (10% Methanol in Chloroform) to yield pure fluorescent DAG

(3.3 mg, 65%). ^1H NMR (400 MHz, CDCl_3) δ 7.10 (s, 1H), 6.89 (d, J = 4.1 Hz, 1H), 6.30 (d, J = 4.1 Hz, 1H), 6.12 (s, 1H), 5.85–5.79 (m, 1H), 5.05–5.05 (m, 1H), 4.30 (dd, J = 11.8, 4.6 Hz, 1H), 4.20 (dt, J = 11.7, 5.8 Hz, 1H), 3.75 – 3.63 (m, 2H), 3.29 – 3.14 (m, 4H), 2.62 (t, J = 7.4 Hz, 2H), 2.56 (s, 3H), 2.39 – 2.24 (m, 7H), 1.67 – 1.56 (m, 4H), 1.46 – 1.35 (m, 2H), 1.34–1.22 (m, 26H), 0.87 (t, J = 6.9 Hz, 3H). ^{13}C NMR (101 MHz, CDCl_3) δ 173.40, 173.38, 171.71, 128.34, 123.81, 120.40, 117.60, 77.31, 76.99, 76.67, 71.95, 61.95, 61.32, 39.14, 39.05, 36.06, 34.26, 33.89, 31.91, 29.68, 29.67, 29.64, 29.60, 29.46, 29.35, 29.25, 29.09, 29.08, 29.01, 26.14, 26.11, 24.91, 24.50, 22.68, 14.92, 14.11, 11.30. ESMS: 717.4 $[\text{M}+\text{H}]^+$

Synthesis of (*R*)-1-((6-(((benzyloxy)carbonyl)amino)hexanoyl)oxy)-3-((bis(benzyloxy)phosphoryl)oxy)propan-2-yl palmitate (22). To a solution of tetrazole (12 mg, 0.045 mmol) in anhydrous DCM (2 mL) was added dibenzyl *N,N*-diisopropyl phosphoramidite (25 μL , 0.045 mmol) under argon followed by the addition of free hydroxyl C15 lipid **3d** (24 mg, 0.041 mmol) in 0.5 mL of anhydrous DCM. The reaction stirred overnight and was then cooled to -40°C followed by the addition of di-*tert*-butyl peroxide (15 μL of 5.5 M solution) and the mixture was allowed to slowly warm to room temperature. The crude mixture was then purified via flash chromatography (1:1 Hex:EtOAc, R_f ~0.35) to yield pure protected intermediate (13 mg, 75%).

^1H NMR (400 MHz, CDCl_3) δ 7.41 – 7.27 (m, 15H), 5.22 – 5.13 (m, 1H), 5.09 (s, 2H), 5.05 – 5.00 (m, 4H), 4.97 – 4.91 (m, 1H), 4.25 (dd, J = 11.9, 4.4 Hz, 1H), 4.12 – 4.03 (m, 3H), 3.22 – 3.12 (m, 2H), 2.34 – 2.17 (m, 4H), 1.67 – 1.44 (m, 6H), 1.38 – 1.20 (m, 26H), 0.87 (t, J = 6.9 Hz, 3H). ^{13}C NMR (101 MHz, CDCl_3) δ 172.84, 172.78, 156.38,

136.63, 135.59, 135.57, 135.52, 128.61, 128.58, 128.46, 128.06, 128.02, 127.93, 127.91, 127.84, 127.81, 77.32, 77.20, 77.00, 76.68, 69.50, 69.45, 69.26, 69.18, 66.53, 65.34, 65.28, 61.62, 40.80, 34.07, 33.90, 33.72, 31.89, 29.67, 29.66, 29.63, 29.60, 29.57, 29.45, 29.33, 29.24, 29.07, 29.04, 26.11, 24.77, 24.72, 24.35, 24.28, 22.66, 14.10. ^{31}P NMR (162 MHz, CDCl_3) δ -1.04 (1P). ESMS: 839.0 $[\text{M}+\text{H}]^+$

Synthesis of (*R*)-1-((6-aminohexanoyl)oxy)-3-(phosphonooxy)propan-2-yl palmitate (23). Protected intermediate **22** (18 mg, 0.021 mmol) was dissolved in ethyl acetate (8 mL) and Pd/C (10 mol %, 5 mg) was added. The mixture was stirred overnight under a balloon of hydrogen gas and the catalyst was filtered via celite and washed with 1:1 chloroform:methanol. The fully deprotected intermediate was used directly in the next reaction without further purification (10 mg, 96%).

^1H NMR (400 MHz, CDCl_3) δ 5.23 – 5.12 (m, 1H), 4.34 – 4.17 (m, 2H), 4.05 – 3.93 (m, 2H), 2.95 (s, 2H), 2.45 – 2.35 (m, 3H), 2.35 – 2.27 (m, 2H), 1.74 – 1.55 (m, 4H), 1.51 – 1.40 (m, 2H), 1.34-1.18 (m, 26H), 0.87 (t, J = 6.9 Hz, 3H). ^{13}C NMR (101 MHz, CDCl_3) δ 206.95, 173.12, 172.88, 77.31, 76.99, 76.67, 69.69, 62.66, 61.46, 39.70, 34.12, 33.59, 31.91, 30.91, 29.71, 29.68, 29.66, 29.64, 29.60, 29.54, 29.46, 29.36, 29.27, 29.17, 29.11, 26.84, 25.46, 24.83, 24.78, 24.26, 22.68, 21.03, 14.10. ^{31}P NMR (162 MHz, CDCl_3) δ 0.37 (1P). ESMS: 524.7 $[\text{M}+\text{H}]^+$

Synthesis of (*R*)-1-((6-(3-(5,5-difluoro-7,9-dimethyl-5*H*-4 β ,5 β -dipyrrolo[1,2-*c*:2',1'-*f*][1,3,2]diazaborinin-3-yl)propanamido)hexanoyl)oxy)-3-(phosphonooxy)propan-2-yl palmitate (BODIPY-PA; 24) Free amine **23** (10 mg, .019 mmol) was dissolved in DMF (150 μL) and 100 μL of TEAB buffer (0.5 M) were added followed by an addition 10 μL of chloroform to fully solubilize the compound. After spinning for 10 min, BODIPY-

NHS was added in 150 μ L of DMF. The reaction was stirred for 1 hour and checked for completion by TLC (0.1% AcOH in 65:35:4 CHCl_3 :MeOH:H₂O) followed by concentration under vacuum. The crude mixture was purified on silica gel (65:35:4 CHCl_3 :MeOH:H₂O Rf- 0.5) to yield pure fluorescent PA (7.5 mg, 50%). ¹H NMR (400 MHz, CDCl_3) δ 7.09 (s, 1H), 6.87 (d, *J* = 4.0 Hz, 1H), 6.27 (d, *J* = 4.0 Hz, 1H), 6.10 (s, 1H), 5.25 – 5.12 (m, 1H), 4.33 (dd, *J* = 11.9, 3.8 Hz, 1H), 4.14 (dd, *J* = 11.9, 6.0 Hz, 1H), 3.99 (t, *J* = 6.0 Hz, 2H) 3.24 (t, *J* = 7.4 Hz, 2H), 3.16 (d, *J* = 6.2 Hz, 2H), 2.61 (t, *J* = 7.4 Hz, 2H), 2.54 (s, 3H), 2.38-2.18 (m, 7H), 1.59 – 1.50 (m, 6H), 1.47 – 1.34 (m, 2H), 1.31 – 1.15 (m, 26H), 0.87 (t, *J* = 6.9 Hz, 3H). ¹³C NMR (101 MHz, CDCl_3) δ 207.05, 177.24, 143.83, 128.31, 123.78, 84.62, 77.31, 76.99, 76.67, 39.24, 35.73, 34.23, 33.82, 31.91, 30.91, 29.72, 29.68, 29.66, 29.35, 29.19, 29.09, 24.85, 24.33, 22.67, 21.45, 14.87, 14.10, 11.27. ³¹P NMR (162 MHz, CDCl_3) δ 2.12 (1P). ESMS: 798.7 [M+H]⁺

CHAPTER 3. CELLULAR DELIVERY OF SYNTHETIC PIP REPORTERS

3.1 Introduction

With fluorescent reporters **BODIPY-DAG-C15**, **BODIPY-PIP₂-C15**, **BODIPY-PtdIns-C15** in hand we sought to investigate various methods of cellular delivery of these reporters. Because of the negative resting potential of the plasma membrane it is difficult to achieve the delivery of a negatively charged substrate [39]. Further complicating delivery is the presence of a solvation shell of water molecules around the hydroxyl groups in the head group of PIP reporters, which makes delivery through the hydrophobic core of the membrane also a challenge [92, 93]. A large problem in achieving systematic analysis of PIPs is the difficulty and unreliability of current delivery methods of synthetic PIP reporters [20, 93]. A carrier: cargo method utilizing charge-charge interaction with histones is the most frequently cited for PIP delivery. Pipette perfusion and microinjection are other methods that have been used though we sought only to explore passive methods of delivery [62, 87, 94]. Unfortunately, these methods have a number of drawbacks that may not make them effective for a systematic approach to studying PIP metabolism. The concentration of synthetic PIP₂ used in this method are 4-10 times the concentration of endogenous substrate at 40 and 100 μ M, which can greatly alter the pool of PIPs [87, 94]. Because the concentration and ratio of PIPs drive biological processes, such a perturbation of the pathway can result in unwanted pathway activation. Indeed, a large calcium flux is seen in this method as well as reporters exclusively metabolized to DAG due to the activation of intrinsic signaling

pathways making this method highly unsuitable when attempting to discern the roles of multiple metabolites within the pathway [87, 94] To effectively measure PIP metabolism using fluorescent reporter technology, a simple and non-intrusive cellular delivery method is required [87, 95]. Such a delivery method must definitively show the delivery of a reporter that is therein capable of metabolism via multiple enzymes. Photocaging methods have also been described for synthetic lipid reporters, including PIPs, and are an excellent method for analysis as it gives temporal control over release of the substrate[92, 93, 96-99]. Various caged, non fluorescent, PIPs have been synthesized and delivered to cells including PIP₃ and PI(3)P as wells IP₃ and have indeed been useful tools in dissecting specific locations of PIP biology[92, 93, 96, 99]. In the method, the phosphate esters are 'caged' with a photocleavable group, often coumarin or nitrobenzyl, which allows for passive diffusion into the cell (**Figure**

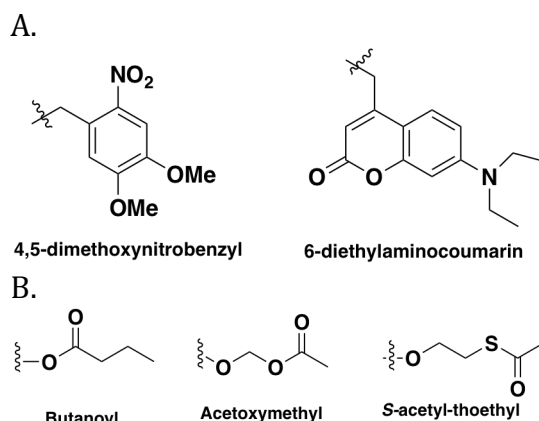


Figure 3.1 Common Chemical Moieties in Photocaging of Phospholipids: **A.** Structures of common photocaging moieties **B.** Structures of bioactivateable protecting groups.

3.1 A). The caging groups can then be released by rapid exposure to UV light releasing the active metabolite [92, 93, 96-99]. These tools often contain a bioactivatable protecting group used for masking of hydrophilic groups on lipid reporters, such as the hydroxyls of PIPs to reduce the energy penalty of entering the hydrophobic region of the lipid bilayer [92, 93, 99] (**Figure 3.1B**). These groups are cleaved over time via nonspecific esterases within the cell leaving only the photo cleavable group to be

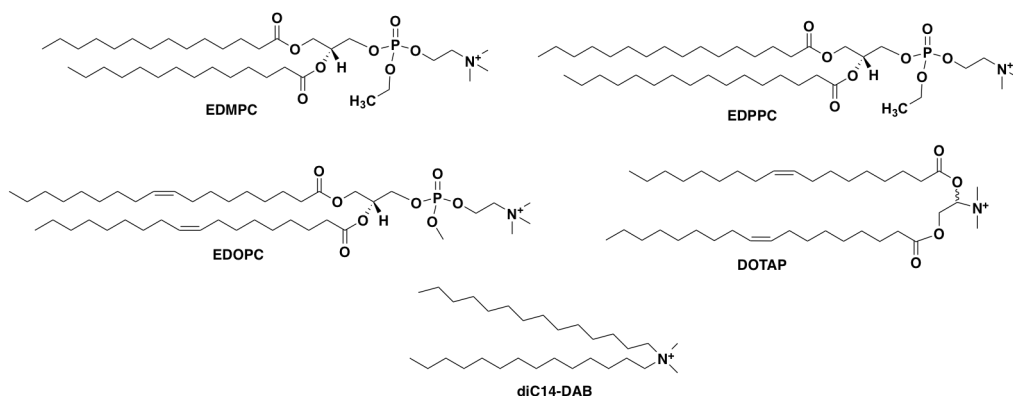
removed. Various caged, non-fluorescent, PIPs have been synthesized and delivered to cells including and have indeed been useful tools in dissecting PIP biology [92, 93, 96, 99]. For instance, caged PI(3)P was successful in inducing endosomal fusion following uncaging [92]. Likewise, various caged tri-functional lipid probes of DAG and sphingosine have been developed and has proven to be a powerful technology for the temporal release of active metabolite [98]. A major drawback of this approach the synthesis of such lipids is a long and arduous process. Further utility of this system to systematically analyze PIP metabolism has yet to be examined as previous studies focused on biological outcomes or proteomics and not metabolite identification [92, 93, 98, 99].

Another system that has proven effective⁹⁹ at the delivery of a variety of cargo is the use of cationic lipids, seen in **Figure 3.2**, to formulate various liposomes capable of cellular entry [100, 101]. When mixed with negatively charged cargo, such as DNA or other cargo, lipid complexes have shown significant efficacy in cellular transfection and subsequent protein expression[100, 102-105]. Cationic liposomes have also proven effective at delivery of cytotoxic agents such as chemotherapy drugs in clinical applications [100, 101, 106]. Because of the effectiveness of cationic liposomes for cellular delivery of various charged substrates, and their composition made up of amphiphilic lipids similar to our reporters, it is plausible that a cationic liposome could be formulated to include a fluorescent PIP reporter for use in delivery and cellular analysis.

Another class of liposomes with fusogenic properties composed of 1,2-dioleoylphosphatidylethanolamine (DOPE) and 1,2-dioleoyl-3-trimethylammonium-propane (DOTAP), shown in **Figure 3.2B**, have also been shown to be effective at

delivery of charged substrates including mRNA and intracellular proteins. In this method, the liposome fuses with the plasma membrane instead of entering the cell via endocytosis, which can lead to lysosomal degradation of the cargo [107]. Further, this method has been previously reported to be capable of delivering phospholipids tagged with fluorophores for membrane visualization via fluorescence microscopy [84, 108]. Interestingly, the addition of the delocalized π electron system of the fluorophores appeared to have a beneficial effect to the efficacy of membrane fusion of the liposome, with BODIPY being one of the most effective [84, 107, 108]. While fusogenic liposomes have been reported to contain fluorescent lipids for visualization the utility of such a system to systematically analyze PIP metabolism has yet to be determined.

A.



B.

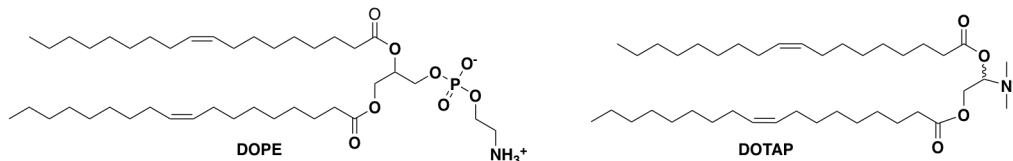


Figure 3.2 Common lipids used in Liposome Formulation for Cellular Transfection: **A.** Cationic lipids commons found in combination with neutral 'helper lipids' to achieve a cationic liposome for cellular transfection. **B.** Common lipids in fusogenic liposome formulations

In this chapter, we describe our attempts at cellular delivery of fluorescent **BODIPY-DAG-C15**, **BODIPY-PtdIns-C15** and **BODIPY-PIP₂-C15** reporters, as well as a model phospholipid to explore a variety of delivery options. We detail our attempts at previously described delivery methods, liposome delivery, intra-molecular charge masking, photocaging, and unique carrier-cargo complexes for use in cellular PIP analysis.

3.2 Results and Discussion

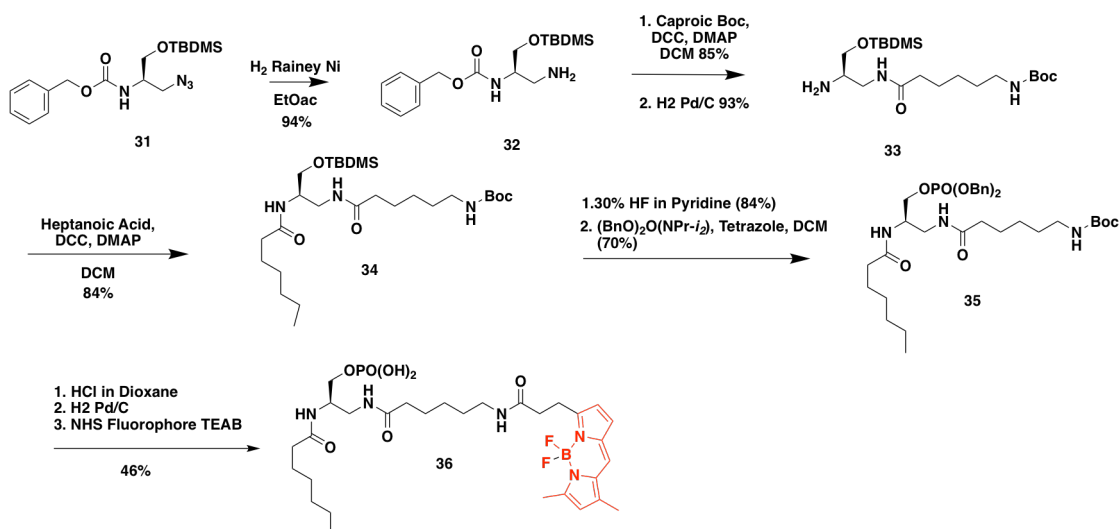
3.2.1 Delivery of **BODIPY-DAG-C15**, **BODIPY-PIP₂-C15**, and model phospholipid **36** to Cells

To investigate the effects of charge on the delivery of fluorescent PIP metabolites, we first compared the effectiveness of delivering the neutral **BODIPY-DAG-C15** and **BODIPY-PIP₂-C15** without the use of a carrier system. HEK293AD cells were incubated with 1 μ M **BODIPY-DAG-C15** or **BODIPY-C15-PIP₂** and cells were then analyzed via fluorescence microscopy after 15 min of incubation with the probe. As expected, and consistent with literature precedent, fluorescent DAG is efficiently taken up by the cells as indicated by the increase in fluorescent signal whereas no fluorescent PIP₂ is present in the cell [21, 61, 109]. This confirmed that indeed charge was a factor for the delivery of PIP reporters, though the difference in structures with PIP₂ containing multiple phosphates on the inositol head group could also have played a part in the delivery efficiency.

To further confirm that charge was a major factor in delivery, a model phospholipid **36** was synthesized that more closely resembles DAG and PA to further test this theory and for comparison to other delivery techniques. The development of the

model phospholipid allows for the exploration and comparison of multiple novel delivery methods due to easier synthesis compared to inositol containing PIP derivatives. The compound contains a phosphate group to examine the effect of charge and a fluorophore for detection. The synthetic route is shown in **Scheme 3.1**. Compound **32** was synthesized via reduction over Ra-Ni/ H₂ of azide intermediate synthesized as previously reported [110]. Next, the amine was coupled N-Boc caproic acid with coupling reagent DCC and DMAP followed by Cbz deprotection via hydrogenolysis over Pd/C to yield compound **33**. Heptanoic acid was coupled to the free amine again using DCC and DMAP to give compound **34**. The silyl ether was removed via hydrogen fluoride in pyridine to yield a free alcohol, which was subsequently phosphorylated via phosphoramidite coupling resulting in fully protected intermediate **35**. Deprotection of the amino-Boc group was achieved via HCl in dioxane followed by final deprotection of the Benzyl protecting groups again via hydrogenolysis over Pd/C. Finally, the free amine was tagged with BODIPY fluorophore using **9** in basic conditions as previously

described to yield fluorescent model compound **36**.



Scheme 3.1 Synthesis of Fluorescent Model Phospholipid 36.

When 1 μ M of **compound 36** was incubated with HEK293-AD cells no increase in cellular fluorescence after 15 min was observed as seen in **Figure 3.3**, again indicating the presence of a negative charge is the largest obstacle to overcome in cellular delivery and neutralization of the charge may deem our reporters suitable for cellular delivery.

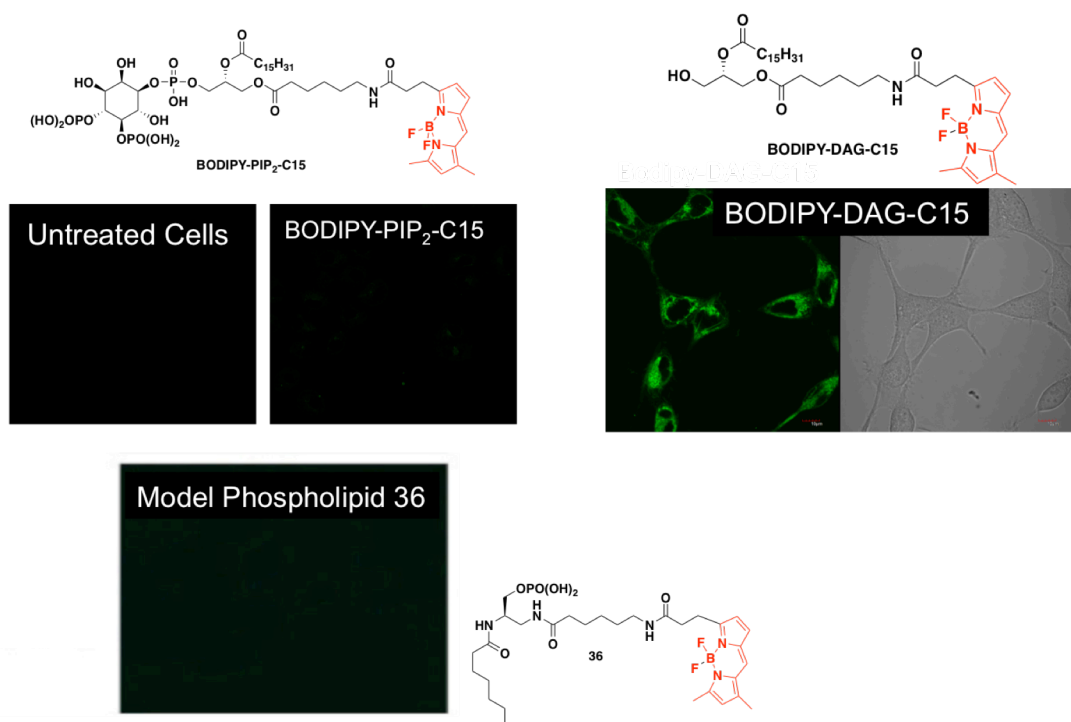


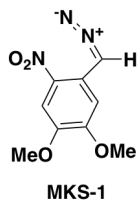
Figure 3.3 Carrier Free Delivery of Fluorescent Lipid Reporters HEK293AD cells (0.5 million) in growth medium (DMEM with 10% FBS, 2 mL) were plated into a 35 mm dish and were grown in an incubator at 37 C with 5% CO₂. After 24 h, the cells were treated with 1 μ M of the indicated fluorescent compound. Cells were visualized with a confocal microscope 15 minutes after incubation.

3.2.2 Photocaging for the Delivery of Model Phospholipid 36

In our lab, we have developed a general, one-step method to enable phospholipids cell permeable and photoactivatable, **MKS-1**, shown in **Figure 3.4A**, which reduces the need for complex synthesis to achieve a caged phospholipid and instead could be applied directly to our suite of PIP reporters [111]. Trimethylsilyldiazomethane (TMS) has been shown to selectively alkylate phosphoric acid under mild conditions. By replacing the methyl group with photocleavable nitrobenzyl yields a useful tool for the general caging of free phosphates using compound **MKS-1**. **Compound 36** was easily caged using **MKS-1** in MeOH yielding

compound 54 and could be effectively uncaged back to **compound 36** following treatment with light between 300-400 nm in wavelength as shown in **Figure 3.4B** [111].

A.



B.

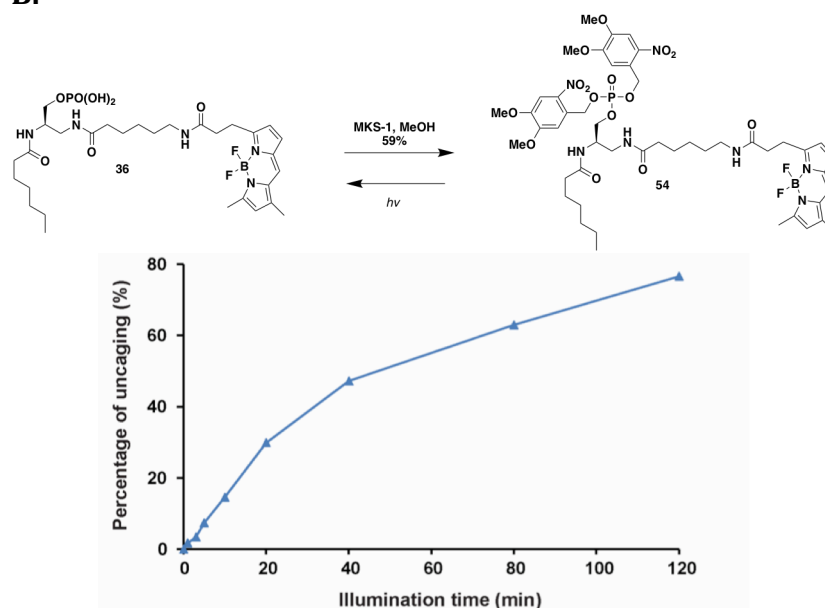


Figure 3.4 Generation and Uncaging of Compound 54 with MKS-1: A. Structure of photocaging reagent **MKS-1**. **B.** Caging of phospholipid **36** with **MKS-1** generated **54** which could be uncaged following treatment with UV light.

With the caged **54** in hand, we tested whether caging the phosphoric acid **36** was sufficient to make it cell-permeable in HEK293-AD cells. Cells were treated with either 1 μ M of uncaged **36** or caged **54** and the cellular fluorescence was examined 15 min after

compound treatment. As shown in **figure 3.5**, strong fluorescence that was primarily in cytosol was detected for caged **54**-treated cells. In contrast, no fluorescence signals were detected in cells treated with uncaged **36**. These results clearly demonstrated that caging the phosphate group in **54** was sufficient to make it cell-permeable and thereby validated our approach of neutralizing charge for the delivery of phospholipids [111].

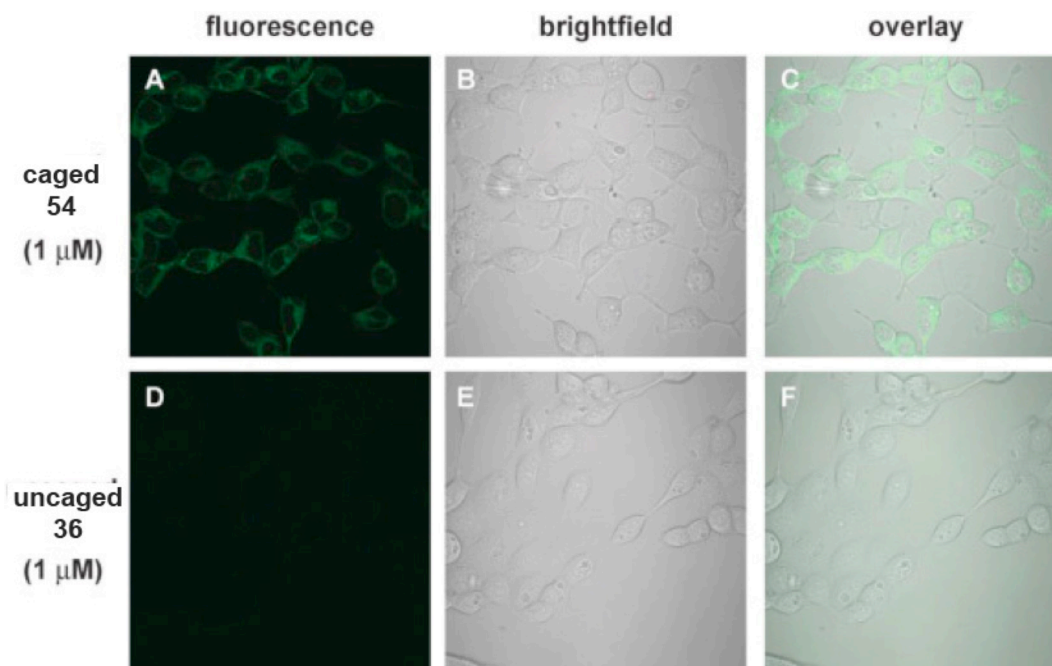


Figure 3.5 Delivery of Uncaged 36 and Caged 54 to Cells: HEK293AD cells (0.5 million) in growth medium (DMEM with 10% FBS, 2 mL) were plated into a 35 mm dish and were grown in an incubator at 37 C with 5% CO₂. After 24 h, the cells were treated with 1 μ M of **36** or **54**. Cells were visualized with a confocal microscope 15 minutes after incubation.

3.2.3 Histone Delivery of PIPs

Despite the previously described drawbacks of using histones as a delivery method, we used this carrier-cargo method as a starting point to analyze the effectiveness of cellular delivery of fluorescent PIPs with this carrier system in our hands with a lower concentration of fluorescent reporter to avoid activation if intrinsic

signaling pathways. **BODIPY-PtdIns-C15** 1 μ M were mixed with histones and incubated with 293AD cells. Cells were then washed with PBS and analyzed for increase in fluorescence via fluorescence microscopy after 30 minutes of incubation. A BODIPY-tagged QS-11, which is known to be cell permeable, was used as a control [112, 113]. Despite literature reports, we were unable to achieve efficient delivery of fluorescent PIPs as seen in **Figure 3.6**, leading our efforts to focus on new and alternative delivery methods of fluorescent PIPs

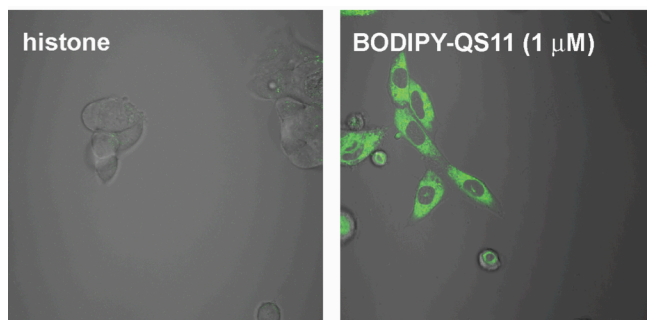


Figure 3.6: Histone Delivery of BODIPY-PtdIns-C15 to Cells
HEK293AD cells (0.5 million) in growth medium (DMEM with 10% FBS, 2 mL) were plated into a 35 mm dish and were grown in an incubator at 37 C with 5% CO₂. After 24 h, the cells were treated with 1 μ M of histone:**BODIPY-PtdIns-C15** or **BODIPY-QS11**. Cells were visualized with a confocal microscope 15 minutes after incubation.

3.2.4 Cationic Liposomes for the Delivery of PIPs

Because of the effectiveness of cationic liposomes for cellular delivery of various charged substrates, we sought to examine the capability of applying this technology to PIP delivery. Cationic liposomes were formulated using 1,2-dimyristoyl-sn-glycero-3-phosphocholine (EDMPC), 1,2-dipalmitoyl-sn-glycero-3-ethylphosphocholine (EDPPC), 1,2-dioleoyl-sn-glycero-3-ethylphosphocholine (EDOPC), N,N-Dimethyltetradecylamine (di-C14 DAB), and 1,2-dimyristoyl-3-trimethylammonium-propane (DMTAP) according

to previous formulations proven effective at delivery of GFP plasmids were formulated include **BODIPY-PtdIns-C15** according to **Table 3.1** [105]. HEK293AD cells were incubated with liposomes to contain a final **BODIPY-PtdIns-C15** of 1 μ M. Cellular fluorescence was examined 15 minutes after incubation. While 2 of the 3 formulations showed an increase in cellular fluorescence as seen in **Figure 3.7** cell morphology indicated that the method was toxic to cells. Due to the toxicity of cationic liposomes with BODIPY-PtdIns-C15, new mechanisms of liposomal delivery were explored.

Table 3.1 Cationic Liposome Formulations for BODIPY-PIP₂-C15 Cellular Delivery

	Formulation (molar ratio)¹⁸
1	EDMPC:EDPPC:BODIPY-PtdIns-C15 (25:75:10)
2	EDOPC:diC14DAB: BODIPY-PtdIns-C15 (30:70:10)
3	EDOPC:DMTAP: BODIPY-PtdIns-C15 (60:40:10)

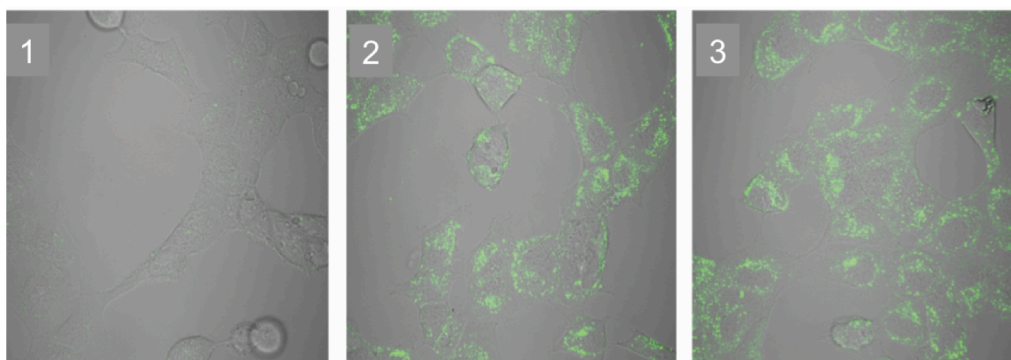


Figure 3.7 Cationic Liposome Delivery of BODIPY-PtdIns-C15 to Cells: HEK293AD cells (0.5 million) in growth medium (DMEM with 10% FBS, 2 mL) were plated into a 35 mm dish and were grown in an incubator at 37 C with 5% CO₂. After 24 h, the cells were treated with a cationic liposomes according to **Table 3.1** for a final **BODIPY-PtdIns-C15** concentration of 1 μ M. Cells were viewed with a confocal microscope following 15 minutes of incubation.

3.2.5 Fusogenic Liposomes for the Delivery of PIPs

Because of the broad range of applications of fusogenic liposomes and effective labeling of the plasma membrane in various cell lines with the addition of fluorescently tagged lipids, we sought to apply this method for the delivery of fluorescent **BODIPY-PtdIns-C15**. Effective labeling of the plasma membrane would present the lipid in the correct cellular location to be metabolized as well as avoid potentially detrimental endosome uptake and lysosome degradation [102]. Liposomes with known fusogenic

properties were formulated according to **Table 3.2** to include DOPE, DOTAP, and **BODIPY-PtdIns-C15** [84, 107, 108].

Liposomes were prepared by the lipid film method; briefly the lipids dissolved in chloroform were mixed in the desired ratios following by removal of solvent under a stream of N₂ and then dried under vacuum for 1 hour. Lipids were then resuspended in 25 mM HEPES (pH 7.4) for a lipid concentration of 2 mg/mL. HEK293-AD cells were treated with liposomes for a final concentration of **BODIPY-PtdIns-C15** of 1 µM and the cellular fluorescence was examined following 15 minutes of incubation. As seen in **Figure 3.8**, an increase in cellular fluorescence was observed for the liposomes and moreover the liposomes did not result in cellular toxicity as was the case previously using cationic liposome formulations.

Table 3.2 Fusogenic Liposome Formulations for BODIPY-PIP₂-C15 Cellular Delivery

	Formulation (Mass Ratio)^[20-22]
4	DOPE:DOTAP:BODIPY-PtdIns-C15 (1:1:0.2)
5	DOPE:DOTAP:BODIPY-PtdIns-C15 (1:1:0.1)
6	DOPE:DOTAP:DIR:BODIPY-PtdIns-C15I (1:1:0.1:0.2)

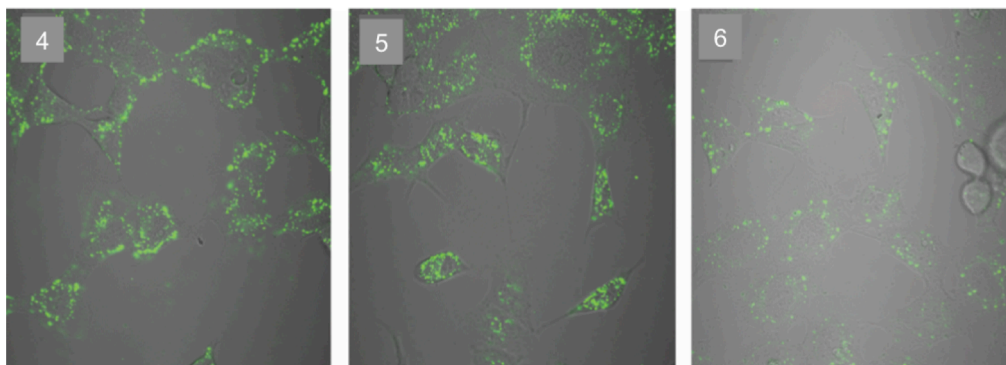


Figure 3.8 Fusogenic Liposome Delivery of BODIPY-PtdIns-C15 to Cells. HEK293AD cells (0.5 million) in growth medium (DMEM with 10% FBS, 2 mL) were plated into a 35 mm dish and were grown in an incubator at 37 C with 5% CO₂. After 24 h, the cells were treated with fusogenic liposomes formulated according to **Table 3.2** (2mg/mL final concentration) with a final **BODIPY-PtdIns-C15** concentration of 1 μ M. Cells were viewed with a confocal microscope following 15 minutes of incubation.

Next, we sought to do a preliminary evaluation of reporter stability/lipid metabolites to see if the method would be amenable to systematic metabolic analysis. We would expect to see a large concentration of **BODIPY-PtdIns-C15** with possible metabolites that could be compared with previously synthesized standards. Cell pellets were harvested and lipid contents were extracted via Folch extraction with acidic chloroform:methanol mixture and analyzed for the fluorescent lipid contents by TLC and

CE [62, 65, 71, 76]. The CE analysis was carried out by Dr. Angela Proctor in Dr. Nancy Allbritton's lab. Unfortunately, very little intact BODIPY-PtdIns-C15 was observed, with ~70% of the reporter converted to fluorescent DAG for each sample as seen in a representative CE trace and quantification in **Figure 3.9**. An unknown metabolite was also generated that was unable to be identified with available standards. It is unknown whether this was through PIP family of enzymes or non-specific cleavage occurring in the endosome/lysosome as the punctate structure of the fluorescence indicates this as the most likely mode of entry.

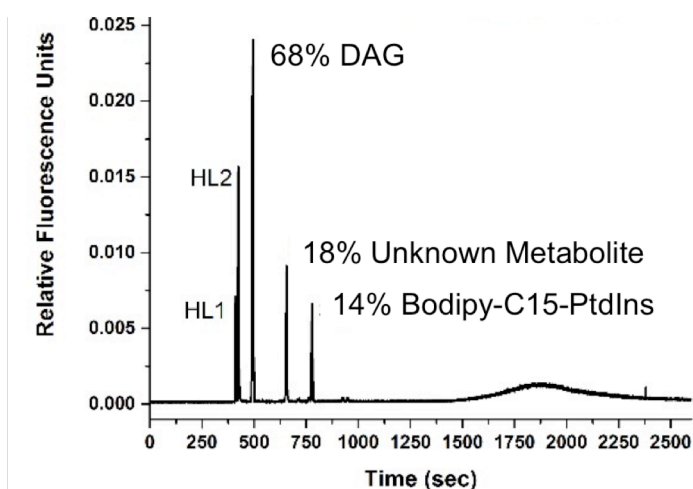


Figure 3.9 CE Analysis of Metabolites Generated using Fusogenic Liposome Delivery of BODIPY-PtdIns-C15. HEK293AD Cells were treated with fusogenic liposomes as described in **Figure 3.8** followed by lipid extraction after 15 minutes of incubation. Lipids were resuspended in propanol and analyzed by CE-LIF using synthesized fluorescent for peak identification.

The breakdown of the reporter lead to this method to be abandoned for a non-liposomal based mode as delivery. Overall, it does not appear liposomes are an effective method to use for the quantification of cellular PIP metabolites, most likely due to endosomal uptake of the liposome [100, 103, 105].

3.2.6 Intramolecular Charge Masking Strategy with Guanidine for the Delivery of Phospholipids

A unique and recently widely used cellular transfection is the use of guanidine rich molecular transporters on a variety of scaffolds[114]. Since the discovery that the HIV Tat protein was capable of crossing the cell membrane which is facilitated by the 9-mer Tat₄₉₋₅₇ (RKKRRQRRR) there has been increased interest in the mechanism of cell penetration by this peptide [115, 116]. When the 9-mer was modified to contain lysines instead of arginines, the efficacy of the cell penetrating peptide (CPP) dropped remarkably indicating that it was not simply the cationic charge carried by either of the residues[114, 117, 118]. This can be attributed to the ability of forming a bidentite hydrogen bond assisted ion pair with phosphate groups shown in **Figure 3.10**. When the hydrogen bond assisted interaction is removed by replacing the hydrogen atoms on the terminal guanidine amino groups with methyl groups, the cell penetrating properties of the peptide are lost further indicating the interaction is a vital part of cell penetration versus that of just charge [119].

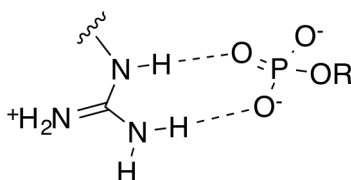
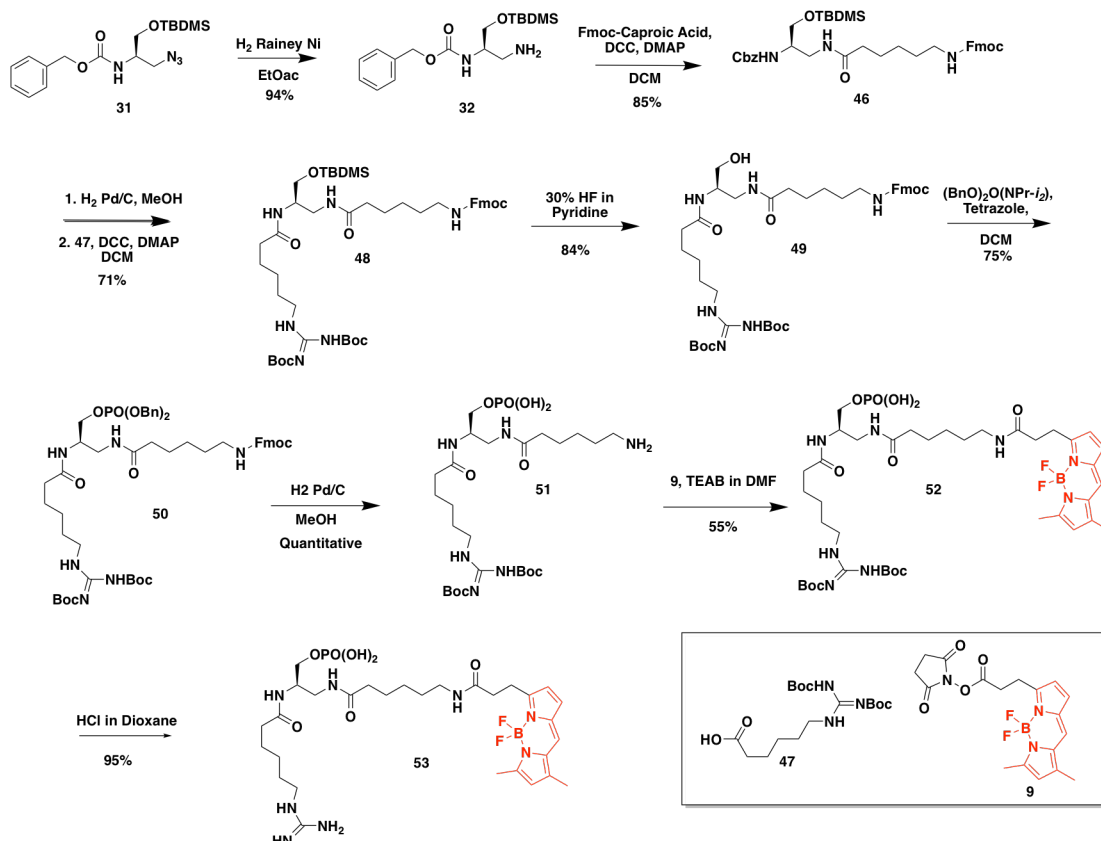


Fig. 3.10 Bidentite Interaction Between Guanidine and Phosphates. Hydrogen bond assisted ion pair between guanidine and phosphate groups resulting in a net neutral charge.

Since this discovery of guanidine promoting cell-penetration, guanidinium rich CPPs have been used for cellular transfection of various cargoes including small molecules, peptides, proteins, and oligonucleotides both non-covalently and covalently attached to the cargoes[114, 120, 121]. Various non-peptidic scaffolds such as glycosides, dendrimers, and carbohydrates have also been modified to contain guanidine moieties and have retained cell-penetrating functions again showing the power of guanidine to induce cellular uptake [95, 114, 117, 120, 122, 123]. Various modes of cellular uptake have been proposed including adaptive translocation where charge-neutralization moves the cargo through the membrane as well as induction of endocytosis because blocking of endocytosis does not fully negate cell-penetrating capability [114, 120].

Based on the success of an intermolecular carrier-cargo system with guanidine scaffolds, and the variety of modes of cellular uptake, we examined if inclusion of a guanidine moiety could allow for the cellular delivery of phospholipids. We explored an intramolecular phosphate masking strategy via a derivative of compound **36** by the addition of a guanidine group at the terminal end of the alkyl chain to generate compound **53** with the hopes of neutralizing the negative charge. We hypothesized that an intramolecular interaction would induce charge neutralization via proximity while also allowing for the guanidine to interact with the cell membrane and allow for cell-penetration. When applied to a fluorescent PIP reporter, such a technology would provide a simple and effective strategy for reporter delivery that does not require the use of multiple reagents and/or chemical manipulation of the reporters.

Guanidine containing model phospholipid compound **53** was synthesized according to **Scheme 3.2**. Azide **31** was synthesized according to literature protocol followed by reduction via H₂/Raney Ni to yield primary amine **32** [110]. Fmoc-caproic acid was then coupled via DCC and catalytic DMAP coupling to yield compound **46**. To generate compound **48**, the Cbz group was cleaved via hydrogenolysis in methanol followed by DCC/DMAP coupling of guanidine caproic acid **47**, which was synthesized according to literature protocol [124]. The silyl ether was removed via hydrogen fluoride in pyridine to yield a free alcohol **49**, which was subsequently phosphorylated via phosphoramidite coupling as previously described resulting in intermediate **50**. Cleavage of the Cbz as well as Bn deprotection of the phosphate group via hydrogenolysis yielded intermediate **51** which was then tagged with the fluorophore BODIPY using reagent **9** as described previously to yield fluorescent intermediate **52**. Finally, Boc deprotection of the guanidine was achieved with HCl in dioxane to yield final guanidine containing phospholipid compound **53**.



Scheme 3.2: Synthesis of Intramolecular Charge Masking Model Compound 53

With guanidine containing compound **53** in hand, we tested whether intramolecular masking of the phosphonic acid would render the compound cell permeable when compared to the cell uptake of compound **36**. HEK-293AD cells were incubated with 1 μM of compound **36** or compound **53** and cellular fluorescence was examined following 15 min of incubation. Unfortunately, the presence of a guanidine group did not increase cellular uptake of the model phospholipid as there was no discernable fluorescence increase for compound **36**, as previously described, and no fluorescence increase seen following treatment with compound **53**. Because of these

findings, this guanidine approach was not applied to PIP reporters and lead us to explore a novel carrier: cargo system that utilized polyamines and guanidine moieties.

3.2.7 Charge Altering Releasable Transporters (CARTs) for the Delivery of PIPs

A recent development in cellular delivery is the synthesized charge altering releasable transporters (CARTs) shown in **Figure 3.11** [96, 114, 125-127]. These transporters have been synthesized to contain both lipid units that contribute to required hydrophobicity for membrane interaction, which we have seen in the case of photocaging equally as important as neutralizing charge, as well as various cationic moieties to interact with polyanionic cargo and the negatively charged membrane. Interestingly, guanidine is a popular cationic moiety included in CARTs, again verifying our attempt at using guanidines previously in delivery [117, 125-127].

This technology is attractive because the oligomers can be ‘tuned’ using different monomers and degrees of polymerization for increased interaction with a specific cargo. In this method, polyanionic cargo is mixed in a 1:1 molar ratio with a CART to form a protective and CART-cargo complex that neutralizes the negatively charged cargo. This complex is then delivered to the cell via hydrophobic interaction and charge-charge interaction with the membrane where the cargo is released via hydrolysis of the CART releasing a neutral non-toxic small molecule and the polyanionic cargo to the cytosol [117, 125-127].

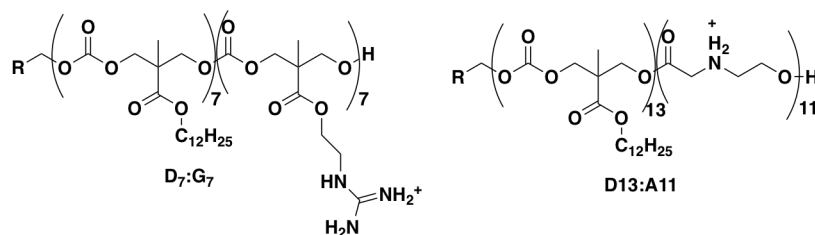


Figure 3.11 CARTs for the Delivery of BODIPY-PIP₂-C15: Structure of CARTs previously shown efficacious for the delivery of plasmids and inositol phosphates examined for their transfection capability of fluorescent PIP₂ reporters [108, 116-118].

Because of the stability of the cargo in complex with CARTs, they have been effective at the delivery of a wide range of cargos including small molecules, metals, imaging agents, siRNA and even proteins to both a variety of cell lines and animal models. D13:A11 (A11) was effective at EGFP mRNA delivery across a panel of cell lines with greater than 90% transfection efficiency in all cell lines, whereas lipofectamine achieved only 20-60% efficiency and results varied greatly amongst cell lines [125]. Likewise, A11 was effective at delivery of EGFP mRNA in mice making this a viable delivery vector for both *in vitro* experiments in both cell culture and animal models, and could potentially be used in therapeutic applications [125]. Guanidinium rich transporter D7:G7 (G7) was effective at the delivery of polyanionic *myo*-inositol derivative 5-diphospho-*myo*-inositol pentakisphosphate (InsP₇) [96]. Further, this structure contains guanidine groups that have been previously described as promising for delivery. Because of the similarity in the core structure to IP₃, it is probable, that this technology could be utilized to deliver other polyanionic inositol containing molecules. Therefore, we examined the ability of CARTs to deliver **BODIPY-PIP₂-C15** because of the polyanionic state of the inositol head group. HeLa cells were incubated with CART:PIP₂ complex with a final BODIPY-PIP₂-C15 concentration of 500 nM and cellular fluorescence was examined 2 hours

after incubation. As shown in **Fig 3.12**, CART:PIP₂ complexes resulted in a strong increase in cellular fluorescence compared to cells treated only with **BODIPY-PIP₂-C15** indicating delivery is indeed a result of the addition of the CART and charge neutralization.

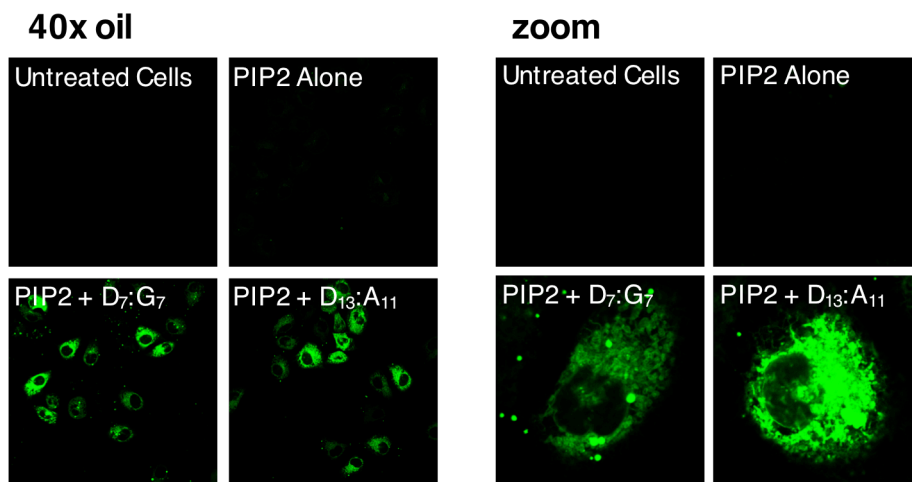


Figure 3.12 Delivery of BODIPY-PIP₂-C15 to Cells via CART systems A11 and G7. HeLa cells were incubated with PIP₂:CART complexes for 2 hours in serum free media. Cells were washed 2X with media and analyzed via confocal microscopy. Both G7 and A11 showed significant fluorescence increase with no fluorescence increase without the use of a transporter. Experiment performed by Dr. Collin McKinlay.

We next examined the basal metabolic profile produced from the CART delivery. Again HEK293-AD cells were incubated with CART:BODIPY-PIP₂-C15 (500 nM PIP₂) and cell pellets were collected following 30 minutes and 2 hours incubation. A Folch lipid extraction was performed to obtain all lipid metabolites followed by concentration of the bottom lipid layer under a stream of N₂. Lipid films were then resuspended in 1:1 chloroform:methanol for TLC analysis. As seen in **Figure 3.13**, both CARTs were successful in achieving cellular delivery, with the G7 CART delivering a larger amount of PIP₂ over 30 minutes than that of A7, with time dependent increase in cellular

fluorescence. Synthesized standards **BODIPY-DAG-15**, **BODIPY-PtdIns-C15**, and **BODIPY-PIP₂-C15** were used to identify new metabolic products produced in the experiment as well as confirm the presence of delivered PIP₂ reporter. A large amount of intact BODIPY-C15-PIP₂ was still present in the sample after 2 hours, a result that had yet to be achieved in the lab previously or with any other delivery method. Likewise, only small amounts of DAG were produced compared liposomal delivery. Following 2-hours of incubation, a strong BODIPY-PtdIns-C15 signal begins to appear as well as a small amount of **BODIPY-PIP₂-C15** though the regioisomer of PIP cannot be distinguished by TLC.

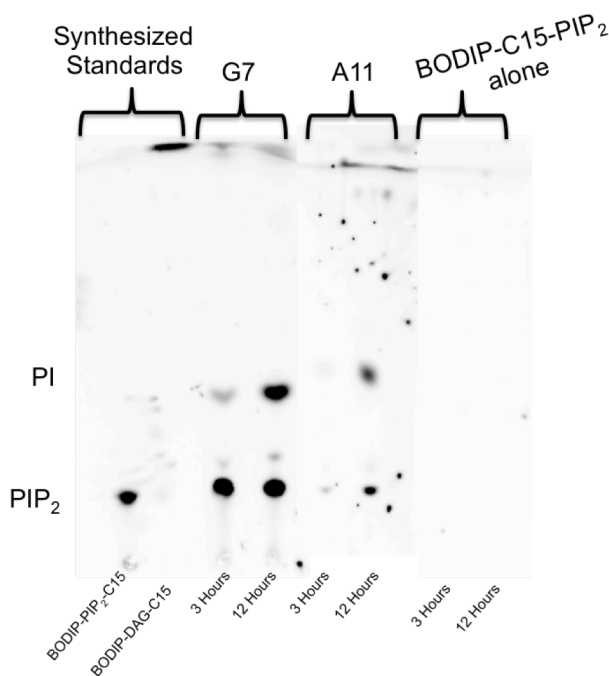


Figure 3.13 TLC analysis of Fluorescent Metabolites Generated from BODIPY-PIP₂-C15 in Cells using the CART System. HEK293-AD cells were treated with 500 nM of BODIPY-PIP₂-C15:CART complexes for the indicated time points followed by lipid extraction. Lipids were suspended in 1:1 chloroform:methanol and analyzed by TLC and fluorescent scanning.

3.3 Conclusions and Future Directions

We have examined a plethora of delivery techniques for the cellular delivery of fluorescent PIP reporters. Consistent with literature protocol, fluorescent DAG freely enters the cells. In contrast negatively charged PIP₂ and compound **36** are not cell permeable. In our attempts at histone delivery, we were unable to achieve cellular delivery with this method in multiple experiments. Likewise, literature reports of this method and analysis of metabolite generation look similar to our studies with fusogenic liposomes with DAG being the most abundant metabolite. Because of the inability to easily reproduce this method, as well as a metabolic profile that does not match the cellular distribution of lipids, this method is not effective for the systematic analysis of PIPs.

Direct neutralization of the negative charge, via covalent photocaging methods using MKS-1 greatly increased the delivery of caged **54** compared to **36**. However, preliminary examinations of caging **BODIPY-PtdIns-C15** or **BODIPY-PIP₂-C15**, not described in this thesis, was not effective in delivering reporters to cells. Due to the presence of bioactive hydrophobic moieties, such as butonyl, used in previous reports of photocaged PIPs it is likely we must increase the hydrophobic properties of **MKS-1**. Another potential problem for the photocaging of PIP₂ with **MKS-1** is the creation of a diphosphate ester, which is chemically unstable and can induce phosphate migration to neighboring hydroxyls. A possible change to the structure would be the introduction of a guanidine moiety or other cationic amine. This would create full charge neutralization with only the addition of a single photocaging group to each phosphate thus eliminating problems of stability. This could also increase delivery by

interacting directly with the membrane and result in a higher release efficiency because of the presence of fewer photo-cleavable groups.

Both cationic liposomes and fusogenic liposomes are not applicable to systematic analysis of PIPs. Cationic liposomes caused a high level of cell toxicity with suboptimal delivery as seen by fluorescence microscopy. This is more likely due to the entry mechanism or cellular perturbation by the liposome more so than BODIPY-PtdIns-C15 because of the low level of cellular delivery. Similarly, fusogenic liposomes showed low level of cellular delivery in punctate structures most likely to be endosomes. While the cells remained healthy, analysis of the metabolites revealed that in a short amount of time the reporter had been metabolized to DAG and an unknown metabolite. It is unknown if this is a result of nonspecific cleavage in the endosome or enzymatic turnover, however this profile does not represent the endogenous distribution of metabolites and is not applicable for use in biological studies.

Despite the widespread use of scaffolds containing guanidine for cellular delivery, our intramolecular charge masking strategy was ineffective at achieving cellular delivery of compound **53**. This, however, does not rule out future application of this design. It is possible that the alkyl chain containing the guanidine is not long enough to interact directly. Therefore future compounds should be synthesized altering the chain length and examining any changes in cellular delivery potential. This could also underscore the importance of the ratio between charge masking and hydrophobicity. It is possible that without intramolecular interaction, the reporter could enter via adaptive translocation through interaction with the guanidine and the membrane phospholipids and an increase in hydrophobicity may stimulate these effects.

. The most successful and promising delivery method was the use of CARTs in a carrier-cargo complex with **BODIPY-PIP₂-C15**. Both **A11** and **G7** were able to achieve significant delivery the fluorescent PIP₂, though the time dependent increase between the 2 carts was different suggesting a more efficient escape for the reporter using CART **G7**. **G7** also contains a guanidine moiety consistent with the hypothesis of guanidine containing compounds being effective at PIP delivery. Incubation with only 500 nM final concentration of fluorescent PIP₂ is far less than used in previous reporters of PIP₂ delivery while still providing enough reporter to visualize via fluorescence microscopy and for extraction to use for TLC and CE analysis [87, 94]. Further, extractions and analysis of lipid metabolites showed a distribution of metabolites consistent with endogenous substrates [39, 128]. Because of the consistency with previously reported distribution, we will begin to use this method for examining cellular distribution of metabolites in cancer cell lines in response to various stimuli and pharmacological agents. Further optimization of experimental parameters such as incubation time will need to be explored in a variety of cell lines as HEK293AD cells yielded different transfection efficiencies between **A11** and **G7**. This will ensure that loading and cellular concentration of reporter will be a factor in the experimental results. Overall this method is the most promising one in hand for use in systematic PIP cellular analysis, which will be detailed in chapter 4 of this dissertation.

3.4 Experimental

All reagents were obtained from commercial sources and were used without further purification. Thin layer chromatography was performed on 250 µm silica plates and column chromatographic purifications were performed on 200–300 mesh silica gel. ¹H

NMR and ^{13}C NMR spectra were recorded at 400 MHz and 100 MHz, respectively. Chemical shifts (δ) are reported in parts per million (ppm) with residual solvent resonances as references.

MKS-1 and **caged compound 54** were synthesized by Dr. Manish K. Singh

Dr. Colin McKinlay and Dr. Paul Wender from Stanford University generously provided all CARTs (A11 and G7).

3.4.1 Confocal Microscopy HEK293AD cells (0.5 million) in growth medium (DMEM with 10% FBS, 2 mL) were plated into a 35 mm dish and were grown in an incubator at 37 °C with 5% CO₂. After 24 h, the cells were treated with fluorescent reporter (1 µM). Cells were washed 2X with DMEM and visualized with a confocal microscope.

3.4.2 Preparation of Cationic Liposomes Cationic lipids and **BODIPY-PtdIns-C15** in chloroform (10 mg/mL) were mixed to their desired molar ratios (**Table 3.1**) followed by removal of solvent under a stream of N₂ and drying for 1 hour. The lipid film was resuspended in 25 mM HEPES buffer to give a final lipid concentration of 2 mM with 200 µM **BODIPY-PtdIns-C15** followed by sonication for 10 minutes. Liposome mixtures were then incubated with cells for a final **BODIPY-PtdIns-C15** concentration of 1 µM

3.4.3 Preparation of Fusogenic Liposomes Lipids and **BODIPY-PtdIns-C15** in chloroform (10 mg/mL) were mixed according to **Table 3.2** for a final lipid concentration of 2 mg/mL with 200 µM **BODIPY-PtdIns-C15** followed by removal of solvent under a stream of N₂ and drying for 1 hour. The lipid film was resuspended in 25 mM HEPES buffer followed by sonication for 10 minutes. Liposome mixtures were then incubated with cells for a final **BODIPY-PtdIns-C15** concentration of 1 µM.

3.4.4 Extraction of Lipid Metabolites

150 µL of 40:20:1 (v:v:v) CHCl₃:Methanol:HCl was added to the cell pellet and left at room temperature for 10 minutes. 50 µL of CHCl₃ and 50 µL of water were added and the mixture vortexed heavily for 3 minutes. The mixture was then centrifuged at 4°C at 3200 RPM for 8 minutes resulting in phase separation. The bottom layer was collected, dried under a stream of N₂ and resuspended in 30 µL of 1:1 CHCl₃:MeOH (v:v) for TLC analysis.

3.4.5 TLC analysis of Lipid Metabolites

TLC plates (Merck, Silica Gel-60) were pre-treated with a solution of 1.2% potassium oxalate and 1.2 mM EGTA in MeOH/water ($v:v = 2:3$) and heated at 110 °C for 20 min before use. Lipid films were diluted in CHCl₃/ MeOH ($v:v = 1:1$) and spotted on a TLC plate directly. The TLC plate was then developed in CHCl₃:Acetone:MeOH:AcOH:water ($v:v:v:v:v = 80:30:26:24:14$) and scanned on a Typhoon 9400 Variable Mode Imager ($\lambda_{\text{ex}}/\lambda_{\text{em}} = 488 \text{ nm}/520 \text{ nm}$). The fluorescence intensity of various spots on the TLC plate was quantified with ImageQuant software (V.5.0).

3.4.6 CE Analysis of Lipid Analytes

Capillary electrophoresis coupled with laser induced fluorescence detection (CE-LIF, 488 nm excitation) was performed on a custom-built system mounted to the stage of an inverted microscope, described previously in detail[75]. Fused silica capillaries were 38 cm long with a 20.5 cm effective length [30 μm inner diameter and 360 μm outer diameter (Polymicro Technologies; Phoenix, AZ)] and were conditioned prior to use by rinsing for 1 h in DI H₂O, 12 h in 0.1 M NaOH, 1 h in DI H₂O, 6 h in 0.1 M HCl, and 12 h in DI H₂O. Prior to each run, capillaries were rinsed with 1 M NaOH and DI H₂O for 5 min each and with electrophoretic buffer for 10 min by application of pressure to the capillary outlet. Buffer at the capillary inlet and outlet was completely refreshed prior to each electrophoretic run. The composition of the electrophoretic buffer was 80 mM NaH₂PO₄, pH 6.8 containing 15% 2-propanol and a field strength of 210 V cm⁻¹ was used for all separations. Internal standards and samples were hydrodynamically loaded by raising the inlet 3 cm relative to the outlet and holding the capillary inlet in the sample for 10 sec. The inlet was then lowered to the height of the outlet and electrophoresis

was initiated by application of a negative voltage to the outlet while grounding the inlet. Electropherograms were plotted and analyzed utilizing OriginLab 9.0 (OriginLab Corporation; Northampton, MA).

3.4.7 Chemical Synthesis

Synthesis of Benzyl (R)-(1-amino-3-((*tert*-butyldimethylsilyl)oxy)propan-2-yl)carbamate (32): To a solution of azide **31** (synthesized as previously described [110]) (620 mg, 1.7 mmol) in ethyl acetate (25 mL) was added a slurry of Rainey Ni. The reaction proceeded under a balloon of H₂ at room temperature for 3 h and was then filtered through celite. The filtrate was concentrated to afford amine **7** that was used directly without further purification (540 mg, 94%). ¹H NMR (400 MHz, CDCl₃) δ 7.24-7.33 (m, 5H), 5.33 (br. s, 1H), 5.08 (s, 2H), 3.60-3.70 (m, 3H), 2.82 (br. s, 2H), 1.95 (br. s, 2H), 0.80 (s, 9H), 0.02 (s, 6H). ¹³C NMR (CDCl₃, 100.5 MHz) δ 156.44, 136.62, 128.58, 128.42, 128.16, 128.02, 77.36, 66.76, 63.12, 54.19, 42.81, 25.92, 25.82, 18.29, 18.11 -3.42, -5.44. LC-MS Calcd [M+H] 339.20; found 339.2

Synthesis of Tert-butyl (R)-(6-((2-amino-3-((*tert*-butyldimethylsilyl)oxy)propyl)amino)-6-oxohexyl)carbamate (33): To a solution of **32** (250 mg, 0.74 mmol) in CH₂Cl₂ (15 mL) was added N-Boc caproic acid (205 mg, 0.87 mmol) followed by the addition of DCC (182 mg, 0.87 mmol) and DMAP (18 mg, 0.15 mmol). The reaction proceeded at room temperature for 4 h followed by removal of solvent and subsequent addition of EtOAc. The mixture was filtered and the filtrate concentrated under vacuum. The resulting residue was purified by column chromatography (67% EtOAc in hexane) to yield protected intermediate (345 mg, 85%).

The fully protected intermediate (150 mg, 0.27 mmol) was dissolved in methanol followed by the addition of 10 mol% Pd/C and the reaction proceeded overnight at room temperature under a balloon of hydrogen. The catalyst was filtered over celite, the filtrate was concentrated and the resulting residue was purified by flash chromatography (10% MeOH in CH₂Cl₂) over silica gel to yield pure free amine **8** (105 mg, 93%). ¹H NMR (400 MHz, CD₃OD) δ 3.64 (dd, *J* = 10.1, 4.8 Hz, 1H), 3.54 (dd, *J* = 10.1, 5.9 Hz, 1H), 3.34 – 3.26 (m, 2H), 3.14 (dd, *J* = 13.5, 7.0 Hz, 1H), 3.04 (t, *J* = 7.0 Hz, 2H), 2.99 – 2.89 (m, 1H), 2.22 (t, *J* = 7.5 Hz, 2H), 1.71 – 1.58 (m, 2H), 1.45-1.40 (m, 12H), 1.41 – 1.29 (m, 3H), 0.94 (s, 9H), 0.11 (s, 6H). ¹³C NMR (CD₃OD, 100.52 MHz) δ 176.50, 158.51, 79.76, 66.32, 65.85, 61.99, 57.65, 53.69, 49.85, 43.28, 41.17, 37.01, 34.76, 30.66, 28.81, 27.48, 26.65, 26.39, 19.15, -5.32. LC-MS Calcd [M+H] 418.30; found 418.3

Synthesis of *tert*-butyl (*R*)-(6-((3-((*tert*-butyldimethylsilyl)oxy)-2-heptanamidopropyl)amino)-6-oxohexyl)carbamate (34**):** To a solution of free amine **33** (120 mg, 0.29 mmol) and heptanoic acid (41 mg, 0.32 mmol) in CH₂Cl₂ (10 mL) was added DCC (65 mg, 0.32 mmol) and DMAP (7 mg, 0.06 mmol). The reaction proceeded at room temperature for 4 h followed by removal of solvent and subsequent addition of EtOAc. The mixture was filtered and the filtrate concentrated under vacuum. The residue was then purified by flash chromatography (67% EtOAc in hexane) over silica gel to yield compound **9** (122 mg, 89%). ¹H NMR (400 MHz, CD₃OD) δ 4.02 – 3.90 (m, 1H), 3.73 – 3.54 (m, 2H), 3.36 – 3.25 (m, 4H), 3.00 (t, *J* = 7.0 Hz, 2H), 2.26 – 2.11 (m, 3H), 1.57 (dt, *J* = 12.2, 7.4 Hz, 3H), 1.68 – 1.25 (m, 19H), 1.47 – 1.39 (m, 13H), 1.31 (q,

$J = 7.0, 5.1$ Hz, 6H), 0.99 – 0.88 (m, 12H), 0.06 (s, 6H). ^{13}C NMR (CD_3OD , 100.5 MHz) δ 176.62, 176.34, 64.18, 52.79, 49.85, 41.24, 41.18, 37.35, 37.04, 32.74, 30.68, 30.02, 28.80, 27.47, 27.03, 26.71, 26.38, 26.20, 23.59, 19.16, 14.41, -5.29, -5.33 . LC-MS Calcd $[\text{M}+\text{H}]$ 530.39; found 530.4

Synthesis of Tert-butyl (R)-(6-((3-((bis(benzyloxy)phosphoryl)oxy)-2-heptanamidopropyl)amino)-6-oxohexyl)carbamate (35): Silylated intermediate **34** (67 mg, .13 mmol) in THF (3.0 mL) was added commercial 30% HF in pyridine (250 μL). The reaction proceeded for 2.5 hours at room temperature followed by the addition of saturated sodium bicarbonate and extracted into EtOAc. The organic layer was collected, dried under Na_2SO_4 and concentrated under vacuum. The crude residue was purified by flash chromatography (5% MeOH in CH_2Cl_2) over silica gel to afford a free hydroxyl intermediate (48 mg, 89%). The free hydroxyl (48 mg, .12 mmol) was added to a solution of tetrazole (64 mg, .24 mmol) and commercial dibenzyl N,N-Diisopropylphosphoramidite (83 mg, .24 mmol) in anhydrous CH_2Cl_2 (4 mL) under Argon gas. The mixture stirred for 18 hours and was then cooled to -40°C followed by the addition of 5.5 M TBUOOH (85 μL). The mixture was allowed to warm to room temperature slowly followed by removal of solvents and the residue purified by flash chromatography (5% MeOH in CH_2Cl_2) over silica to afford pure phosphorylated compound **10** (60 mg, 75%) ^1H NMR (400 MHz, CD_3OD) 7.31-7.36 (m, 10H), 5.06 (s, 2 H), 5.04 (s, 2H) 4.15-4.21 (m, 1H), 3.96-4.06 (m, 2H), 3.80-3.89 (m, 1H), 3.22-3.44 (m, 4H), 2.98-3.5 (m, 2H), 2.09-2.20 (m, 4H), 1.44-1.68 (m, 6H), 1.40-1.43 (m, 9H), 1.20-1.39 (m, 6H), 0.88 (t, $J = 8$ Hz, 3H). ^{13}C NMR (CD_3OD , 100.5 MHz) δ 176.60, 176.35, 129.78, 129.70, 129.25, 128.18, 128.55, 128.43, 105.62, 105.27, 70.96, 70.91, 68.32,

68.27, 68.21, 68.14, 68.00, 62.76, 50.78, 50.75, 50.70, 50.47, 41.17, 40.47, 37.20, 37.02, 36.94, 36.71, 33.18, 32.72, 32.69, 30.65, 30.00, 29.95, 28.80, 27.46, 27.00, 26.88, 26.66, 26.60, 23.58, 23.56, 14.42. ^{31}P NMR (CD_3OD , 162 MHz) δ -1.38 (1P). LC-MS Calcd $[\text{M}+\text{H}]$ 676.36; found 676.3

Synthesis of (*R*)-3-(6-(3-(5,5-difluoro-7,9-dimethyl-5*H*-4 β ,5 β -dipyrrolo[1,2-*c*:2',1'-*f*][1,3,2]diazaborinin-3-yl)propanamido)hexanamido)-2-heptanamidopropyl

dihydrogen phosphate (36): Fully protected intermediate **34** (20 mg, 0.03 mmol) was dissolved in dioxane (2 mL) and added 4M HCl (500 μL). The reaction was monitored for completion by TLC (10% MeOH in CH_2Cl_2) for 3 h followed by removal of solvent under vacuum. The so-formed HCl salt (18 mg, 0.03 mmol) was dissolved in methanol (10 mL) followed by the addition of 10 mol% Pd/C and stirred overnight under a balloon of hydrogen at room temperature. The mixture was filtered through celite and filtrate concentrated under vacuum to yield fully deprotected free amine intermediate which was used directly in the next reaction. To the free amine (3.6 mg, 0.008 mmol) in 0.5 M TEAB buffer (150 μL) was added NHS-BODIPY (4.7 mg, 0.016 mmol) in DMF (150 μL). The mixture stirred overnight in the dark followed by removal of solvent under a stream of nitrogen gas. The crude reaction mixture was purified via HPLC (30-80% 0.1% TFA in MeOH over 60 min) to yield pure fluorescent compound **11** (3.6 mg, 46% combined from compound **10**). ^1H NMR (400 MHz, CD_3OD) δ 7.44 (s, 1H), 7.02 (d, J = 4.0 Hz, 1H), 6.33 (d, J = 4.1 Hz, 1H), 6.22 (s, 1H), 4.18 (s, 1H), 4.03 – 3.91 (m, 2H), 3.44 – 3.35 (m, 2H), 3.25 – 3.12 (m, 4H), 2.60 (t, J = 7.6 Hz, 2H), 2.52 (s, 3H), 2.29 (s, 3H), 2.23 – 2.15 (m, 4H), 1.55 – 1.40 (m, 6H), 1.38-1.25 (m, 6H), 0.90 (t, J =7.9 Hz, 3H). ^{13}C NMR

(CD₃OD, 100.5 MHz) δ 176.49, 176.18, 174.53, 129.66, 125.78, 121.30, 117.74, 111.44, 50.75, 50.66, 49.85, 49.50, 49.28, 49.07, 47.82, 40.98, 40.29, 37.27, 37.05, 36.02, 32.75, 30.09, 30.06, 27.60, 26.96, 26.64, 25.67, 23.60, 14.41, 11.19, 9.31; ³¹P NMR (CD₃OD, 162 MHz) δ 0.02 (1P) ESMS 670.30 [M+H]⁺

Synthesis of (9H-fluoren-9-yl)methyl (R)-(6-((2-(((benzyloxy)carbonyl)amino)-3-((tert-butyldimethylsilyl)oxy)propyl)amino)-6-oxohexyl)carbamate (46): To Fmoc-Caproic Acid (350 mg, 0.99 mmol) was added DCC (205 mg, 0.99 mmol), catalytic DMAP (23 mg, 0.19 mmol), and anhydrous DCM. The mixture was spun for 30 min followed by the addition of free amine (320 mg, 0.94 mmol) in DCM. The reaction proceeded for 4 hours followed by removal of solvent under vacuum. The mixture was then suspended in ethyl acetate and filtered followed by column chromatography (2:1 EtOac:Hex) to afford pure product (541 mg, 85%). ¹H NMR (400 MHz, CDCl₃) ¹H NMR (400 MHz, CDCl₃) δ 7.74 (d, *J* = 7.6, 2H), 7.58 (d, *J* = 7.6 2H), 7.47 – 7.30 (m, 6H), 6.18 – 5.97 (m, 1H), 5.44 – 5.27 (m, 1H), 5.07 (s, 2H), 4.88 (s, 1H), 4.37 (d, *J* = 7.0 Hz, 2H), 4.22 – 4.16 (m, 1H), 3.84 – 3.73 (m, 1H), 3.71 – 3.54 (m, 2H), 3.48 – 3.37 (m, 1H), 3.21 – 3.09 (m, 2H), 1.63 – 1.23 (m, 6H), 0.87 (s, 9H), 0.04 (s, 6H). ¹³C NMR (CDCl₃, 100.52 MHz) δ 173.74, 156.92, 156.58, 144.14, 141.34, 136.49, 128.65, 128.29, 128.17, 127.76, 127.14, 125.18, 120.07, 77.36, 66.95, 66.62, 63.80, 52.66, 49.94, 49.24, 47.43, 42.23, 41.70, 40.91, 36.49, 34.09, 29.83, 29.73, 26.36, 25.98, 25.81, 25.75, 25.22, 25.08, 18.35, 0.13, -5.38, -5.41 ESMS: 674.74[M+H]⁺

Synthesis of (Z)-6-(2,3-bis(tert-butoxycarbonyl)guanidino)hexanoic acid (47): To a solution of N-Caproic acid in MeOH at 0°C was added TEA slowly followed by addition of commercial diboc-triflyl-guanidine. The reaction proceeded overnight and was

monitored for disappearance of starting material (2:1 Hex: EtOAc). EtOAc was added and the mixture was then washed with 2M Sodium Bisphosphate. The organic layer was dried over Sat. sodium sulfate followed by column chromatography to afford pure N-guanidiny caproic acid (95%). ^1H NMR (400 MHz, CD_3OD) δ 3.34 (t, J = 7.1 Hz, 2H), 2.29 (t, J = 7.4 Hz, 2H), 1.72 – 1.54 (m, 4H), 1.50 (s, 9H), 1.45 (s, 9H), 1.40 – 1.35 (m, 2H). ^{13}C NMR (101 MHz, CD_3OD) δ 177.50, 164.55, 157.58, 154.23, 84.45, 80.36, 49.85, 49.64, 49.50, 49.43, 49.28, 49.21, 49.07, 49.00, 48.79, 48.57, 48.36, 41.64, 34.84, 29.86, 28.57, 28.22, 27.39, 25.72. ESMS: 174.3 $[\text{M}+\text{H}-\text{Boc}]^+$

Synthesis of 48: To a solution of CBz amine (200 mg, 0.130mmol) in methanol was added Pd/C (5 mol %). The reaction proceeded under a balloon of hydrogen for and monitored ever 30 minutes by TLC (10% MeOH in DCM) until completion to avoid the slower Fmoc deprotection. Following filtration and vacuum concentration, flash chromatography (10% MeOH in DCM) yielded pure amine as a colorless oil (135 mg, 85%). The free amine (80 mg, 0.15 mmol) was added immediately following addition of anhydrous DCM at 0°C to a solution of N-Guanidine Caproic Acid (85 mg, 0.22 mmol), DCC (45 mg, 0.22 mmol), and DMAP (3.8 mg, 0.03 mmol) The reaction proceeded for 4hr until the starting material was consumed. The reaction proceeded at RT for 2hr until starting material was consumed whereas solvent was evaporated EtOAc was added and solid filtered followed by column chromatography (5% MeOH in DCM) to afford pure material as a colorless oil (110mg, 84%). ^1H NMR (400 MHz, CDCl_3) δ 11.77 – 11.18 (m, 1H), 8.31 (d, J = 6.8 Hz, 1H), 7.76 (d, J = 6.8 Hz, 2H), 7.68 – 7.55 (m, 2H), 7.47 – 7.30 (m, 4H), 6.38 – 6.15 (m, 2H), 4.47 – 4.33 (m, 2H), 4.05 – 3.93 (m, 1H), 3.80 – 3.67 (m, 1H), 3.50 – 3.33 (m, 5H), 3.24 – 3.13 (m, 2H), 2.28 –

2.12 (m, 4H), 1.45-1.52 (m, 24H), 1.49 (s, 7H), 1.36 (s, 6H), 0.90 (s, 9H), 0.07 (s, 6H). ^{13}C NMR (CDCl_3 , 100.52 MHz) δ 174.17, 173.82, 156.63, 156.26, 153.47, 144.17, 141.45, 127.79, 127.16, 125.21, 120.09, 110.17, 83.24, 79.42, 77.36, 68.13, 66.65, 63.35, 51.51, 47.47, 40.90, 36.66, 36.58, 29.80, 28.95, 28.47, 28.23, 28.18, 26.63, 26.44, 26.02, 25.41, 25.34, 18.38, 0.15, -5.26, -5.36. ESMS: 894.5 $[\text{M}]^+$

Synthesis of 49: A solution of protected hydroxyl (100 mg, 0.11 mmol) in THF (3.4 mL) was added commercial 30% HF in pyridine (300 μL). The reaction was monitored to completion by TLC (10% MeOH in DCM) and after 2.5 hrs saturated sodium bicarbonate was added followed by extraction into EtOAc. The organic layer was dried over saturated NaSO_4 followed by column purification (10% MeOH in DCM) to afford pure hydroxyl as a colorless oil (74 mg, 85%). ^1H NMR (400 MHz, CDCl_3) δ 11.54-11.45 (m, 1H), 8.34 – 8.29 (m, 1H), 7.76 (d, $J=7.5$ Hz, 2H), 7.59 (d, $J = 7.5$ Hz, 2H), 7.44-7.29 (m, 4H), 6.37 (d, $J = 7.6$ Hz, 1H), 6.25 (s, 1H), 5.08 – 4.84 (m, 1H), 4.40 (d, $J = 6.9$ Hz, 2H), 4.21 (t, $J = 6.7$ Hz, 1H), 3.86 (s, 1H), 3.74 – 3.57 (m, 1H), 3.50 (d, $J = 10.6$ Hz, 2H), 3.38 (q, $J = 6.3$ Hz, 2H), 3.32 – 3.14 (m, 3H), 2.25 – 2.17 (m, 4H), 1.52-1.55 (m, 4H) 1.32-1.59 (M, 30H). ^{13}C NMR (CDCl_3 , 100.52 MHz) δ 173.48, 169.65, 169.08, 163.70, 156.28, 153.47, 144.11, 127.83, 127.18, 125.15, 120.13, 83.27, 79.46, 77.36, 66.70, 61.82, 51.58, 47.44, 40.88, 39.71, 36.50, 36.32, 31.09, 29.76, 28.85, 28.85, 28.23, 26.48, 26.26, 25.40, 25.17, 0.15 ESMS: 781.4 $[\text{M}+\text{H}]^+$

Synthesis of 50: To a solution of tetrazole (44 mg, .167 mmol) and hydroxyl (65 mg, .08 mmol) in anhydrous DCM was added drop-wise commercial Dibenzyl N,N-Diisopropylphosphoramidite (56 μL , .166 mmol). Reaction was monitored by TLC (5% MeOH in DCM) and after 24 hr. the mixture was cooled to -40°C followed by the

addition of 5.5M TBUOOH (60 μ L) . The reaction mixture was warmed slowly, concentrated, and purified via column chromatography (5% MeOH in DCM) to afford pure product (65 mg, 75%) ^1H NMR (400 MHz, CD_3OD) δ 7.76 (d, J = 7.5 Hz, 2H), 7.61 (d, J = 7.5 Hz, 2H), 7.40 – 7.21 (m, 14H), 5.03 (dd, J = 8.4, 1.7 Hz, 4H), 4.30 (d, J = 6.9 Hz, 2H), 4.26 – 4.11 (m, 2H), 4.11 – 3.91 (m, 2H), 3.39 – 3.21 (m, 4H), 3.08 (t, J = 6.9 Hz, 2H), 2.29 – 2.01 (m, 4H), 1.71 – 1.53 (m, 4H), 1.45-1.48 (m, 24H) 1.35 – 1.23 (m, 6H). ^{13}C NMR (CD_3OD , 100.52 MHz) δ 176.52, 176.02, 164.14, 158.78, 157.29, 154.12, 145.31, 144.38, 142.54, 137.06, 137.04, 136.99, 136.98, 129.76, 129.69, 129.22, 129.16, 129.15, 128.74, 128.51, 128.40, 128.11, 126.15, 120.91, 111.37 84.50, 80.54, 70.93, 70.88, 68.28, 68.23, 67.53, 50.76, 50.68, 48.46, 41.70, 41.54, 40.48, 36.92, 30.54, 29.74, 28.58, 28.22, 27.34, 26.53, 26.47. ^{31}P NMR (CD_3OD , 162 MHz) δ 0.15 (1P)

Synthesis of 52: To a solution of benzyl and Fmoc protected intermediate **50** (12 mg, 0.011 mmol) in methanol was added 5 mol% Pd/C. The reaction was stirred overnight under a balloon of hydrogen gas. Following filtration of catalyst free phosphate ester and free amine was achieved in quantitative yield 7.35 mg, 0.011 mmol) as a colorless oil **51**. To **51** (5 mg, .008 mmol) in 0.5M TEAB buffer was added NHS-Fluorophore in DMF in a total reaction volume of 300 μ L. The mixture stirred overnight in the dark followed by removal of solvent under a stream of nitrogen gas. The crude mixture was purified by HPLC (30-80% 0.1% TFA in Methanol over 30 minutes product elutes at 43 minutes) to yield Boc-protected fluorogenic compound (55% 3.8 mg). ^1H NMR (400 MHz, CD_3OD) δ 7.44 (s, 1H), 7.02 (d, J = 4.0 Hz, 1H), 6.32 (d, J = 4.0Hz, 1H), 6.22 (s 1H), 4.15-4.22 (m, 1H), 3.81-4.02 (m, 2H), 3.45-3.55 (m, 2H), 3.35-3.40 (m, 2 H), 3.14-

3.22 (m, 4H), 2.61 (t, $J = 7.6$ Hz, 2H), 2.52 (s, 3H), 2.29 (s, 3H), 2.18-2.27 (m, 4H), 1.30-1.72 (m, 30H). ^{31}P NMR (CD_3OD , 162 MHz δ -0.06 (1P). ESMS: 913.5 $[\text{M}+\text{H}]^+$; 713.5 $[\text{M}-\text{BOC}+\text{H}]^+$

Synthesis of guanidine containing model system 53: Intermediate **52** (0.8 mg, 0.9 μmol) was dissolved in dioxane and treated with 0.5 M HCl. The reaction proceeded 4 hours followed by removal of solvent yielding a fully deprotected HCl Salt (0.5 mg, 84%) ^1H NMR (400 MHz, CD_3OD) ^1H NMR (400 MHz, CD_3OD) δ 7.44 (s, 1H), 7.02 (d, $J = 4.0$ Hz, 1H), 6.33 (d, $J = 4.0$ Hz, 1H), 6.22 (s, 1H), 4.23 – 4.12 (m, 1H), 3.81-4.02 (m, 2H), 3.49 (s, 1H), 3.40 – 3.34 (m, 2H), 3.25 – 3.12 (m, 4H), 2.61 (t, $J = 7.7$ Hz, 2H), 2.52 (s, 2H), 2.29 (s, 2H), 2.26 – 2.15 (m, 3H), 1.72-1.30 (m, 30H). NMR (CD_3OD , 162 MHz δ -0.20 (1P). ESMS: 713.3 $[\text{M}+\text{H}]^+$

Synthesis of (R)-(6-((3-((bis(benzyloxy)phosphoryl)oxy)-2-heptanamidopropyl)amino)-6b-oxo-4,5-dihydro-2H-1,2,4-triazol-2-yl) phosphate (54) :

To an eppendorf tube charged with a stir bar and the bis(triethylammonium) salt of uncaged model compound 10 (0.7mg, 0.0008 mmol) was added MeOH (200 μL) followed by aq. HCl (1 M, 2.4 μL). To the stirring solution was added diazonium compound 2 (1.4 mg, 0.0064 mmol). The reaction mixture was stirred at room temperature for 10 min and evaporated to dryness. ^{31}P NMR of the crude material showed incomplete reaction. To the same crude material was added MeOH (200 μL) followed by HCl (1 M, 3.0 μL). To the stirring solution was added diazonium compound 1 (1.4 mg, 0.0064 mmol). The reaction mixture was stirred for 10 min and the solvent was removed. ^{31}P NMR of crude mixture showed complete consumption of the starting material. The residue was purified by column chromatography over silica gel

(4% MeOH in CH₂Cl₂) to provide 11 (0.5 mg, 59%) as red solid. ¹H NMR (400 MHz, CD₃OD): δ 7.63 (s, 2H), 7.34 (s, 1H), 7.04 (s, 2H), 6.94 (d, J = 3.9 Hz, 1H), 6.27 (d, J = 4.1 Hz, 1H), 6.16 (s, 1H), 5.41 (d, J = 8.1 Hz, 4H), 4.16 (m, 3H), 3.87 (s, 12H), 3.38 (m, 2H), 3.15 (m, 4H), 2.57 (t, J = 8.1 Hz, 2H), 2.46 (s, 3H), 2.24 (s, 3H), 2.16 (q, J = 7.0, 14.0 Hz, 4H), 1.55 (m, 6H, 3 CH₂), 1.28 (br. s, 8H), 0.86 (td, J = 6.5, 13.5 Hz, 3H). ³¹P NMR (161.5 MHz, CD₃OD): δ -1.88 (1P). ESMS: m/z 572.5 (M - C₁₈H₂₀N₂O₁₂P)⁺.

CHAPTER 4. INVESTIGATION OF CELLULAR PHOSPHOLIPID METABOLISM WITH FLUORESCENT REPORTERS

4.1 Introduction

With a suite of fluorescent reporters in hand, shown in **Figure 4.1** and described in Chapter 2 of this dissertation, as well as a successful delivery method for charged PIPs described in Chapter 3, we sought to confirm the capability of these reporters to undergo cellular metabolism to a variety of PIP metabolites. We chose to analyze cellular activity of DAGK using our **BODIPY-DAG-C15** reporter as well as cellular activity of PI3K using **BODIPY-PIP₂-C15** in a variety of breast cancer cell lines due to the prevalence of mutations in multiple PIP modifying enzymes including PI3K and PTEN [5, 17, 37, 44, 129]. In previous studies using classical methods of detection including radiolabeled substrate, PI3K was stimulated under variety of conditions including insulin growth factor (IGF), EGF and N-formyl-met-leu-phe (fMLP). In these studies, a distinct difference in metabolic profiles, specifically PIP₃ production is observed with PIP₃ capable of being resolved by TLC following short (<10 minutes) stimulation whereas limited to no detectable PIP₃ is observed in nonstimulated samples [130]. Likewise, other lipid modifying enzymes including diacylglycerol kinase (DAGK) have also been shown to be important in anchorage independent growth of breast cancer cells [22, 61, 109, 131]. Hepatocyte growth factor (HGF) stimulation lead to an increase in production of PA via activation of DAGK in MDA-MB-231 cells as well as dose dependent DAGK stimulation by synthetic DAG and other lipid metabolites via

radiolabeled TLC analysis[109]. We chose to examine the metabolite distribution in multiple breast cancer cell lines seen in **Figure 4.2A** and possess mutations within the PI3K pathway highlighted in **Figure 4.2B**. MDA-MB-436 cells do not express tumor suppressor enzyme PTEN, which catalyzes the dephosphorylation of the 5-phosphate in PIP₃. Alternatively, MDA-MB-453 cells possess the PI3K mutation H1047R, which leads to increased basal and stimulated activity of the enzyme through increased affinity for lipid binding [46]. These genetic changes should result in higher levels of PIP₃ in MDA-MB-436 and MDA-MB-453 cells. We also chose to compare these 2 cell lines for their overall distribution of metabolites to better understand how the collective of metabolites is controlled in the various disease models and the effects of the pathway mutations on metabolite distribution.

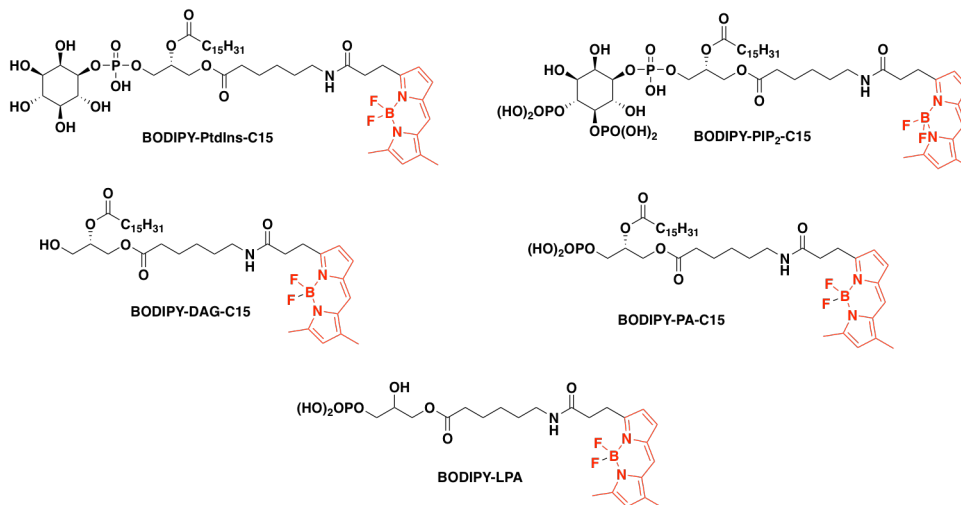


Figure 4.1 Suite of Fluorescent Reporters to Probe Various PIP Metabolic Pathways: A suite of fluorescent reporters with the sn-2 and sn-3 chains held constant for separation by CE. The synthesis for these compounds is described in Chapter 2.

In this chapter, we describe the application of our suite of fluorescent-tagged PIPs and lipid metabolites for monitoring of cellular PIP metabolism first utilizing **BODIPY-DAG-C15** to demonstrate the proof of principle. We then used **BODIPY-PIP₂-C15** in complex with the CART systems for delivery, described in chapter 3, to monitor metabolite distribution following a variety of incubation times. We believe this method when coupled with TLC and fluorescent scanning and/or CE-LIF will be capable of providing a detailed profile of multiple PIPs simultaneously with the capability of monitoring changes due to pathway mutations, stimulation, or inhibition.

A.

Cell Line	PI3K Pathway Mutation	Phenotypic Result
MDA-MB-436	PTEN (-/-)	No PTEN Expression
MDA-MB-453	PI3K (H1047R)	Increased Basal and Stimulated Activity

B.

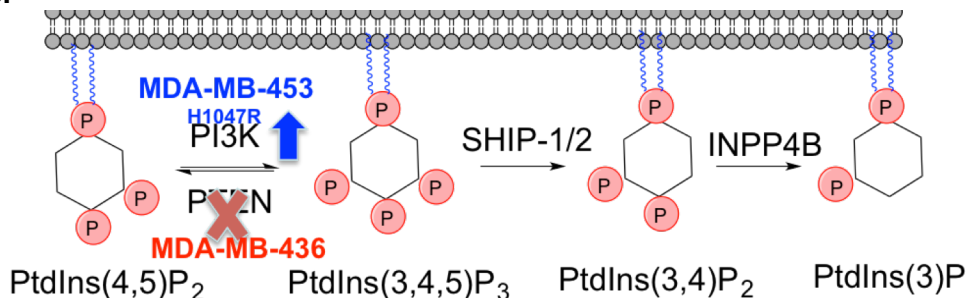


Figure 4.2: Breast Cancer Cell Lines for PI3K Pathway Metabolic Analysis: A. Table of selected breast cancer cell lines, associated PI3K pathway mutation, and phenotype of the cells. B. Schematic showing locations and result of mutations within the PI3K Pathway.

4.2 Results and Discussion

4.2.1 Concentration Dependent Production of PA using BODIPY-DAG-C15

As a proof of concept, we first examined the conversion of **BODIPY-DAG-C15** to its corresponding phosphorylated metabolite by DAGK, **BODIPY-PA-C15**. It has been

demonstrated on various occasions that cellular PA production increases when incubated with increasing concentrations of DAG using radiolabeled substrate and TLC analysis [11, 21]. We sought to duplicate this result using our fluorescent **BODIPY-DAG-C15** reporter. Previously, we have demonstrated that **BODIPY-DAG-C15** is cell permeable. HEK293-AD cells were thus incubated with 2, 10, 50, or 100 μM of BODIPY-DAG-C15 for 5 minutes which lead to optimal PA production as PA is quickly degraded with little remaining radiolabeled PA present after 15 minutes of incubation [11, 21]. Folch lipid extraction of slightly acidic chloroform:methanol was performed to isolate the fluorescent metabolites and subsequently analyzed by TLC [21, 59]. A stronger fluorescent signal consistent with the same *R_f* of synthesized BODIPY-PA-C15 standard is observed when incubated with increasing concentrations of DAG as seen in **Figure 4.3**, consistent with previous reports using a di-C8 DAG substrate [11, 21].

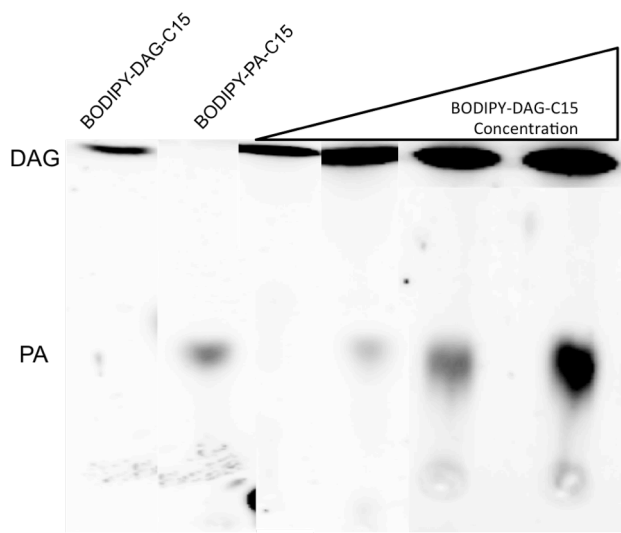


Figure 4.3 Concentration Dependent Increase of PA Production with BODIPY-DAG-C15: HEK293AD cells were treated with increasing concentrations (2-100 μM) of **BODIPY-DAG-C15** for 5 minutes followed by lipid extraction and TLC analysis. A spot consistent with PA is produced in increasing intensity in a dose dependent manner.

This experiment highlighted the utility in using our fluorescent suite of molecules as both a reporter, in the case of DAG-C15, and a metabolic product in the form of PA. Likewise, it demonstrates that it is feasible to use our technology to monitor environmental changes within the cell.

4.2.2 Delivery of BODIPY-PIP₂-C15:CART Complex to Breast Cancer Cells

With the ultimate goal of monitoring PIP₃ generation in breast cancer cells, we wanted to ensure that our previously explored method of delivery utilizing a CART: BODIPY-PIP₂-C15 complex was also effective for delivery to breast cancer cell lines. MDA-MB-436 and 453 cells were incubated with CART:PIP₂ complex with a final **BODIPY-PIP₂-C15** concentration of 500 nM. Cellular fluorescence was examined after of incubation for 1 and 18 hours, respectively. As seen in **Figure 4.4** the CART system was capable at efficient and robust delivery of fluorescent reporter, with only 453 cells pictured.

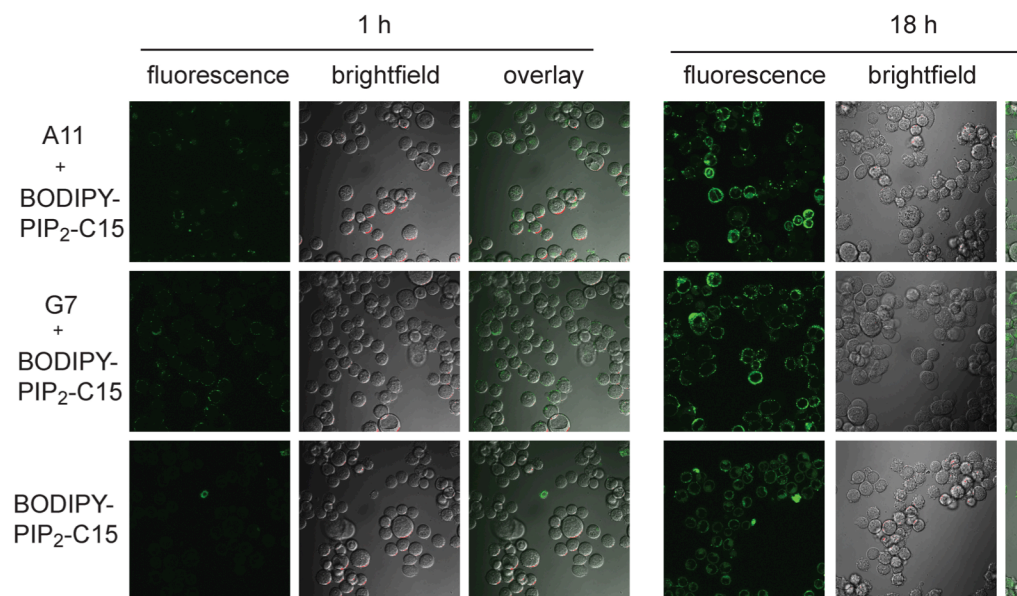


Figure 4.4. Delivery of BODIPY-PIP₂-C15 into MDA-MB-453 cells with CARTs: MDA-MB-453 cells (200,000 cells) were plated into a 35 mm dish and incubated at 37 °C with 5% CO₂ for 24 h. The growth medium was replaced with serum free DMEM before the cells were treated with a 1:1 complex of **BODIPY-PIP₂-C15** and A11 or G7, or BODIPY-PIP₂-C15 alone. The final concentration of BODIPY-PIP₂-C15 was 500 nM. The cells were washed with DMEM twice before images were recorded with a confocal microscope.

4.2.3 Cellular Analysis of BODIPY-PIP₂ Metabolites in MDA-MBA-436 Cells

Following confirmation of cellular delivery into breast cancer cell lines, we sought to analyze the basal metabolic activity in MDA-MB-436 using both CARTs G7 and A11 with **BODIPY-PIP₂-C15**. Ideally we would be able to monitor basal metabolism with a distribution pattern of fluorescent metabolites that reflects endogenous metabolite distribution. Because these cells lack PTEN expression, we would expect to see a buildup of PIP₃ over time with the inability to metabolize the product back to PIP₂. Cells were treated with CART:PIP₂ complex with a final **BODIPY-PIP₂-C15** concentration of 500 nM. Following incubation for 3 and 12 hours cell pellets were collected and lipids were extracted for analysis. As shown in **Figure 4.5**, multiple metabolites were

generated using both A11 and G7, with slightly different metabolite profiles. Fluorescent standards of **BODIPY-DAG-C15**, **BODIPY-PA-C15** and **BODIPY-PtdIns-C15**, and enzymatically generated **BODIPY-PI(4)P-C15** were used to identify metabolites present in the samples. Both samples lead to the generation of a high level of PtdIns with increasing concentration of PIP over time. TLC analysis cannot assign the identity of the PIP as two possible isomers, PI4P and PI5P, should have similar R_f values. We thought it is likely to be PI4P, because previous studies analyzing the effect of Wnt stimulation on PIP metabolism showed an increase in PIP₂ production that was subsequently blocked by treating cells with siRNA targeting PI4K, indicating PI(4)P is a key intermediate in PIP₂ production [9, 10]. These results closely represent endogenous PIP distribution with PtdIns being the most abundant fluorescent metabolite followed by PIP₂ and the intermediate PIP suggesting our system was successful in monitoring multiple metabolite generation simultaneously while being distributed throughout the PIP metabolic pathway similarly to endogenous metabolites. Interestingly, the 2 CARTs also yielded different profiles of metabolites with the cells treated with A11 showing a large abundance of fluorescent PA whereas little was generated with the G7 delivery system. This could be related to the difference in uptake of the systems that was observed in fluorescence microscopy. This distribution of metabolites is remarkably similar to distribution of metabolites seen when doing long-term (>24 h) incubation with radiolabeled substrate [39, 66, 128].

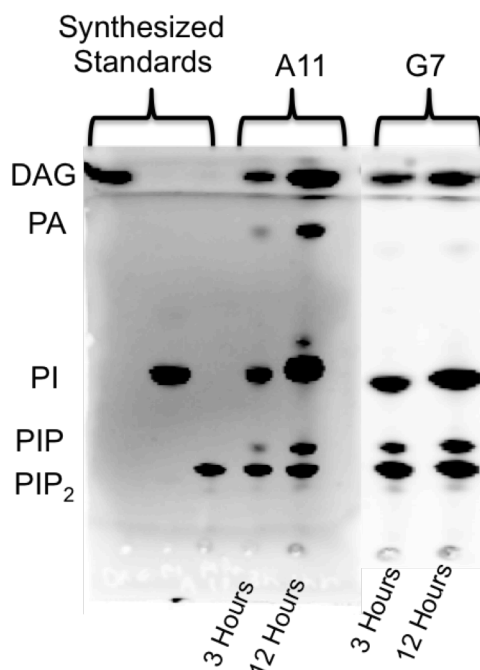


Figure 4.5 Analysis of Fluorescent Metabolite Distribution in MDA-MB-436 Cells: Cells (6 million) were treated with 500 nM of **BODIPY-PIP₂-C15:CART** as complexes as previously described for the indicated time points followed by lipid extraction of cell pellets. Metabolites were assigned using synthesized standards

Despite this positive result, no quantifiable PIP₃ was generated in this experiment. While we would expect to see increased accumulation of PIP₃ due to the lack of PTEN, it is possible PIP₃ could be terminated through SHIP metabolism generating PI(3,4)P₂, which would comigrate with PI(4,5)P₂ on TLC. Future experiments using a SHIP inhibitor should be performed to attempt to ‘trap’ any PIP₃ produced over time as illustrated in **Figure 4.6**.

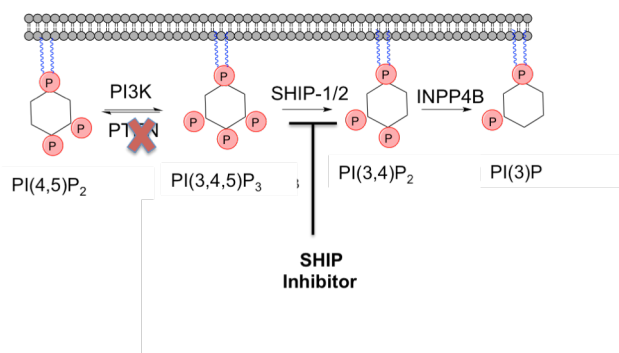


Figure 4.6 Method to ‘Capture’ Fluorescent PIP₃ Produced in MDA-MB-436 Cells: Treating PTEN deficient cells with a SHIP inhibitor over a long-time course incubation may allow for trapping of any PIP₃ produced that is below the detectable limit in previous experiments.

4.2.4 Cellular Analysis of BODIPY-PIP₂-C15 Metabolites in MDA-MB-453 Cells

With the goal of monitoring PIP metabolism in patient samples that will have unique genetic profiles, we wanted to examine and compare the metabolism of our reporter in another breast cancer cell line MDA-MB-453. These cells possess a mutation in the P110a subunit of PI3K that renders the enzyme constitutively active and should result in an increase in PIP₃ generation over time. Cells were treated with G7-CART:PIP₂ complex with a final **BODIPY-PIP₂-C15** concentration of 500 nM. Following incubation for 1 and 3 hours cell pellets were collected and lipids were extracted for analysis. We chose to do a shorter time course to achieve a higher concentration of cellular BODIPY-PIP₂-C15 before it undergoes cellular distribution with the goal of monitoring production of PIP₃. As with the 436 cells, no cellular PIP₃ was observed with a similar distribution of PtdIns and PIP as seen in **Figure 4.7**. However, unlike the 436 cells the most abundant fluorescent signal comes from PIP₂ and not PtdIns suggesting differential metabolism of the reporter despite using the same delivery vehicle. The high concentration of PIP₂ could also be a result of the presence of active PTEN in MDA-MB-

453 cells that could diminish PIP_3 back to PI(4,5)P_2 despite the overactive PI3K. This presence of PTEN could explain the difference in metabolite profiles between MDA-MB-436 and 453 cells suggesting differential mechanisms to diminish total PIP_3 produced.

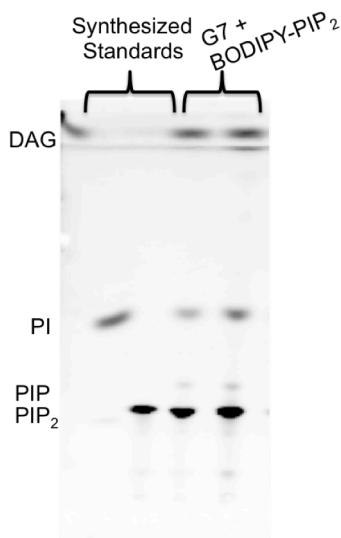


Figure 4.7 Analysis of Fluorescent Metabolite Distribution in MDA-MB-453 Cells: Cells (6 million) were treated with 500 nM of **BODIPY-PIP₂-C15:CART** complexes as previously described for the indicated time points followed by lipid extraction. Metabolites were assigned using synthesized standards.

4.3 Conclusions and Future Directions

We have successfully demonstrated the capability of using a fluorescent reporter for analysis of various lipid metabolites. **BODIPY-DAG-C15**, which freely enters cells, was converted to the corresponding PA in a dose dependent fashion showing that indeed a fluorescent reporter is capable of monitoring changes in lipid metabolism. Further experiments need to be performed using a single low concentration of **BODIPY-DAG-C15** and various stimulation events. One such experiment that could verify the system against literature precedent would be the analysis of PA production using **BODIPY-DAG-C15** and stimulating with the non-fluorescent di-C8-DAG, as this

substrate has been used to stimulate DAGK activity as previously described in this chapter. This will be more representative of a biological application where a small amount of fluorescent reporter would be used to monitor intracellular metabolism. DAGK has been widely studied in Jurkat cell lines, therefore we plan to apply this technology to analysis of PA production and metabolite distribution in a leukemia model system[6, 11, 21, 22, 59, 132].

We have also demonstrated the strategy for PIPs generating multiple metabolites using **BODIPY-PIP₂-C15**. In combination with CARTs **A11** and **G7**, we were successful in delivering **BODIPY-PIP₂-C15** to multiple breast cancer cell lines harboring separate and distinct PI3K pathway mutations. Upon delivery, **BODIPY-PIP₂-C15** underwent cellular metabolism to generate a variety of PIP metabolites that were confirmed using synthesized standards. An incubation time of 3 and 12 hours with **BODIPY-PIP₂-C15** in MDA-MB-436 cells revealed a distribution of metabolites consistent with the endogenous ratios of PIPs [20, 39, 65, 66, 68]. Further, this profile was consistent with previously reported basal PIP analysis using radiolabeled inositol and ATP over a similar time course[66, 133]. Unfortunately we were unable to obtain measurable generation of PIP₃ by TLC. Because PIP₃ is a potent secondary activator, it is quickly generated and degraded by multiple mechanisms; therefore it is likely any PIP₃ is below our measurable range[16, 17, 25]. Comparison of PIP₃ production using mass spectrometry following fMLP stimulation in MCF10A cells showed that in many cases less than 1% of a total PIP₂ population is converted to PIP₃[64, 67]. Likewise, there has been more success in measuring PIP₃ production using radiolabeled substrates under stimulatory conditions such as EGF with maximal PIP₃ production at 5 minutes following

stimulation in HL60 cells. Therefore it is probable that any PIP_3 produced in unstimulated cells is below the level of detection. Future experiments will be performed using cell lines such as MCF10A or HL60 under a variety of stimulatory conditions, including fMLP and EGF, which have previously been demonstrated to produce detectable levels of PIP_3 in bulk cell analysis by TLC and mass spectrometry as well as single-cell analysis by flow cytometry [7, 67, 133]. Such an experiment is important to verify we are capable of measuring changes to cellular metabolism following stimulation events using **BODIPY- PIP_2 -C15**. Likewise, treatment of MDA-MB-436 cells with a SHIP inhibitor to 'trap' any PIP_3 produced would also be a useful experiment in examining the utility of our system following cellular perturbation using pharmacological agents.

In a shorter incubation of **BODIPY- PIP_2 -C15** using carrier **G7** in MDA-MB-453 cells harboring the activating H1047R PI3K mutation we saw the major metabolite present to be the delivered reporter with fluorescent PtdIns present as well. As before we were unable to detect fluorescent PIP_3 in the mixture, which could be a result of numerous previously described mechanisms. However, because the system in this time shows a less complex metabolic profile these conditions can be utilized to monitor future studies performed following receptor stimulation. This will give the greatest opportunity to both analyze production of PIP_3 while also allowing comparison of the distribution of various metabolites following receptor stimulation. Because of the shorter incubation time required with CART G7 it will be used exclusively in future experiments. Studies in previously mentioned cell lines will be performed following a variety of incubation times prior to stimulation to better understand the optimal range for

monitoring PIP₃ production. It is also possible various metabolic pathways will require unique incubation times and metabolite distribution for effective study.

Another future direction for this work is the modification of the reporter to serve as a more efficient substrate toward PIP modifying enzymes. While we have demonstrated here and in chapter 2 that a PIP₂ reporter with a C15 alkyl chain is efficiently metabolized to a variety of metabolites it still possesses less hydrophobicity than endogenous PIP₂ which contains stearic and arachidonic acid on the DAG moiety. This could explain the lack of PIP₃ production as **BODIPY-PIP₂-C15** is competing against endogenous substrate to be metabolized. One such modification would be the addition of more hydrophobic side chain at the sn-2 position and comparing the efficacy of the reporters in a cellular based assay. This could also be beneficial in achieving PM localization as a majority of the delivered **BODIPY-PIP₂-C15** appears in the cytosol.

Another structural change to the reporter would be the removal of the fluorophore for the addition of a terminal alkyne that could be tagged with a fluorophore using 'click-chemistry.' Such an approach has been shown effective on tri-functional DAG and PA reporters for visualization[98, 134]. We have synthesized an alkyne containing PtdIns (**AK-PtdIns-C15; Figure 4.9A**) by replacing the fluorophore with a terminal alkyne at the sn-1 position using an NHS ester as previously described. We have confirmed generation of fluorescent product via 'click chemistry' as shown in **Figure 4.9B**. Getting rid of the bulky and exogenous fluorophore will further allow for reporters to better mimic endogenous substrate. Likewise, modifications can be made to both alkyl chains on DAG to contain a terminal alkyne at either position. Such a method could increase the ability of our reporters to be metabolized in the cell. Future experiments comparing

alkyne containing reporters and fluorescent reporters may give further valuable insight into the structural requirement for effective metabolic measurement.

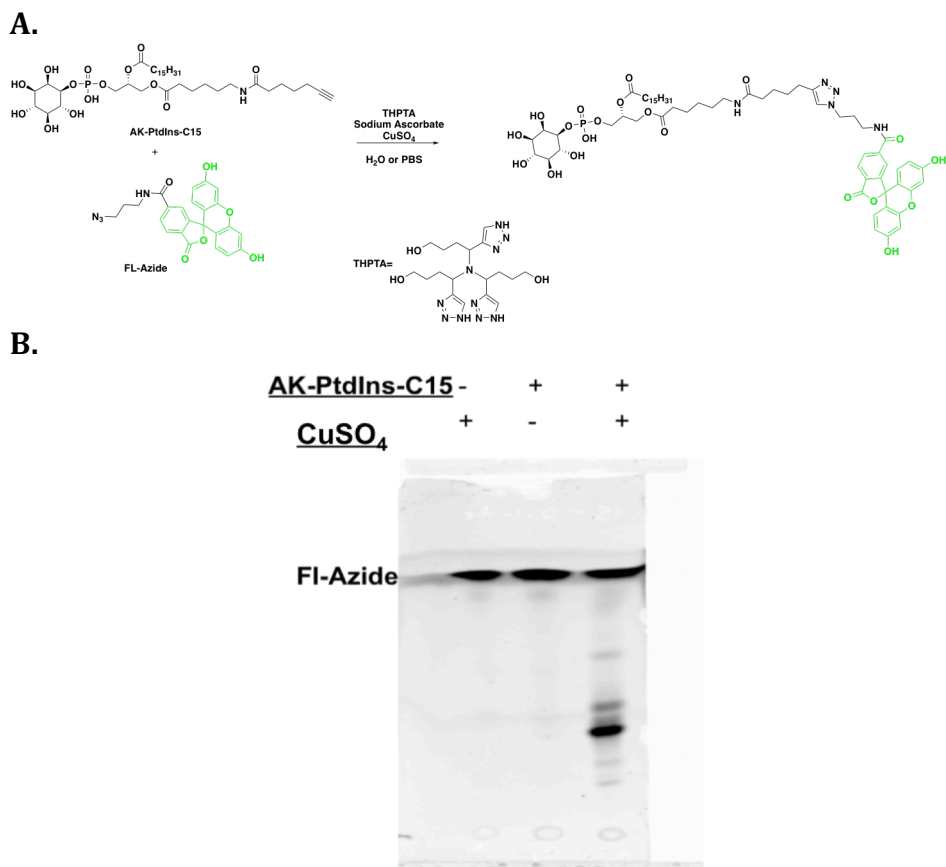


Figure 4.8 Structure of AK-PtdIns-C15 and Fluorophore Addition via ‘Click-Chemistry’: **A.** Structure of AK-PtdIns-C15 which when reacted with FI-Azide under ‘click’ chemistry conditions generates a fluorescent product. **B.** TLC analysis of ‘click-chemistry’ reaction, a new fluorescent spot was generated only in the sample containing both **AK-PtdIns-C15** and catalytic CuSO₄ indicating successful generation of the fluorescent metabolite. Reaction was performed in water with 2 mM CuSO₄, 2 mM sodium ascorbate, and 2 mM THPTA for 30 minutes.

Another potential direction for this platform is the use of dual fluorophores with unique excitation and emission wavelengths that could be used to tag multiple substrates. For instance PIP₂ tagged with BODIPY which is excited and detected using a 488 nm blue

laser line and PtdIns tagged with TAMRA which is excited using a 523 nm green laser line, could be delivered to cells and then the specific pools of metabolites could be monitored using CE-LIF and analyzing separately for BODIPY and TAMRA metabolites through excitation with their unique laser lines [62, 76, 77] .

Overall, this work has demonstrated the feasibility of using PIP reporters for analysis of cellular metabolic activity. Numerous chemical biology approaches can further be applied to this technique to increase the scope of biological processes that can be examined, with long-term aspirations of diagnostic application.

4.4 Experimental

All reagents were obtained from commercial sources and were used without further purification.

4.4.1 Cell Culture

HEK293AD and MDA-MB-453 cells were cultured in DMEM with 10% FBS and 1% antibiotic-antimycotic. MDA-MB-436 cells were cultured in DMEM with 10% FBS, 10 mg/mL insulin, 16 mg/mL glutathione, and 1% antibiotic-antimycotic. All cells were grown at 37 °C with 5% CO₂, and split when the confluency reached approximately 90%.

4.4.2 Delivery of BODIPY-PIP₂-C15 to Breast Cancer Cells

Cells as indicated (200,000 cells) were plated into a 35 mm dish in growth medium and cultured at 37 °C with 5% CO₂ for 24 h. The medium was replaced with serum free DMEM before the BODIPY-PIP₂-C15/CART complex was added. To form the complex, BODIPY-PIP₂-C15 (1.6 mL, 1.0 mM stock in H₂O) was added to acidified PBS (pH 5.5, 47.5 mL). The CART (A11 or G7, 0.6 mL) was subsequently added and the components

were gently mixed through pipetting. After 1 min, the complex was added to the medium and incubated with the cells for indicated time before analysis was carried out.

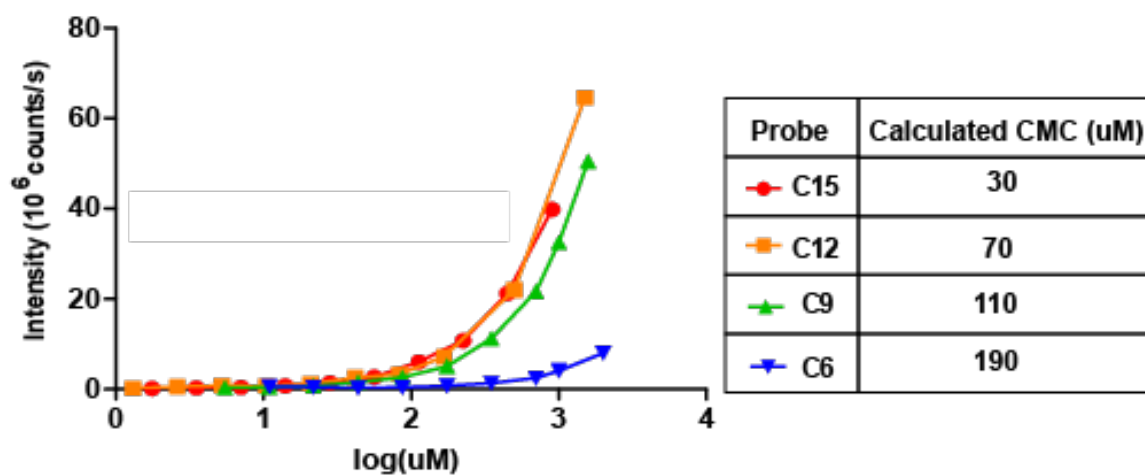
4.4.3 Extraction of Lipids from Cell Pellet

150 μ L of 40:20:1 (v:v:v) Chloroform:Methanol:HCl was added to the cell pellet and left at room temperature for 10 minutes. 50 μ L of CHCl_3 and 50 μ L of water were added and the mixture vortexed heavily for 3 minutes. The mixture was then centrifuged at 4 $^{\circ}\text{C}$ at 3200 RPM for 8 minutes resulting in phase separation. The bottom layer was collected, dried under a stream of N_2 and resuspended in 30 μ L of 1:1 CHCl_3 :MeOH (v:v) for TLC analysis.

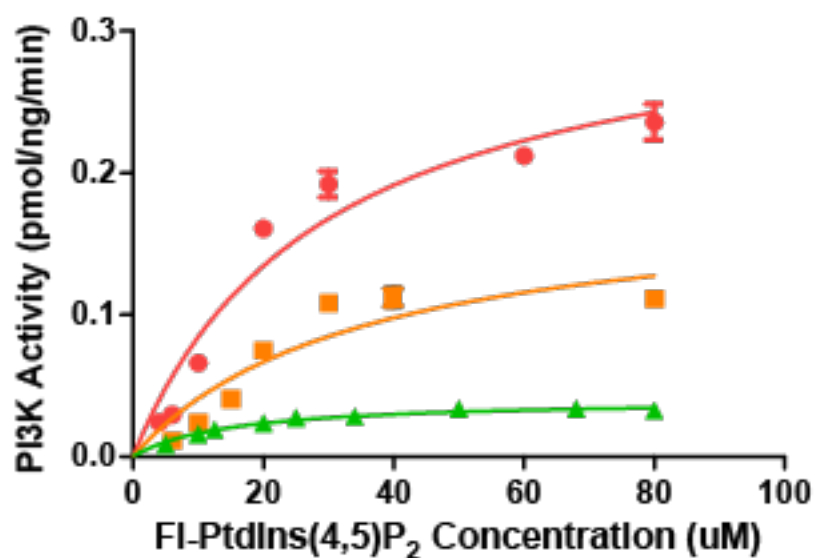
4.4.4 TLC Analysis of Lipid Metabolites

TLC plates (Merck, Silica Gel-60) were pre-treated with a solution of 1.2% potassium oxalate and 1.2 mM EGTA in MeOH/water (v:v = 2:3) and heated at 110 $^{\circ}\text{C}$ for 20 minutes before use. Reaction mixture was diluted in CHCl_3 / MeOH (v:v = 1:1) and spotted on a TLC plate directly. The TLC plate was then developed in CHCl_3 :Acetone:MeOH:AcOH:water (v:v:v:v:v = 80:30:26:24:14) or CHCl_3 :Hexane:Metahnol:Acetic Acid (v:v:v:v= 50:30:10:5) and scanned on a Typhoon 9400 Variable Mode Imager ($I_{\text{ex}}/I_{\text{em}}$ = 488 nm/520 nm). The fluorescence intensity of various spots on the TLC plate was quantified with ImageQuant software (V.5.0)

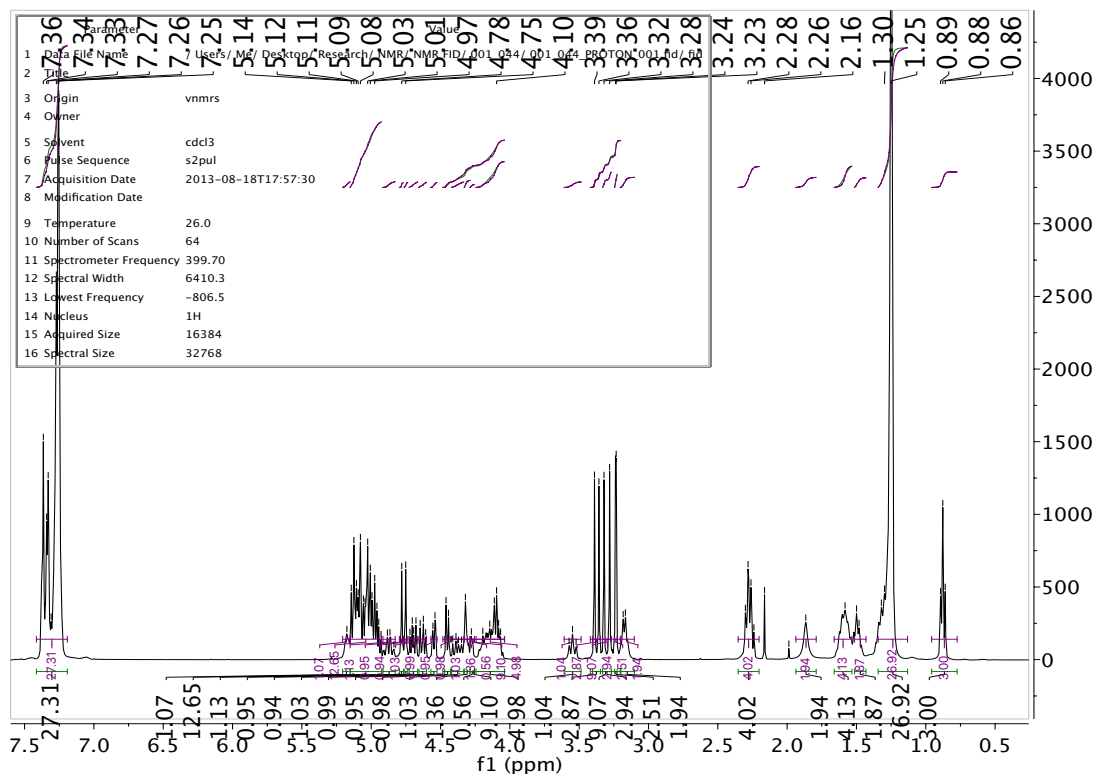
Appendix



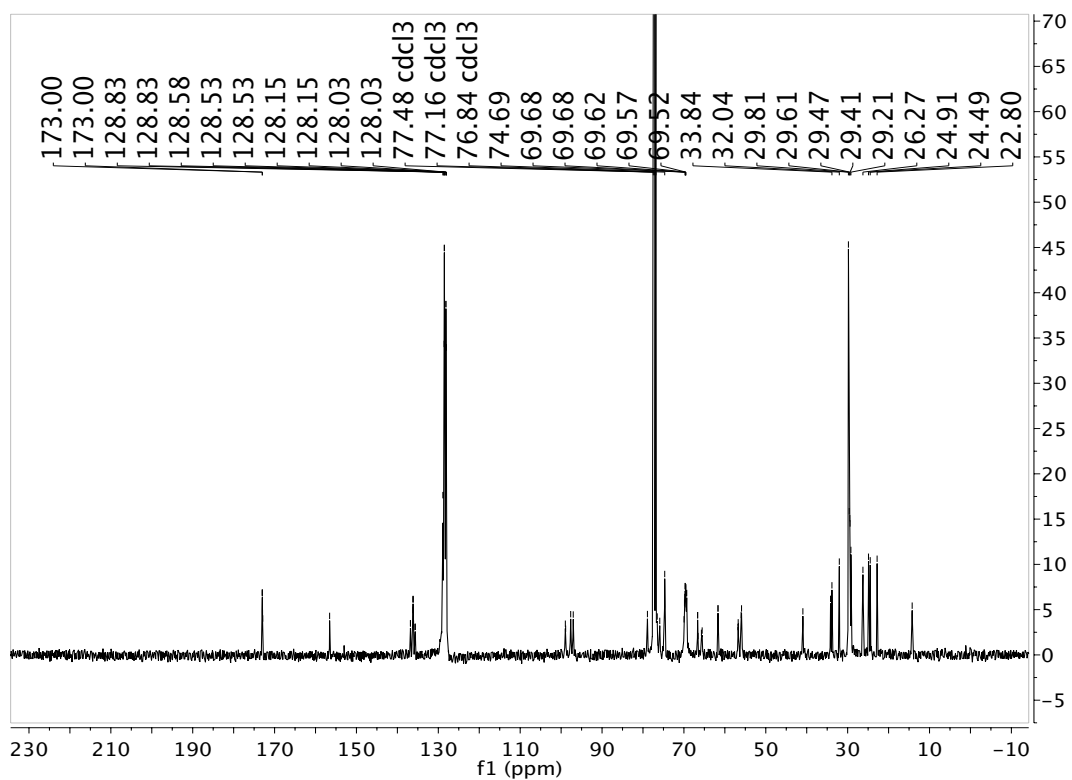
Appendix A CMC Determination of Fluorescent PIP₂ Analogs



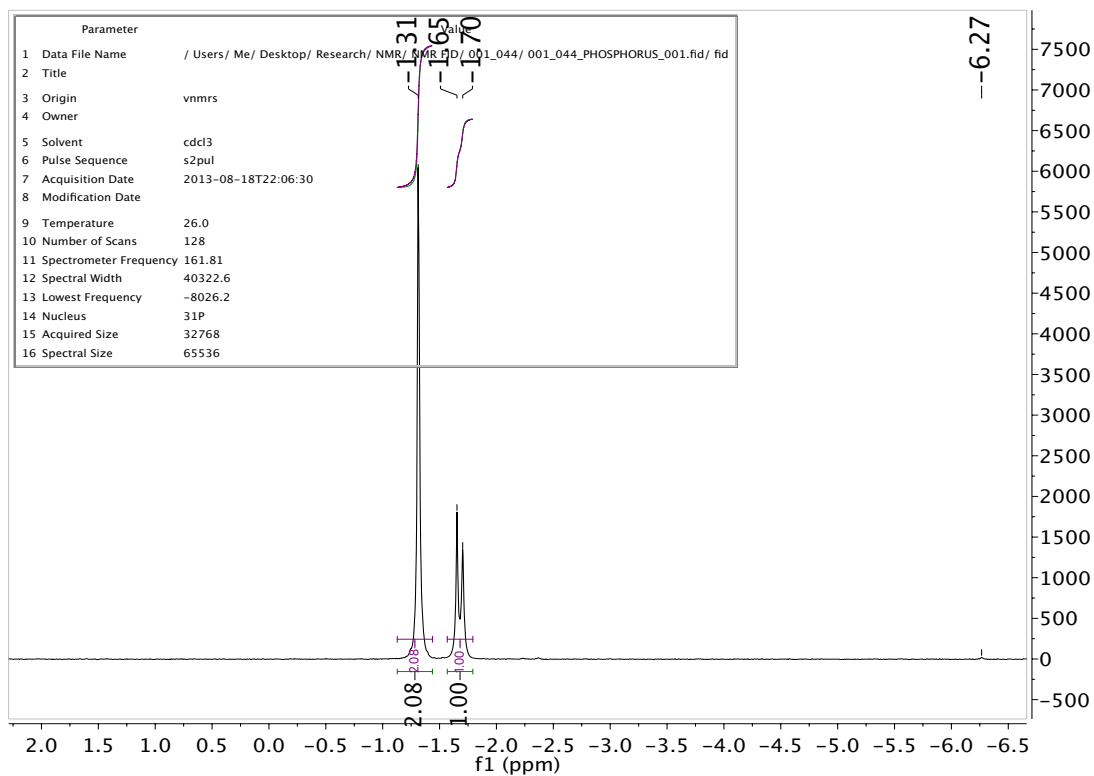
Appendix B Kinetic Analysis of Fluorescent PIP₂ Analogs



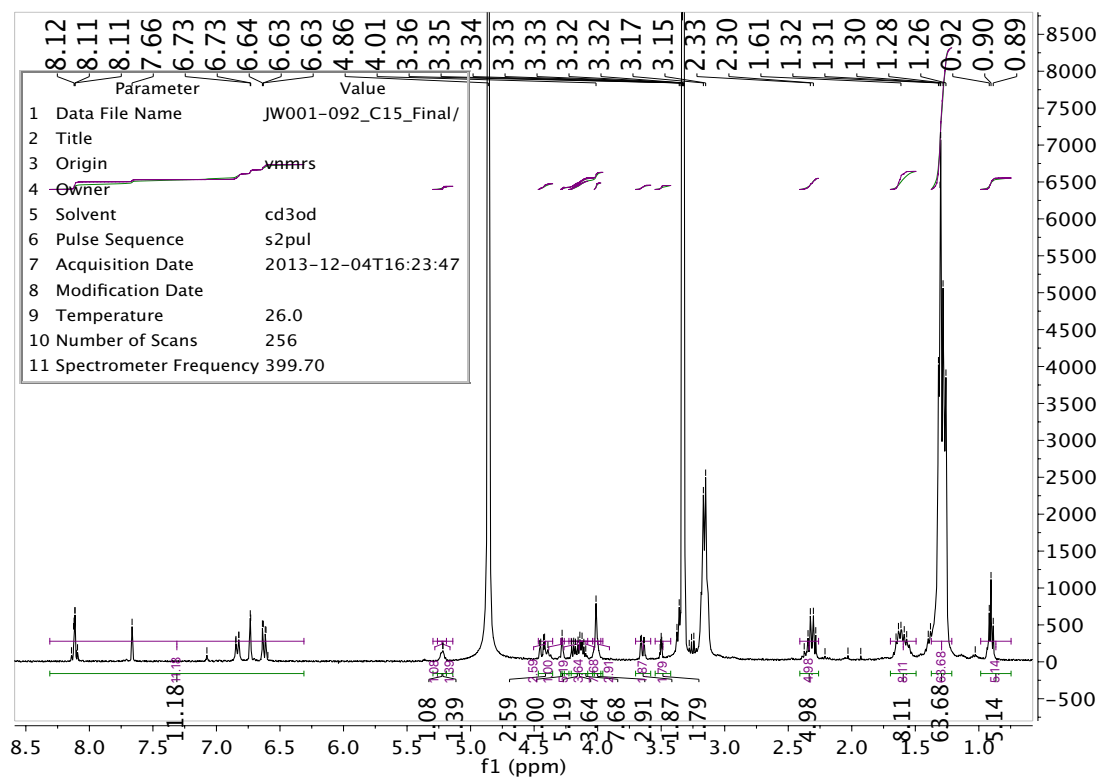
Appendix C ^1H NMR Spectra (CDCl_3) of compound 5D is an example of fully protected intermediate in PIP_2 synthesis



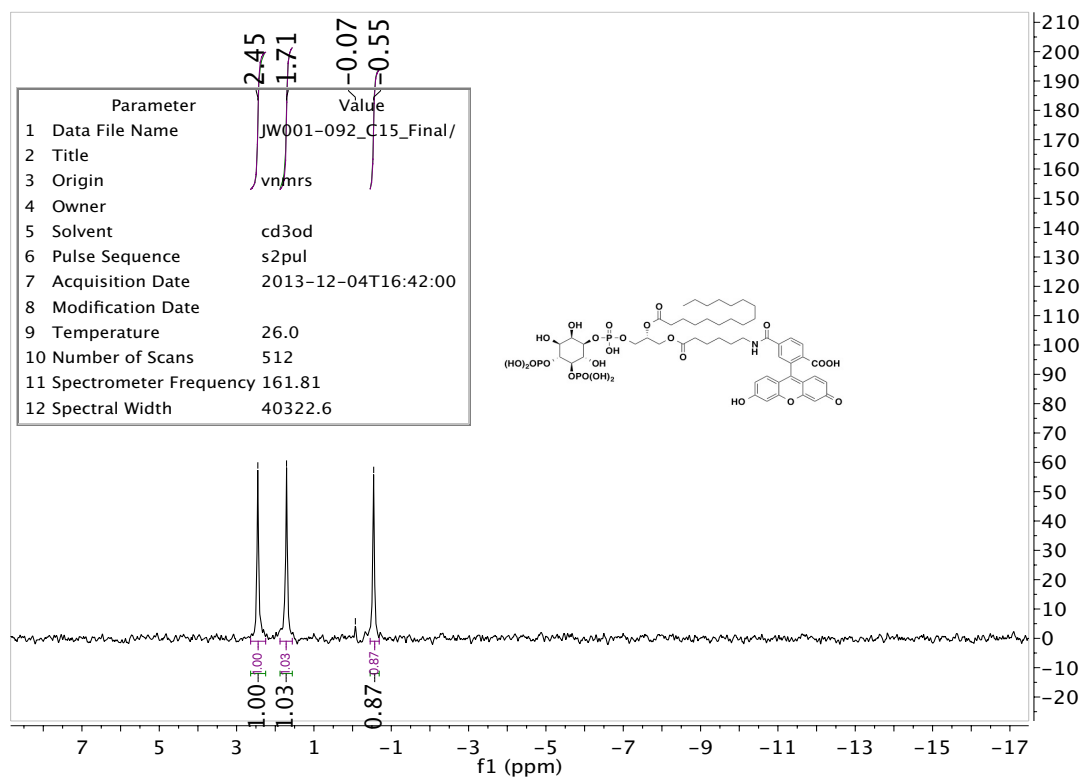
Appendix D ^{13}C NMR Spectra (CDCl_3) of compound 5D is an example of fully protected intermediate in PIP_2 synthesis



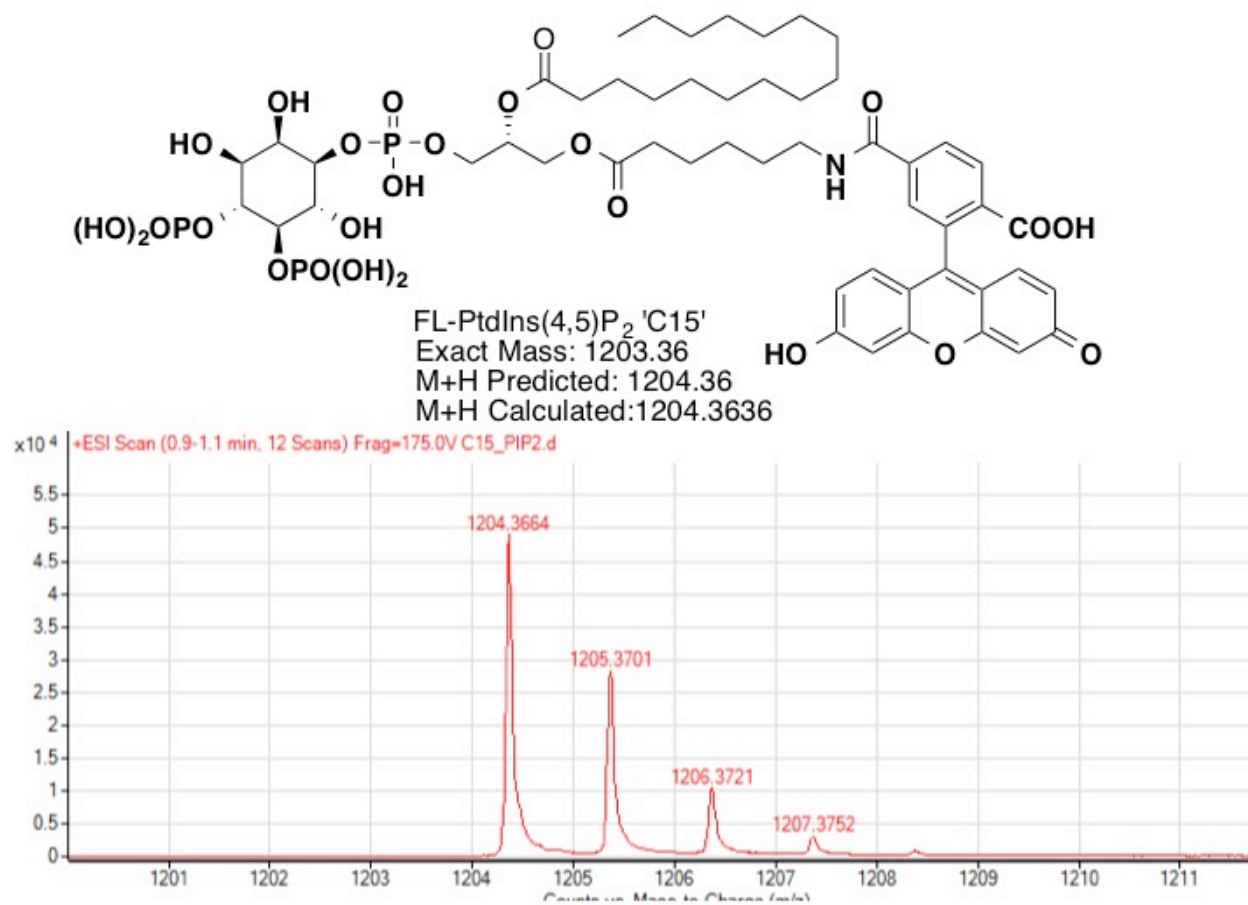
Appendix E ^{31}P NMR Spectra (CDCl_3) of compound 5D is an example of fully protected intermediate in PIP_2 synthesis



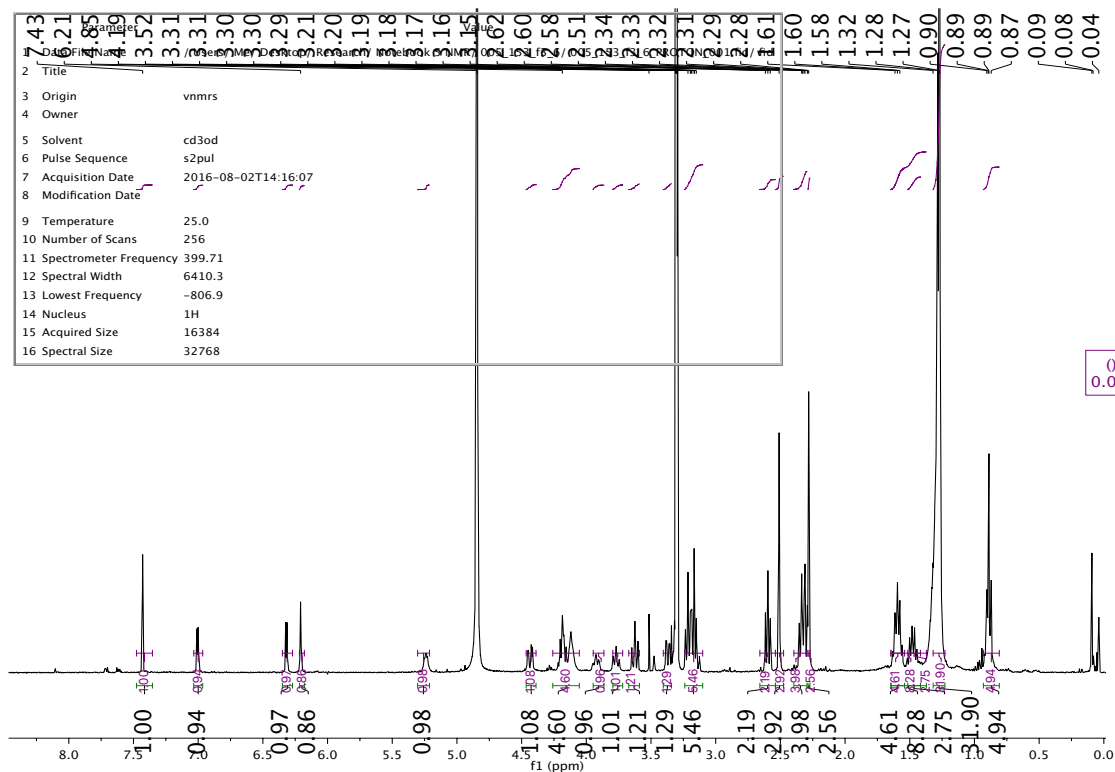
Appendix F ^1H NMR (CD_3OD) of $\text{PIP}_2\text{-C15}$ is an example of a final fluorescent PIP_2 Analog



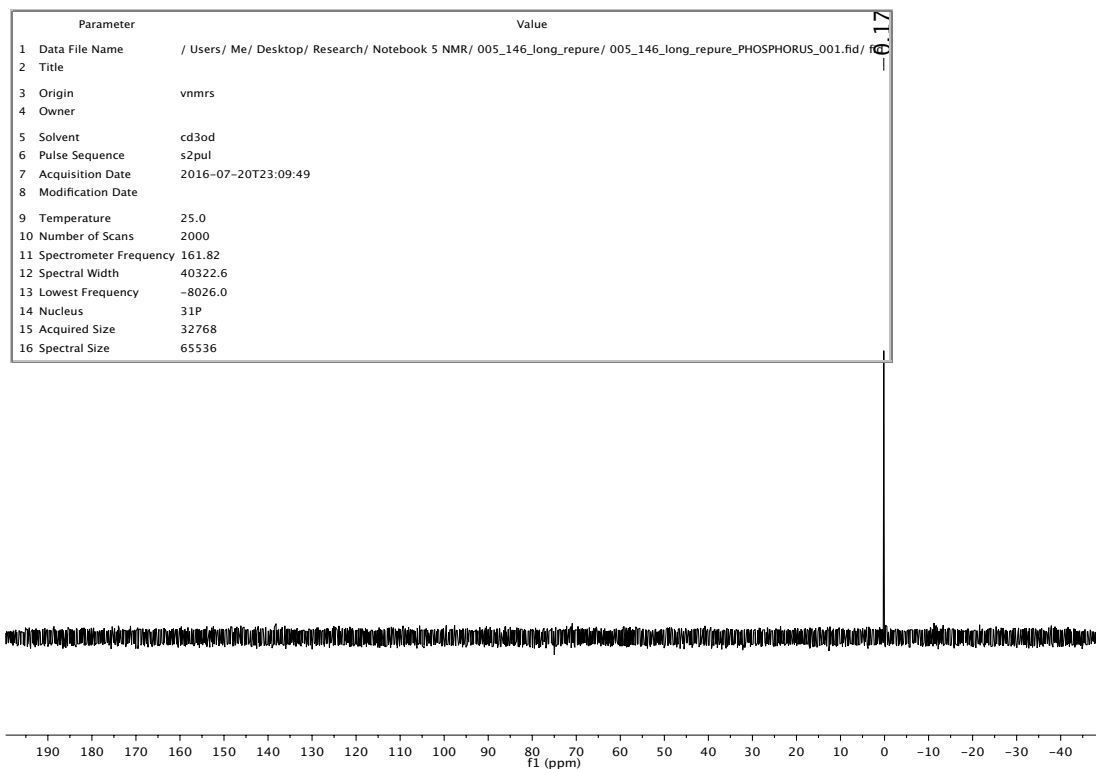
Appendix G ^{31}P NMR (CD_3OD) of $\text{PIP}_2\text{-C15}$ is an example of a final fluorescent PIP_2 Analog



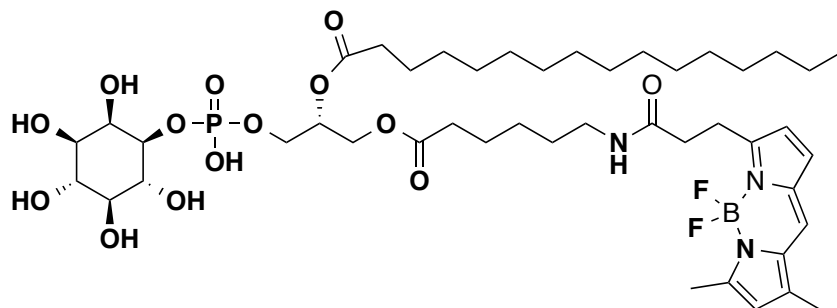
Appendix H HRMS analysis of PIP₂-C15 is an example of a final PIP₂ analog



Appendix I ^1H NMR (CD_3OD) of BODIPY-PtdIns-C15



Appendix J ^{31}P NMR Spectra (CD_3OD) of BODIPY-PtdIns-C15

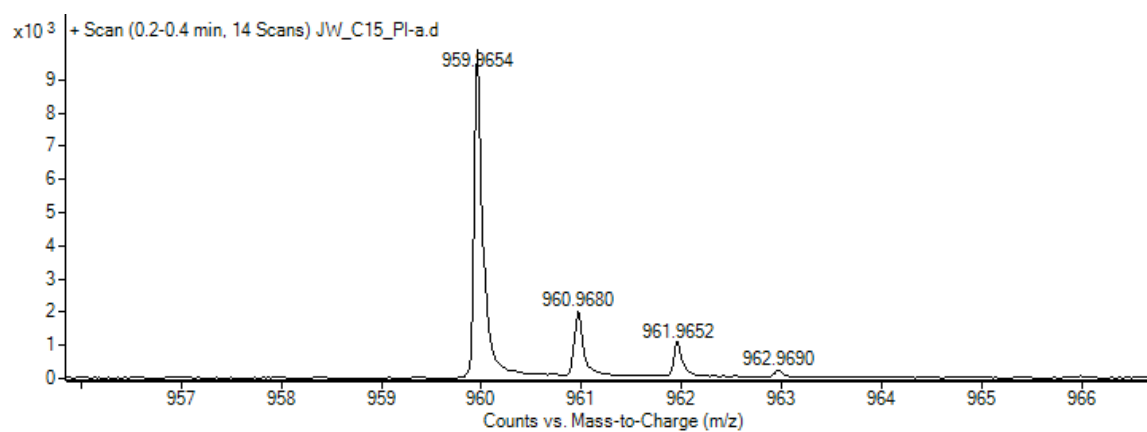


Chemical Formula: $C_{45}H_{73}BF_2N_3O_{14}P$

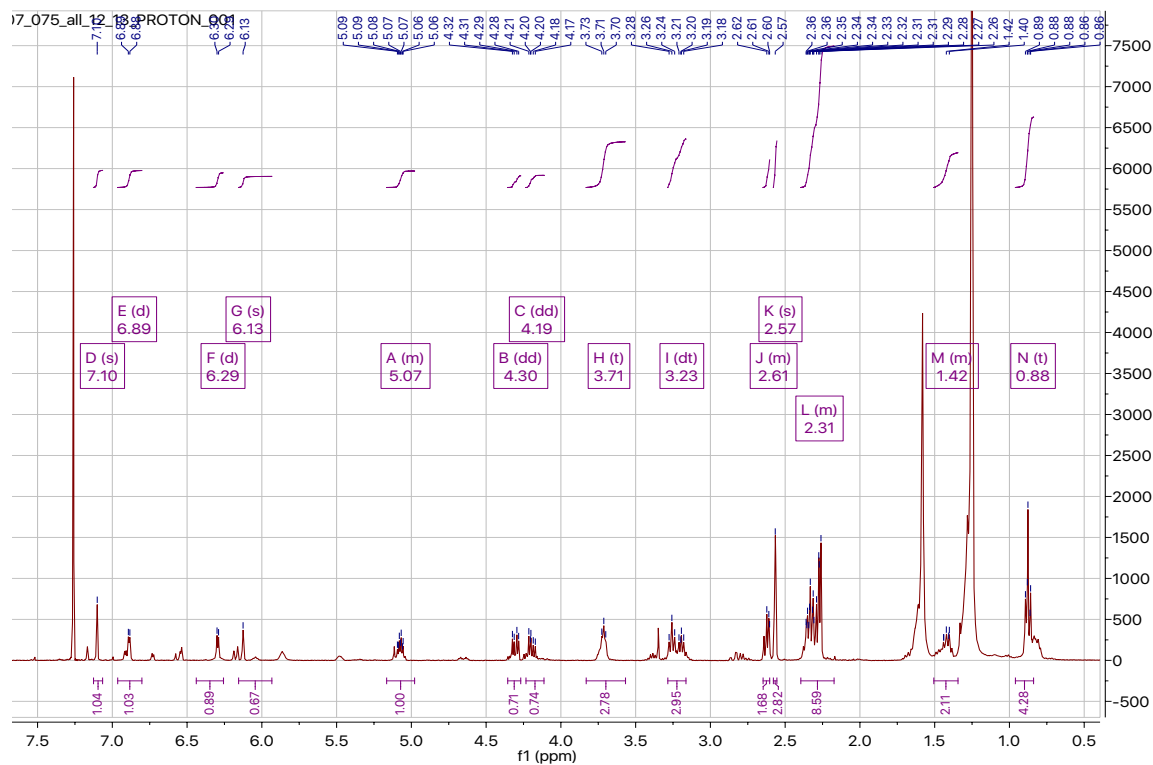
Exact Mass: 959.49

[M+H] Predicted: 960.49

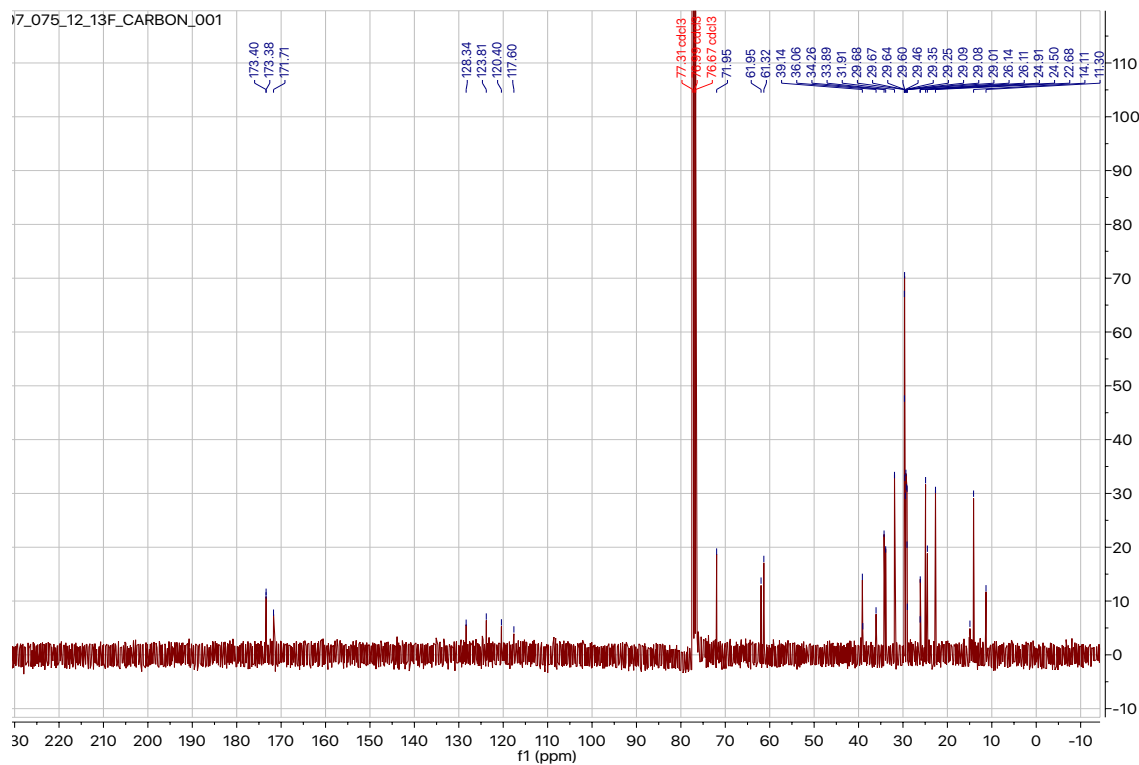
M+H Calculated: 960.96



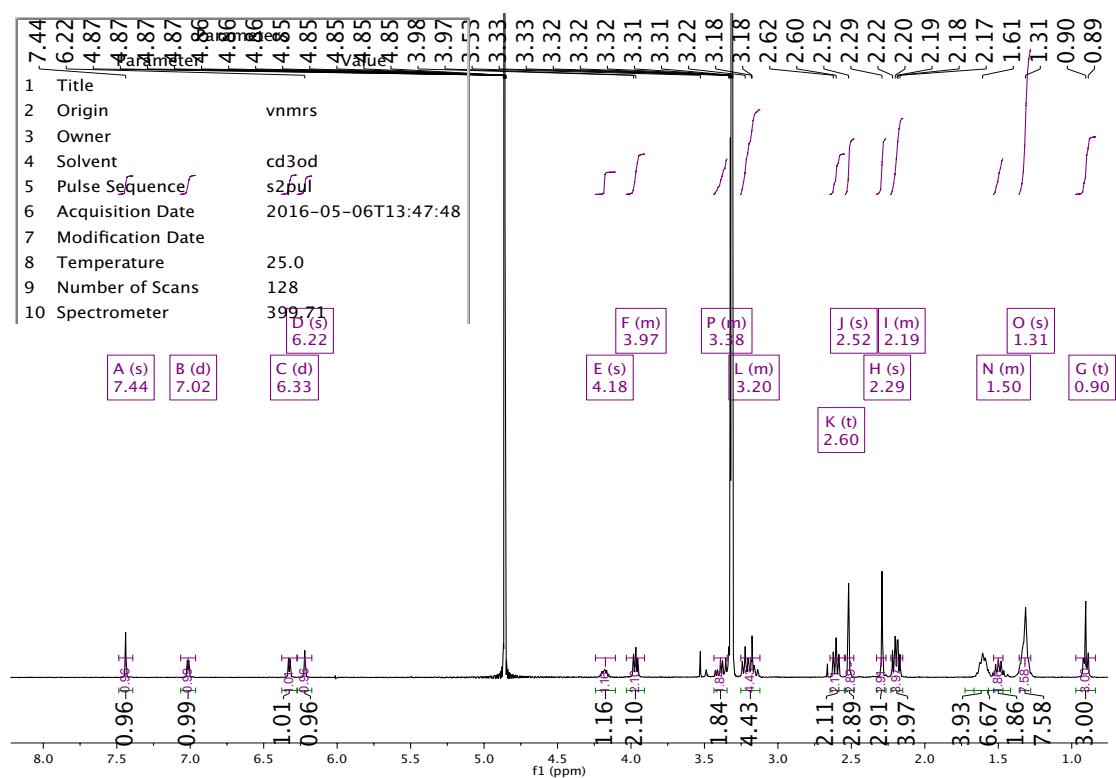
Appendix K HRMS of BODIPY-PtdIns-C15



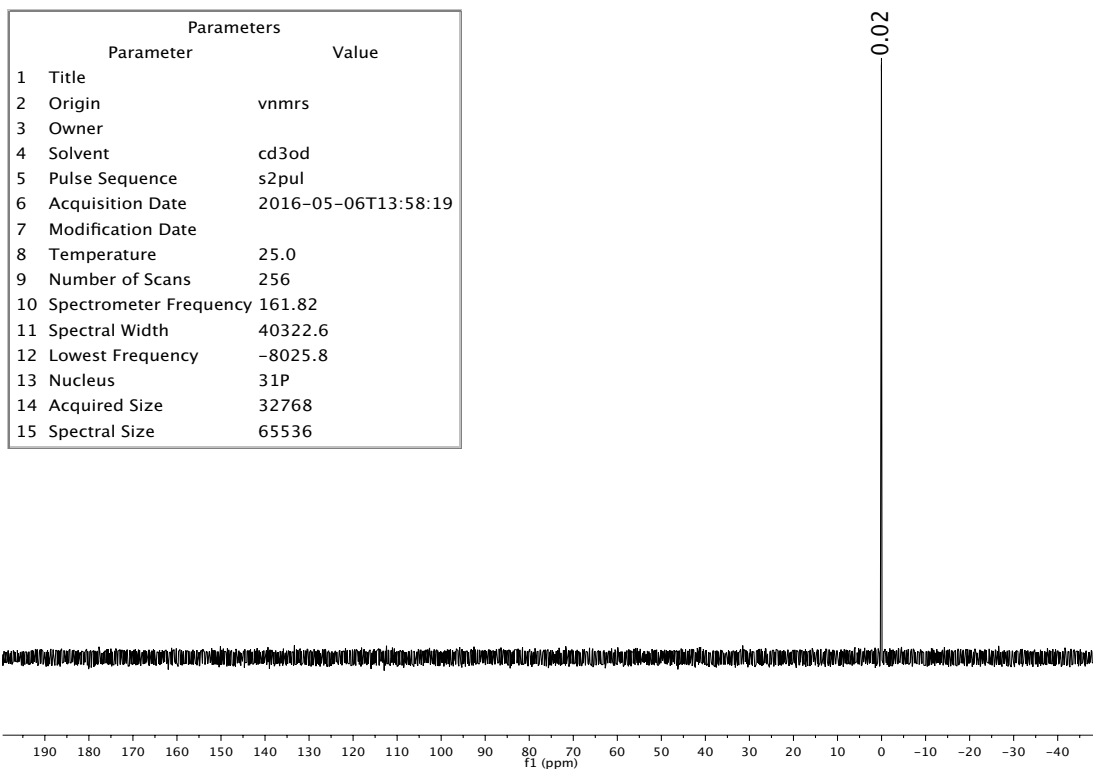
Appendix J ^1H NMR Spectra (CDCl_3) of BODIPY-DAG-C15



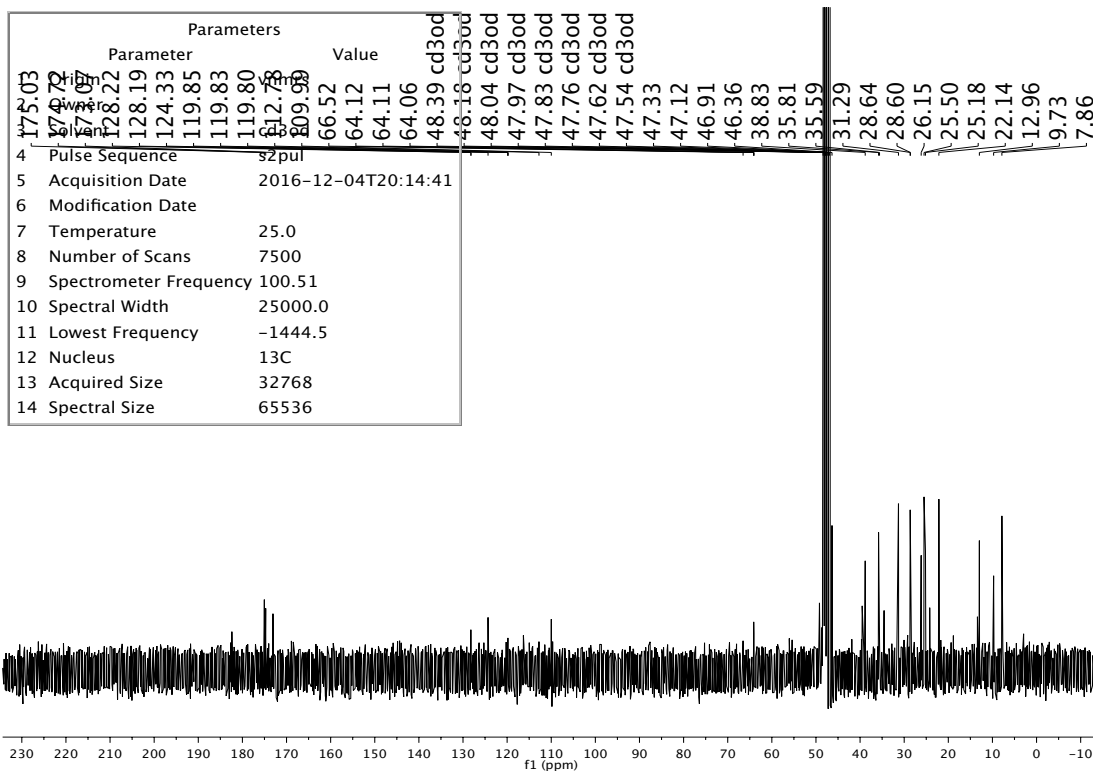
Appendix J ^{13}C NMR spectra of BODIPY-DAG-C15



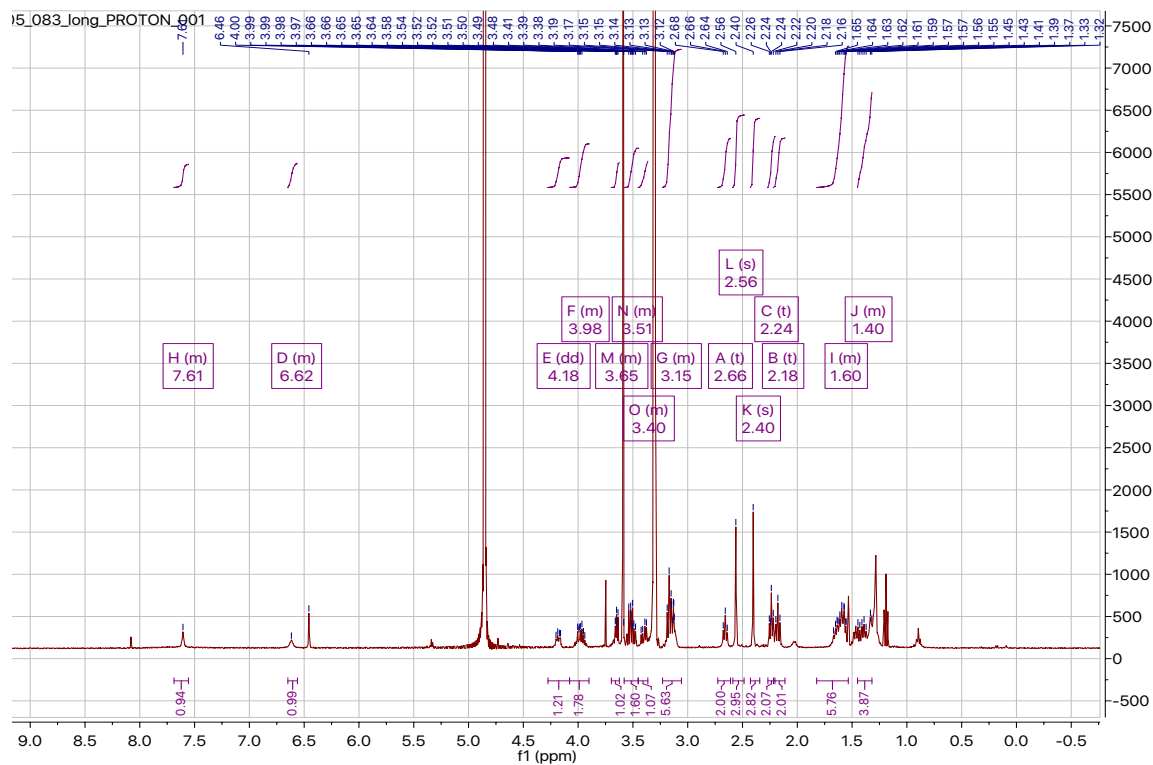
Appendix K ^1H NMR Spectra (CD_3OD) of Compound 36



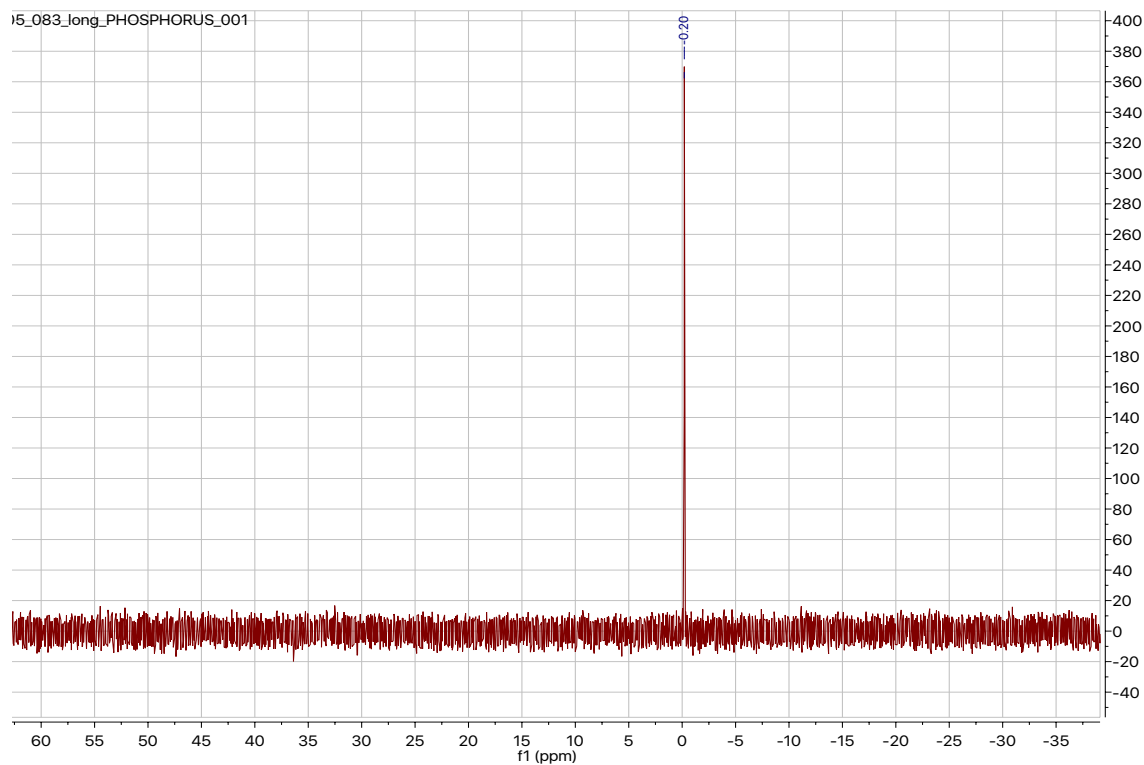
Appendix L ³¹P NMR Spectra (CD₃OD) of compound 36



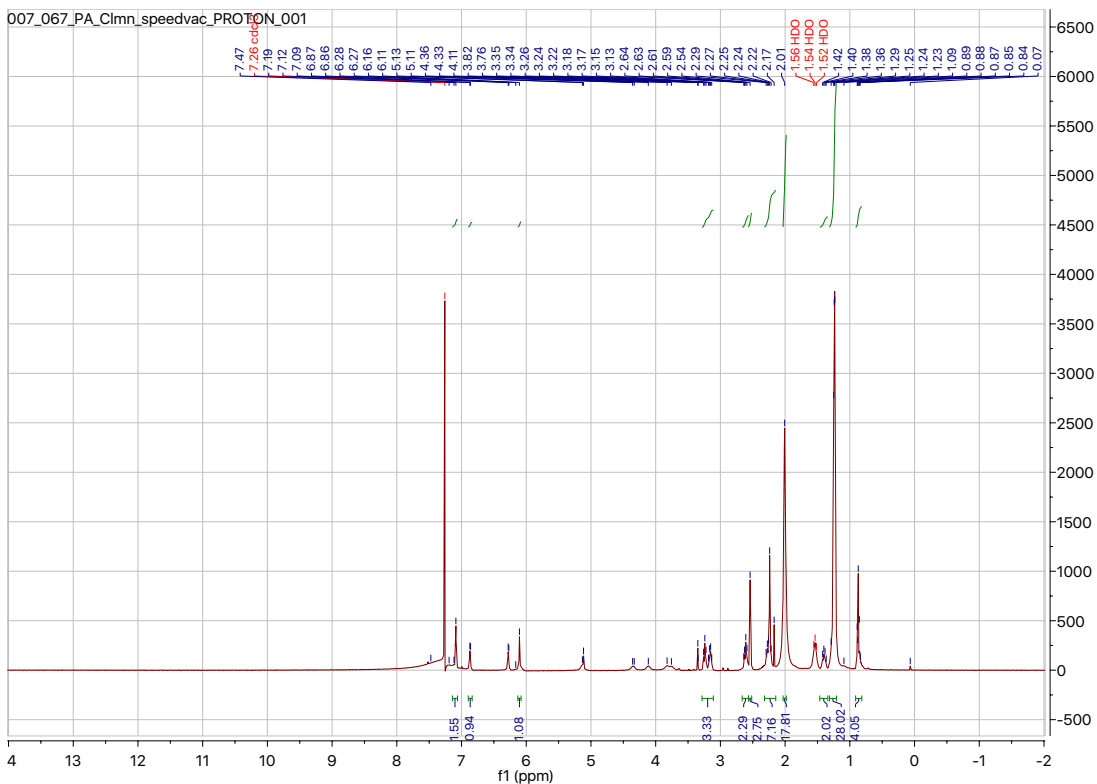
Appendix M ¹³C NMR spectra (CD₃OD) of Compound 36



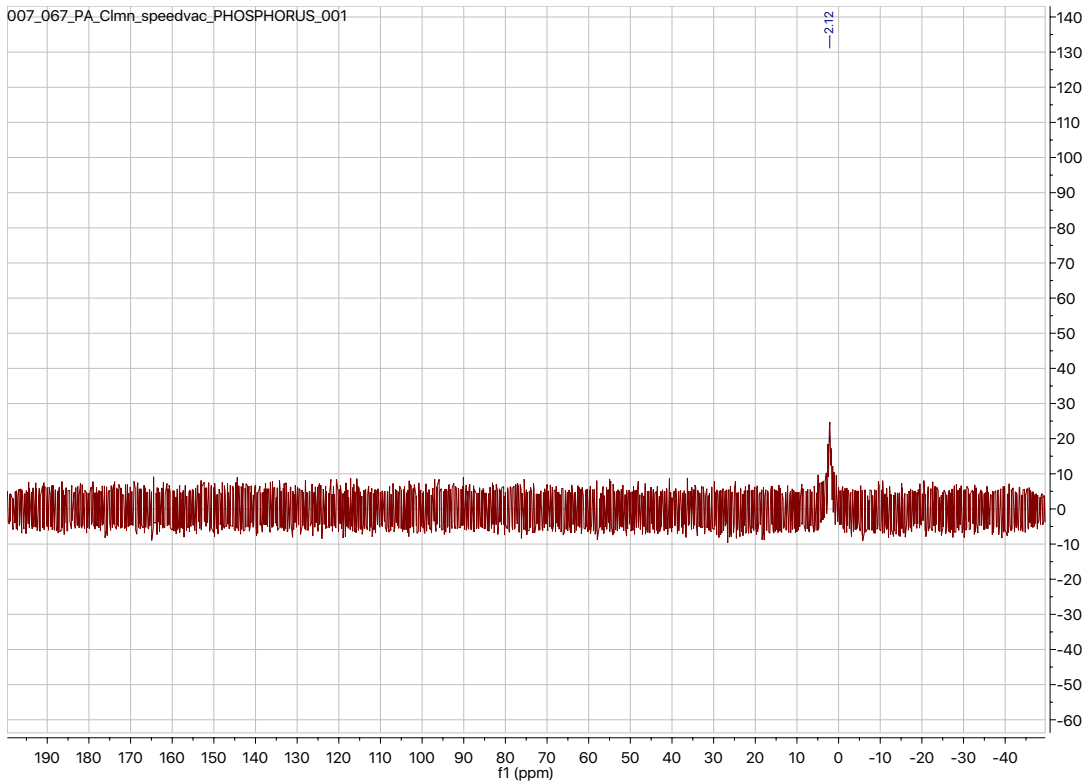
Appendix N ^1H NMR Spectra (CD_3OD) of compound 53



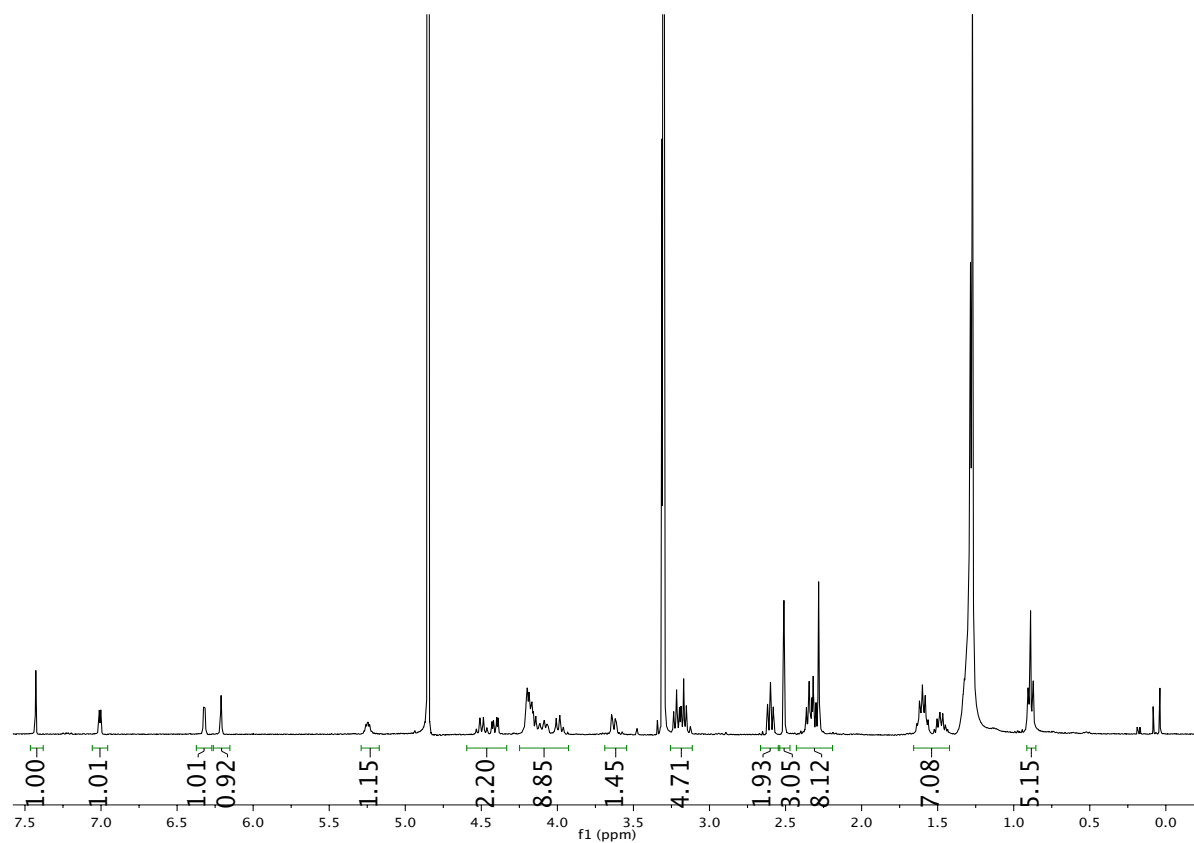
Appendix O ^{31}P NMR spectra (CD_3OD) of compound 53



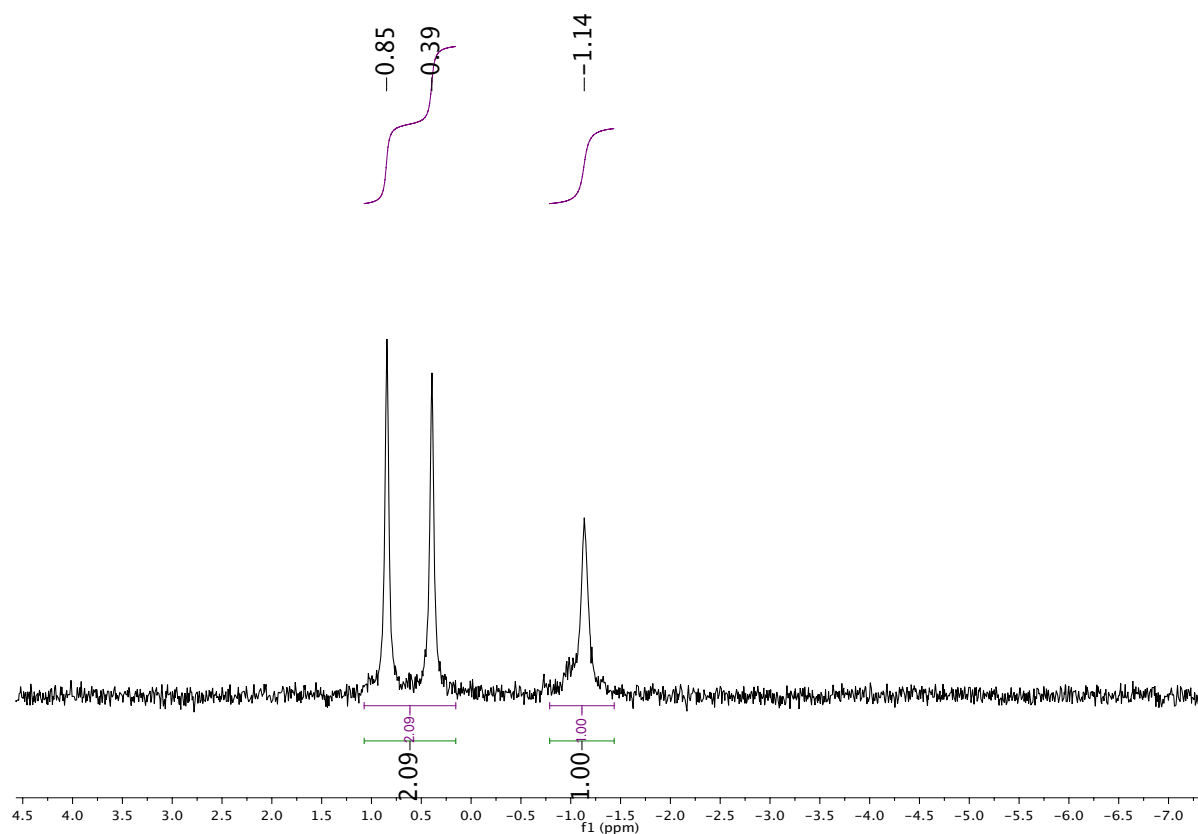
Appendix P ^1H NMR spectra (CDCl_3) of BODIPY-PA-C15



Appendix Q ^{31}P NMR Spectra (CDCl_3) of BODIPY-PA-C15



Appendix R ^1H NMR spectra (CD₃OD) of BODIPY-PIP₂-C15



Appendix S ^{31}P NMR spectra (CD₃OD) of BODIPY-PIP₂-C15

REFERENCES

1. van Meer, G., D.R. Voelker, and G.W. Feigenson, *Membrane lipids: where they are and how they behave*. Nat Rev Mol Cell Biol, 2008. **9**(2): p. 112-24.
2. Kutateladze, T.G., *Translation of the phosphoinositide code by PI effectors*. Nat Chem Biol, 2010. **6**(7): p. 507-13.
3. Shevchenko, A. and K. Simons, *Lipidomics: coming to grips with lipid diversity*. Nat Rev Mol Cell Biol, 2010. **11**(8): p. 593-8.
4. Liu, Y., R.A. Kahn, and J.H. Prestegard, *Structure and membrane interaction of myristoylated ARF1*. Structure, 2009. **17**(1): p. 79-87.
5. Wymann, M.P. and R. Schneiter, *Lipid signalling in disease*. Nat Rev Mol Cell Biol, 2008. **9**(2): p. 162-76.
6. Baldanzi, G., et al., *Activation of diacylglycerol kinase alpha is required for VEGF-induced angiogenic signaling in vitro*. Oncogene, 2004. **23**(28): p. 4828-38.
7. Yuan, T.L., et al., *Cell-to-cell variability in PI3K protein level regulates PI3K-AKT pathway activity in cell populations*. Curr Biol, 2011. **21**(3): p. 173-83.
8. Chu, K.M., et al., *Differential effects of the phosphatidylinositol 4-kinases, PI4KIIalpha and PI4KIIbeta, on Akt activation and apoptosis*. Cell Death Dis, 2010. **1**: p. e106.
9. Qin, Y., et al., *Regulation of phosphatidylinositol kinases and metabolism by Wnt3a and Dvl*. J Biol Chem, 2009. **284**(34): p. 22544-8.
10. Pan, W., et al., *Wnt3a-mediated formation of phosphatidylinositol 4,5-bisphosphate regulates LRP6 phosphorylation*. Science, 2008. **321**(5894): p. 1350-3.
11. May, W.S., E.G. Lapetina, and P. Cuatrecasas, *Intracellular activation of protein kinase C and regulation of the surface transferrin receptor by diacylglycerol is a spontaneously reversible process that is associated with rapid formation of phosphatidic acid*. Proc Natl Acad Sci U S A, 1986. **83**(5): p. 1281-4.

12. Cully, M., et al., *Beyond PTEN mutations: the PI3K pathway as an integrator of multiple inputs during tumorigenesis*. Nat Rev Cancer, 2006. **6**(3): p. 184-92.
13. Stjernstrom, A., et al., *Alterations of INPP4B, PIK3CA and pAkt of the PI3K pathway are associated with squamous cell carcinoma of the lung*. Cancer Med, 2014. **3**(2): p. 337-48.
14. Liu, P., et al., *Targeting the phosphoinositide 3-kinase pathway in cancer*. Nat Rev Drug Discov, 2009. **8**(8): p. 627-44.
15. Engelman, J.A., *Targeting PI3K signalling in cancer: opportunities, challenges and limitations*. Nat Rev Cancer, 2009. **9**(8): p. 550-62.
16. Fruman, D.A. and C. Rommel, *PI3K and cancer: lessons, challenges and opportunities*. Nat Rev Drug Discov, 2014. **13**(2): p. 140-56.
17. Wong, K.K., J.A. Engelman, and L.C. Cantley, *Targeting the PI3K signaling pathway in cancer*. Curr Opin Genet Dev, 2010. **20**(1): p. 87-90.
18. Ihle, N.T. and G. Powis, *Take your PIK: phosphatidylinositol 3-kinase inhibitors race through the clinic and toward cancer therapy*. Mol Cancer Ther, 2009. **8**(1): p. 1-9.
19. Skwarek, L.C. and G.L. Boulianne, *Great expectations for PIP: phosphoinositides as regulators of signaling during development and disease*. Dev Cell, 2009. **16**(1): p. 12-20.
20. Schultz, C., *Challenges in studying phospholipid signaling*. Nat Chem Biol, 2010. **6**(7): p. 473-5.
21. Yamada, K., et al., *Sphingosine activates cellular diacylglycerol kinase in intact Jurkat cells, a human T-cell line*. Biochim Biophys Acta, 1993. **1169**(3): p. 217-24.
22. Torres-Ayuso, P., et al., *Diacylglycerol kinase alpha promotes 3D cancer cell growth and limits drug sensitivity through functional interaction with Src*. Oncotarget, 2014. **5**(20): p. 9710-26.

23. Yarden Samuels, et al., *High Frequency of Mutations of the PIK3CA Gene in Human Cancers*. Science, 2004. **304**(5670).
24. Gutierrez, A., et al., *High frequency of PTEN, PI3K, and AKT abnormalities in T-cell acute lymphoblastic leukemia*. Blood, 2009. **114**(3): p. 647-50.
25. Cantley, L.C., *The phosphoinositide 3-kinase pathway*. Science, 2002. **296**(5573): p. 1655-7.
26. Gabelli, S.B., et al., *Somatic mutations in PI3Kalpha: structural basis for enzyme activation and drug design*. Biochim Biophys Acta, 2010. **1804**(3): p. 533-40.
27. Vadas, O., et al., *Structural Basis for Activation and Inhibition of Class I Phosphoinositide 3-Kinases*. Science Signaling, 2011. **4**(195): p. re2-re2.
28. Perez-Lorenzo, R., et al., *A tumor suppressor function for the lipid phosphatase INPP4B in melanocytic neoplasms*. J Invest Dermatol, 2014. **134**(5): p. 1359-68.
29. Vicinanza, M., et al., *Phosphoinositides as regulators of membrane trafficking in health and disease*. Cell Mol Life Sci, 2008. **65**(18): p. 2833-41.
30. Di Paolo, G. and P. De Camilli, *Phosphoinositides in cell regulation and membrane dynamics*. Nature, 2006. **443**(7112): p. 651-7.
31. Vicinanza, M., et al., *Function and dysfunction of the PI system in membrane trafficking*. EMBO J, 2008. **27**(19): p. 2457-70.
32. Downes, C.P., A. Gray, and J.M. Lucocq, *Probing phosphoinositide functions in signaling and membrane trafficking*. Trends Cell Biol, 2005. **15**(5): p. 259-68.
33. Balla, T., *Phosphoinositides: tiny lipids with giant impact on cell regulation*. Physiol Rev, 2013. **93**(3): p. 1019-137.
34. Wymann, M.P. and C. Schultz, *The chemical biology of phosphoinositide 3-kinases*. Chembiochem, 2012. **13**(14): p. 2022-35.

35. Fruman, D.A., R.E. Meyers, and L.C. Cantley, *Phosphoinositide kinases*. Annu Rev Biochem, 1998. **67**: p. 481-507.
36. Ferguson, C.J., G.M. Lenk, and M.H. Meisler, *PtdIns(3,5)P₂ and autophagy in mouse models of neurodegeneration*. Autophagy, 2009. **6**(1): p. 170-1.
37. Courtney, K.D., R.B. Corcoran, and J.A. Engelman, *The PI3K pathway as drug target in human cancer*. J Clin Oncol, 2010. **28**(6): p. 1075-83.
38. Fresno Vara, J.A., et al., *PI3K/Akt signalling pathway and cancer*. Cancer Treat Rev, 2004. **30**(2): p. 193-204.
39. Stahelin, R.V., J.L. Scott, and C.T. Frick, *Cellular and molecular interactions of phosphoinositides and peripheral proteins*. Chem Phys Lipids, 2014. **182**: p. 3-18.
40. Gewinner, C., et al., *Evidence that inositol polyphosphate 4-phosphatase type II is a tumor suppressor that inhibits PI3K signaling*. Cancer Cell, 2009. **16**(2): p. 115-25.
41. Hennessey, B.T., et al., *Exploiting the PI3K/AKT pathway for cancer drug discovery*. Nat Rev Drug Discov, 2005. **4**(12): p. 988-1004.
42. Maira, S.M., P. Finan, and C. Garcia-Echeverria, *From the bench to the bed side: PI3K pathway inhibitors in clinical development*. Curr Top Microbiol Immunol, 2010. **347**: p. 209-39.
43. Samuels, Y., et al., *High frequency of mutations of the PIK3CA gene in human cancers*. Science, 2004. **304**(5670): p. 554.
44. Bachman, K.E., et al., *The PIK3CA gene is mutated with high frequency in human breast cancers*. Cancer Biol Ther, 2004. **3**(8): p. 772-5.
45. Bohanes, P., et al., *Predictive molecular classifiers in colorectal cancer*. Semin Oncol, 2011. **38**(4): p. 576-87.

46. Hon, W.C., A. Berndt, and R.L. Williams, *Regulation of lipid binding underlies the activation mechanism of class IA PI3-kinases*. *Oncogene*, 2012. **31**(32): p. 3655-66
47. Vadas, O., et al., *Structural basis for activation and inhibition of class I phosphoinositide 3-kinases*. *Sci Signal*, 2011. **4**(195): p. re2.
48. Brazil, D.P., *Ten Years of Protein Kinase B Signaling: A hard Akt to Follow*. *Trends Biochemical Science*, 2001. **26**: p. 657-664.
49. Rodon, J., et al., *Development of PI3K inhibitors: lessons learned from early clinical trials*. *Nat Rev Clin Oncol*, 2013. **10**(3): p. 143-53.
50. Bunney, T.D. and M. Katan, *Phosphoinositide signalling in cancer: beyond PI3K and PTEN*. *Nat Rev Cancer*, 2010. **10**(5): p. 342-52.
51. Myles C Hodgson, et al., *INPP4B suppresses prostate cancer cell invasion*. *Cell Communication and Signaling*, 2014. **12**(61).
52. Georgescu, M.M., *PTEN Tumor Suppressor Network in PI3K-Akt Pathway Control*. *Genes Cancer*, 2010. **1**(12): p. 1170-7.
53. Myers, A.P. and L.C. Cantley, *Targeting a Common Collaborator in Cancer Development*. *Science Translational Medicine*, 2010. **2**(48): p. 45-48.
54. Snijder, B. and L. Pelkmans, *Origins of regulated cell-to-cell variability*. *Nat Rev Mol Cell Biol*, 2011. **12**(2): p. 119-25.
55. Skommer, J., S. Raychaudhuri, and D. Wlodkowic, *Timing is everything: stochastic origins of cell-to-cell variability in cancer cell death*. *Front Biosci (Landmark Ed)*, 2011. **16**: p. 307-14.
56. Sabbah, D.A., J. Hu, and H.A. Zhong, *Advances in the Development of Class I Phosphoinositide 3-Kinase (PI3K) Inhibitors*. *Curr Top Med Chem*, 2016. **16**(13): p. 1413-26.

57. Workman, P., et al., *Drugging the PI3 kinome: from chemical tools to drugs in the clinic*. Cancer Res, 2010. **70**(6): p. 2146-57.
58. Prestwich, G.D., *Phosphoinositide signaling; from affinity probes to pharmaceutical targets*. Chem Biol, 2004. **11**(5): p. 619-37.
59. Cipres, A., et al., *Regulation of diacylglycerol kinase alpha by phosphoinositide 3-kinase lipid products*. J Biol Chem, 2003. **278**(37): p. 35629-35.
60. Cutrupi, S., et al., *Src-mediated activation of alpha-diacylglycerol kinase is required for hepatocyte growth factor-induced cell motility*. EMBO J, 2000. **19**(17): p. 4614-22.
61. Merida, I., A. Avila-Flores, and E. Merino, *Diacylglycerol kinases: at the hub of cell signalling*. Biochem J, 2008. **409**(1): p. 1-18.
62. Jiang, D., C.E. Sims, and N.L. Allbritton, *Single-cell analysis of phosphoinositide 3-kinase and phosphatase and tensin homolog activation*. Faraday Discuss, 2011. **149**: p. 187-200; discussion 227-45.
63. Kelong Wanga, D.J., Christopher E. Simsa, and Nancy L. Allbritton, *Separation of fluorescently labeled phosphoinositides and sphingolipids by capillary electrophoresis*. J Chromatogr B Analyt Technol Biomed Life Sci., 2012(907): p. 79-86.
64. Kielkowska, A., et al., *A new approach to measuring phosphoinositides in cells by mass spectrometry*. Adv Biol Regul, 2014. **54**: p. 131-41.
65. Pettitt, T.R., et al., *Analysis of intact phosphoinositides in biological samples*. J Lipid Res, 2006. **47**(7): p. 1588-96.
66. Wenk, M.R., et al., *Phosphoinositide profiling in complex lipid mixtures using electrospray ionization mass spectrometry*. Nat Biotechnol, 2003. **21**(7): p. 813-7.
67. Clark, J., et al., *Quantification of PtdInsP3 molecular species in cells and tissues by mass spectrometry*. Nat Methods, 2011. **8**(3): p. 267-72.

68. Milne, S.B., et al., *A targeted mass spectrometric analysis of phosphatidylinositol phosphate species*. J Lipid Res, 2005. **46**(8): p. 1796-802.
69. Markus R Wenk, L.L., Gilbert Di Paolo, Anthony J Romanelli, Sharon F Suchy, Robert L Nussbaum, Gary W Cline, Gerald I Shulman, Walter McMurry and Pietro De Camilli, *Phosphoinositide Profiling in Complex Lipid Mixtures Using Electrospray Ionization Mass Spectrometry*. Nature Biotechnology, 2003. **21**(7): p. 813-817.
70. Balla, T. and P. Varnai, *Visualization of cellular phosphoinositide pools with GFP-fused protein-domains*. Curr Protoc Cell Biol, 2009. **Chapter 24**: p. Unit 24 4.
71. Huang, W., et al., *Kinetic analysis of PI3K reactions with fluorescent PIP2 derivatives*. Anal Bioanal Chem, 2011. **401**(6): p. 1881-8.
72. Várnai, T.B.a.P.t., *Visualizing cellular phosphoinositide pools with GFP-fused protein-modules*. Science Signaling, 2002(125).
73. Huang, W., et al., *Fluorous enzymatic synthesis of phosphatidylinositides*. Chem Commun (Camb), 2014. **50**(22): p. 2928-31.
74. Meredith, G.D., et al., *Measurement of kinase activation in single mammalian cells*. Nat Biotechnol, 2000. **18**(3): p. 309-12.
75. Proctor, A., et al., *Measurement of protein kinase B activity in single primary human pancreatic cancer cells*. Anal Chem, 2014. **86**(9): p. 4573-80.
76. Wang, K., et al., *Separation of fluorescently labeled phosphoinositides and sphingolipids by capillary electrophoresis*. J Chromatogr B Analyt Technol Biomed Life Sci, 2012. **907**: p. 79-86.
77. Sims, C.E. and N.L. Allbritton, *Single-cell kinase assays: opening a window onto cell behavior*. Curr Opin Biotechnol, 2003. **14**(1): p. 23-8.
78. Dickinson, A.J., et al., *Single-cell sphingosine kinase activity measurements in primary leukemia*. Anal Bioanal Chem, 2014. **406**(27): p. 7027-36.

79. Barnett, S.F., et al., *Interfacial catalysis by phosphoinositide 3'-hydroxykinase*. Biochemistry, 1995. **34**(43): p. 14254-62.
80. Liu, S., S. Knapp, and A.A. Ahmed, *The structural basis of PI3K cancer mutations: from mechanism to therapy*. Cancer Res, 2014. **74**(3): p. 641-6.
81. Kubiak, R.J. and K.S. Bruzik, *Comprehensive and Uniform Synthesis of All Naturally Occurring Phosphorylated Phosphatidylinositols*. The Journal of Organic Chemistry, 2003. **68**(3): p. 960-968.
82. Chen, J., A.A. Profit, and G.D. Prestwich, *Synthesis of Photoactivatable 1,2-O-Diacyl-sn-glycerol Derivatives of 1-L-Phosphatidyl-D-myo-inositol 4,5-Bisphosphate (PtdInsP(2)) and 3,4,5-Trisphosphate (PtdInsP(3))*. J Org Chem, 1996. **61**(18): p. 6305-6312.
83. Martin, S.F. and G.E. Pitzer, *Solution conformations of short-chain phosphatidylcholine: Substrates of the phosphatidylcholine-preferring PLC of Bacillus cereus*. Biochimica et Biophysica Acta (BBA) - Biomembranes, 2000. **1464**(1): p. 104-112.
84. Kleusch, C., et al., *Fluorescent lipids: functional parts of fusogenic liposomes and tools for cell membrane labeling and visualization*. Molecules, 2012. **17**(1): p. 1055-73.
85. Bruce, I., et al., *Development of isoform selective PI3-kinase inhibitors as pharmacological tools for elucidating the PI3K pathway*. Bioorg Med Chem Lett, 2012. **22**(17): p. 5445-50.
86. Luo, Z., et al., *Fluorous mixture synthesis: a fluorous-tagging strategy for the synthesis and separation of mixtures of organic compounds*. Science, 2001. **291**(5509): p. 1766-9.
87. Ozaki, S., et al., *Intracellular delivery of phosphoinositides and inositol phosphates using polyamine carriers*. Proc Natl Acad Sci U S A, 2000. **97**(21): p. 11286-91.
88. Bigay, J., et al., *ArfGAP1 responds to membrane curvature through the folding of a lipid packing sensor motif*. EMBO J, 2005. **24**(13): p. 2244-53.

89. Meier, T.I., et al., *Cloning, expression, purification, and characterization of the human Class Ia phosphoinositide 3-kinase isoforms*. Protein Expr Purif, 2004. **35**(2): p. 218-24.
90. Antus, L.L.L.J.M.C.M.H.A.B.S., *Selective removal of the (2-naphthyl)methyl protecting group in the presence of p-methoxybenzyl group by catalytic hydrogenation*. Archive of Organic Chemistry, 2012(5).
91. Sajik, H., *Selective inhibition of benzyl ether hydrogenolysis with Pd/C due to the presence of ammonia, pyridine or ammonium acetate*. Tetrahedron Lett, 1995. **36**: p. 3465-3468.
92. Subramanian, D., et al., *Activation of membrane-permeant caged PtdIns(3)P induces endosomal fusion in cells*. Nat Chem Biol, 2010. **6**(5): p. 324-6.
93. Hoglinger, D., A. Nadler, and C. Schultz, *Caged lipids as tools for investigating cellular signaling*. Biochim Biophys Acta, 2014. **1841**(8): p. 1085-96.
94. Dewald, D.B., et al., *Cellular calcium mobilization in response to phosphoinositide delivery*. Cell Calcium, 2005. **38**(2): p. 59-72.
95. Kui Huang, et al., *Dendritic Molecular Transporters Provide Control of Delivery to Intracellular Compartments*. Bioconjugate Chemistry, 2007. **18**: p. 403-409.
96. Pavlovic, I., et al., *Cellular delivery and photochemical release of a caged inositol-pyrophosphate induces PH-domain translocation in cellulo*. Nat Commun, 2016. **7**: p. 10622.
97. Hovelmann, F., et al., *Optotaxis: Caged Lysophosphatidic Acid Enables Optical Control of a Chemotactic Gradient*. Cell Chem Biol, 2016. **23**(5): p. 629-34.
98. Hoglinger, D., et al., *Trifunctional lipid probes for comprehensive studies of single lipid species in living cells*. Proc Natl Acad Sci U S A, 2017. **114**(7): p. 1566-1571.

99. Mentel, M., et al., *Photoactivatable and cell-membrane-permeable phosphatidylinositol 3,4,5-trisphosphate*. *Angew Chem Int Ed Engl*, 2011. **50**(16): p. 3811-4.
100. Hirko, A., F. Tang, and J.A. Hughes, *Cationic lipid vectors for plasmid DNA delivery*. *Curr Med Chem*, 2003. **10**(14): p. 1185-93.
101. Sercombe, L., et al., *Advances and Challenges of Liposome Assisted Drug Delivery*. *Front Pharmacol*, 2015. **6**: p. 286.
102. Popplewell, L.J., et al., *Novel cationic carotenoid lipids as delivery vectors of antisense oligonucleotides for exon skipping in Duchenne muscular dystrophy*. *Molecules*, 2012. **17**(2): p. 1138-48.
103. Ilies, M.A., W.A. Seitz, and A.T. Balaban, *Cationic lipids in gene delivery: principles, vector design and therapeutical applications*. *Curr Pharm Des*, 2002. **8**(27): p. 2441-73.
104. Martin, B., et al., *The design of cationic lipids for gene delivery*. *Curr Pharm Des*, 2005. **11**(3): p. 375-94.
105. Koynova, R., L. Wang, and R.C. MacDonald, *Synergy in lipofection by cationic lipid mixtures: superior activity at the gel-liquid crystalline phase transition*. *J Phys Chem B*, 2007. **111**(27): p. 7786-95.
106. Kshirsagar, N.A., et al., *Liposomal drug delivery system from laboratory to clinic*. *J Postgrad Med*, 2005. **51 Suppl 1**: p. S5-15.
107. Kube, S., et al., *Fusogenic Liposomes as Nanocarriers for the Delivery of Intracellular Proteins*. *Langmuir*, 2017. **33**(4): p. 1051-1059.
108. Csiszar, A., et al., *Novel fusogenic liposomes for fluorescent cell labeling and membrane modification*. *Bioconjug Chem*, 2010. **21**(3): p. 537-43.

109. Filigheddu, N., et al., *Diacylglycerol kinase is required for HGF-induced invasiveness and anchorage-independent growth of MDA-MB-231 breast cancer cells*. Anticancer Res, 2007. **27**(3B): p. 1489-92.
110. Madhuri, V. and V.A. Kumar, *Design, synthesis and DNA/RNA binding studies of nucleic acids comprising stereoregular and acyclic polycarbamate backbone: polycarbamate nucleic acids (PCNA)*. Org Biomol Chem, 2010. **8**(16): p. 3734-41.
111. Singh, M.K., J. Waybright, and Q. Zhang, *A facile method to enable a model phospholipid cell-permeable and photoactivatable*. Tetrahedron, 2017. **73**(26): p. 3677-3683.
112. Zhang, Q., et al., *Small-molecule synergist of the Wnt/beta-catenin signaling pathway*. Proc Natl Acad Sci U S A, 2007. **104**(18): p. 7444-8.
113. Singh, M.K., et al., *Structure-activity relationship studies of QS11, a small molecule Wnt synergistic agonist*. Bioorg Med Chem Lett, 2015. **25**(21): p. 4838-42.
114. Stanzl, E.G., et al., *Fifteen years of cell-penetrating, guanidinium-rich molecular transporters: basic science, research tools, and clinical applications*. Acc Chem Res, 2013. **46**(12): p. 2944-54.
115. Frankel, A.D. and C.O. Pabo, *Cellular uptake of the tat protein from human immunodeficiency virus*. Cell, 1988. **55**(6): p. 1189-93.
116. Vives, E., P. Brodin, and B. Lebleu, *A truncated HIV-1 Tat protein basic domain rapidly translocates through the plasma membrane and accumulates in the cell nucleus*. J Biol Chem, 1997. **272**(25): p. 16010-7.
117. Wender, P.A., et al., *The design, synthesis, and evaluation of molecules that enable or enhance cellular uptake: peptoid molecular transporters*. Proc Natl Acad Sci U S A, 2000. **97**(24): p. 13003-8.
118. Mitchell, D.J., et al., *Polyarginine enters cells more efficiently than other polycationic homopolymers*. J Pept Res, 2000. **56**(5): p. 318-25.

119. Rothbard, J.B., et al., *Role of membrane potential and hydrogen bonding in the mechanism of translocation of guanidinium-rich peptides into cells*. J Am Chem Soc, 2004. **126**(31): p. 9506-7.
120. Bonduelle, C.V. and E.R. Gillies, *Dendritic Guanidines as Efficient Analogues of Cell Penetrating Peptides*. Pharmaceuticals (Basel), 2010. **3**(3): p. 636-666.
121. Wexselblatt, E., J.D. Esko, and Y. Tor, *On guanidinium and cellular uptake*. J Org Chem, 2014. **79**(15): p. 6766-74.
122. Lee, W.S., et al., *Synthesis and cellular uptake properties of guanidine-containing molecular transporters built on the sucrose scaffold*. Mol Biosyst, 2009. **5**(8): p. 822-5.
123. Gillies, E.R. and J.M. Frechet, *Dendrimers and dendritic polymers in drug delivery*. Drug Discov Today, 2005. **10**(1): p. 35-43.
124. Feichtinger, K., et al., *Triurethane-Protected Guanidines and Triflyldiurethane-Protected Guanidines: New Reagents for Guanidinylation Reactions*. The Journal of Organic Chemistry, 1998. **63**(23): p. 8432-8439.
125. McKinlay, C.J., et al., *Charge-altering releasable transporters (CARTs) for the delivery and release of mRNA in living animals*. Proc Natl Acad Sci U S A, 2017. **114**(4): p. E448-E456.
126. Geihe, E.I., et al., *Designed guanidinium-rich amphipathic oligocarbonate molecular transporters complex, deliver and release siRNA in cells*. Proc Natl Acad Sci U S A, 2012. **109**(33): p. 13171-6.
127. Cooley, C.B., et al., *Oligocarbonate molecular transporters: oligomerization-based syntheses and cell-penetrating studies*. J Am Chem Soc, 2009. **131**(45): p. 16401-3.
128. Duffy, C. and M.T. Kane, *Investigation of the role of inositol and the phosphatidylinositol signal transduction system in mouse embryonic stem cells*. J Reprod Fertil, 1996. **108**(1): p. 87-93.

129. Yuan, T.L. and L.C. Cantley, *PI3K pathway alterations in cancer: variations on a theme*. Oncogene, 2008. **27**(41): p. 5497-510.
130. Sun, H., et al., *PTEN modulates cell cycle progression and cell survival by regulating phosphatidylinositol 3,4,5,-trisphosphate and Akt/protein kinase B signaling pathway*. Proc Natl Acad Sci U S A, 1999. **96**(11): p. 6199-204.
131. Dominguez, C.L., et al., *Diacylglycerol kinase alpha is a critical signaling node and novel therapeutic target in glioblastoma and other cancers*. Cancer Discov, 2013. **3**(7): p. 782-97.
132. Athenstaedt, K. and G. Daum, *Phosphatidic acid, a key intermediate in lipid metabolism*. Eur J Biochem, 1999. **266**(1): p. 1-16.
133. Yamamoto, M., et al., *Phosphatidylinositol 4,5-bisphosphate induces actin stress-fiber formation and inhibits membrane ruffling in CV1 cells*. J Cell Biol, 2001. **152**(5): p. 867-76.
134. Neef, A.B. and C. Schultz, *Selective fluorescence labeling of lipids in living cells*. Angew Chem Int Ed Engl, 2009. **48**(8): p. 1498-500.